Fifth DELTA
User- meeting

Dortmund
25. November 2009

Dear reader,

The last Wednesday of November is DELTA User-Meeting's day. It is since 2005 and we will continue this short tradition in the next years.

As you probably know from the previous meetings the number of contributions is continuously increasing. The offer for all participants to present the results in an oral contribution could not be followed for the fifth DELTA User Meeting. In order to have a more convenient schedule for this day, we decided to share and to present about 50 % of the contribution as posters. I hope you will support the new modality.

Most of the contributions are related to measurements preformed at beamline 9 (58 %) followed by beamline 8 (18 %). Both lines can be regarded as user-friendly parts of a dedicated synchrotron source. For the efforts and the support given to the users by the DELTA-crew and by the beamline scientists providing us an operating system I would like to express my compliments again.

I am very curious about the results of your research obtained at DELTA in the past year.

Alex von Bohlen

Beamline overview:

BL 0 not in use

- Technische Universität Dortmund
- White beam at DELTA bending magnet, critical energy 2.2 keV
- (Infrared)

BL 1 in preparation

- Technische Universität Dortmund
- White beam at DELTA bending magnet, critical energy 2.2 keV
- Lithography

BL 2

- ISAS Dortmund
- White/monochromatic beam bending magnet, critical energy 2.2 keV
- Energy and wavelength dispersive x-ray fluorescence spectroscopy

BL 3 and BL 4

- FEL

BL 5

- Forschungszentrum Jülich
- U250 electromagnetic undulator
- Energy range: 5 - 400 eV
- Photoemission, coincidence measurements, spectroscopy

BL 8

- Universität Wuppertal
- Superconducting asymmetric wiggler (SAW), critical energy 7.9 keV
- Energy range: 1 - 30 keV
- Focus on material science, EXAFS, QEXAFS, ReflEXAFS, XRD

BL 9

- Technische Universität Dortmund
- Superconducting asymmetric wiggler (SAW), critical energy 7.9 keV
- Energy range: 4 - 30 keV
- X-ray reflectivity, (surface) x-ray diffraction, SAXS, XSW, inelastic x-ray scattering

BL 10 in preparation

- Universität Siegen/Universität Wuppertal
- Superconducting asymmetric wiggler (SAW), critical energy 7.9 keV
- Energy range: 4.5 - 16 keV
- X-ray diffraction, absorption spectroscopy (EXAFS)

BL 11

- Technische Universität Dortmund
- U55 permanent magnet undulator
- Energy range: 55-1500 eV
- Photoemission spectroscopy, photoelectron diffraction

BL 12

- Technische Universität Dortmund
- White beam at DELTA bending magnet, critical energy 2.2 keV
- Energy range: 5 - 220 eV
- Photoemission spectroscopy

Deep X-ray lithography – Progress at BL1
D. Lietz, M. Paulus, C. Sternemann, U. Berges, H. Conrad, B. Hippert, M. Tolan

Report – U250 PBM Beamline 5; Angle- and spin-polarized photoemission system with the upgraded in –situ sample preparation system
C. Gottlob, M Gulik, A. Herdt, L. Plucinski, S. Cramm, F. Matthes, B. Küpper , C.M. Schneider

Commissioning of the YB_{66}- monochromator at DELTA beamline BL8
A. Herdt, R. Wagner, R. Frahm, D, Lützenkirchen-Hecht

Practical courses for physics students using synchrotron radiation at DELTA
D. Lützenkirchen-Hecht, T. Heim, S. Rutkowski, R. Wagner, R. Frahm

An EXAFS study of GaN thin films prepared by Pulsed Laser Deposition
J. Brendt, M. Martin

EXAFS investigations of functionalized ZnO(0001) surfaces
V. Moellmann, O. Ozcan, C. Kunze, P. Keil, R. Wagner, D. Lützenkirchen-Hecht, R. Frahm, G. Grundmeier

XSW analysis of dynamical interface processes
M. Brücher, A. von Bohlen, B. Holland, R. Wagner, D. Lützenkirchen-Hecht, R. Hergenröder

Protein adsorption at hydrophobic surfaces
A.K. Hüsecken, F. Evers, M. Paulus, C. Sternemann, T. Brenner, K. Shokuie, S. Bieder, M. Tolan, C. Czeslik

Biomineralization at lipid membranes
S. Bieder, D.C.F. Wieland, M.A. Schroer, M. Paulus, C. Sternemann, P. Degen, M. Tolan

SAXS studies on proteins under extreme conditions
M.A. Schroer, V. Khangulov, J.-B. Rouget, J. Roche, C. Jeworrek, M. Paulus, C. Sternemann, H. Conrad, C.J. Sahle, A. Steffen, D.C.F. Wieland, C.A. Royer, B. Garcia- Moreno, M. Tolan, R. Winter

Bulk amorphous SiO studied by SAXS
M.A. Schroer, C.J. Sahle, O.M. Feroughi, C. Sternemann, A. Hohl, M. Tolan

Structure determination of polyethylene materials by means of X-ray diffraction
S. Schmacke, M. Paulus, C. Sternemann, D. Grahl, T. Theisen, M. Tolan

Self-assembly of iron oxide nanoparticles characterized by X-ray scattering
D. Mishra, M.J. Benitez, O. Petracic, P. Szary, F. Brüssing, M. Feyen, A. Lu, H. Zabel

The adsroption of nanoparticles at interfaces
T. Brenner, M. Paulus, P. Degen, S. Tiemeyer, H. Rehage, M. Tolan

The X-ray investigation of GaAs nanorods grown onto Si[111] substrate
A. Davydok, A. Biermanns, U. Pietsch, S. Breuer, L. Geelhaar

Phase separation and nanocrystal formation in GeO_x
C.J. Sahle, C. Sternemann, A. Hohl, H. Conrad, A. Herdt, O.M. Feroughi, R. Wagner, D. Lützenkirchen-Hecht, A.Sakko, R. Frahm, K. Hämäläinen, M. Tolan

Structural changes of a metal-organic framework under temperature load
D.C.F. Wieland, O. Shekhah, M.A. Schroer, M. Paulus, C. Sternemann, M. Tolan, C. Wöll

The structure of protein adsorbates affected by short- and long- range forces studied by X-ray reflectivity
H. Hähl, F. Evers, M. Paulus, A.K. Hüsecken, T. Brenner, C. Sternemann, S. Grandthyll, M. Tolan, K. Jacobs

Effect of non-ionic cosolvents on protein adsorption studied by X-ray reflectivity
F. Evers, A.K. Hüsecken, T. Brenner, C. Sternemann, C. Jeworrek, M. Tolan, C. Czeslik

Ultrathin Co films on glass studied by MOKE, XRR and XRD using the 2D-MAR-detector
T. Kuschel, T. Becker, D. Bruns, M. Suendorf, F. Bertram, C. Sternemann, M. Paulus, L. Böwer, J. Wollschläger

Ultrathin Fe films on MgO(001) studied by MOKE, XRR and XRD
T. Kuschel, H. Bardenhagen, D. Bruns, M. Suendorf, B. Zimmermann, F. Bertram, C. Sternemann, H. Wollschäger

Laser-induced strain in InAs/GaAs quantum dots
S. Tiemeyer, M. Bombeck, M. Paulus, C. Sternemann, D.C.F. Wieland, M. Bayer, M. Tolan

Investigation of Langmuir films by grazing incidence diffraction
D.C.F. Wieland, S. Bieder, M.A. Schroer, M. Paulus, C. Sternemann, P. Degen, M. Tolan

X-ray diffraction studies on cobalt diamond composites
C. Kronholz, A. Steffen, M. Ferreira, M. Paulus, C.H. Sahle, M. Tolan, W. Tillmann

Residual stress measurements on PVD-TiAlN layers of a multilayer coating under low incident beam angle
U. Selvadurai-Lassl, H.-A. Crostack

Structural studies on $Eu_xSr_{1-x}C_2$ by synchrotron powder diffraction
P. Link, U. Ruschewitz

Structural and morphological changes in P3HT thin film transistors applying an electrical field
D.K. Tiwari, S. Grigorian, U. Pietsch, H.-G. Flesch, R. Resel

Structural and mobility analysis of edge on oriented poly(3-hexylthiphzene) OFET devices prepared by low temperature drop casting technique
T.S. Shabi, P. Pingel, U. Pietsch, N. Koenen, U. Scherf

Soft X-ray standing-wave excited photoelectron spectroscopy studies on the system MgO/Fe
S. Döring, F. Schönbohm, D. Weier, U. Berges, R. Schreiber, D.E. Bürgler, C.S. Fadley, C.M. Schneider, C. Westphal

Photoelectron spectroscopy (XPS) studies on zirconium oxide on nitrided Si(100)
A. Wadewitz, F. Schönbohm, D. Weier, T. Lühr, C. Westphal

X-PEEM of antiferromagnetic domains in single crystalline nickel oxide
F. Nickel, C. Wiemann, U. Berges, C. Westphal, C.M. Schneider

Deep X-Ray Lithography - Progress at BL1

D. Lietz*, M. Paulus, C. Sternemann, U. Berges, H. Conrad, B. Hippert, and M. Tolan
Fakultät Physik/DELTA, TU Dortmund, Maria-Goeppert-Mayer-Str. 2, D-44227 Dortmund

*email: daniela.lietz@tu-dortmund.de

During the last years the demand for micromechanical devices used in micro drives, hard disks, mobile phones etc. has increased rapidly. Due to the small size, such components cannot be fabricated by classical manufacture. For these industrial applications high structures (up to several millimeters) with a lateral resolution of sub-micrometers are required. The components must fulfill high quality standards concerning surface topology and geometry. To achieve the high lateral resolution in combination with a very good edge steepness deep x-ray lithography is used [1]. X-ray lithography uses contact less shadow projection to transcribe the lateral structure of the components which shall be produced to a photosensitive resist which is deposited on a silicon wafer. The x-ray mask is realized by a gold absorber applied on an x-ray transparent membrane, e.g. beryllium or carbon. The exposed areas are changed concerning the chemical structure. In a subsequent chemical development the unradiated regions can be removed. The micromechanical components can be produced by subsequent galvanic precipitation. Synchrotron radiation is used because of the high penetration depth of the radiation in the resist and the small vertical divergence which enables the production of high quality structures.

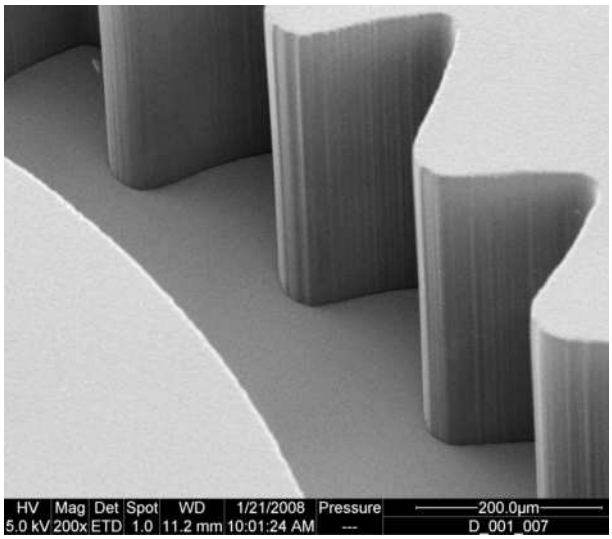

Fig. 1: Scanning electron microscopy micrograph of an exposed and chemical developed microstructure. The good edge steepness and orthogonality between surface and wall as well as substrate and wall becomes clearly visible.

In a first experiment carried out at the ISASline BL2 [2] at DELTA the feasibility of deep x-ray lithography at DELTA was proven. The scanning electron microscopy micrographs are shown in Fig.1. One can clearly see the high edge steepness, the good orthogonality between surface and wall as well as between structure wall and the substrate. The small vertical striations are in the dimension of 1 μm and are caused by the scattering at the mask membrane [3].

A dedicated beamline for deep x-ray lithography is under construction at BL1 at DELTA. At this beamline we are able to expose 4 inch Wafers. Therefore we use the white radiation of a 1.5 T bending magnet with a critical energy of $E_c = 2.2$ keV (Fig.3). This energy is well suited to produce microstructures with a good lateral resolution [4]. The maximum photon flux of $5.7{\cdot}10^{12}$ (photons/s mrad^2 0.1%BW) at 130 mA is reached at 1.8 keV. The most important components of the beamline are the watercooled collimator behind the front-end section, the watercooled beryllium window at the entrance of the experimental hutch and the wafer stepper at the exposure endstation (Fig.2). The collimator aperture is 26 x 16 mm^2 (horizontally x vertically) reducing the original horizontal divergence of 26.2 mrad to a divergence of 8.7 mrad. The vertical divergence is 0.68 mrad. The collimator leads to a beamwidth of 120 mm at the exposure endstation. Thus, it is possible to expose 4 inch wafers homogenously over the full width.

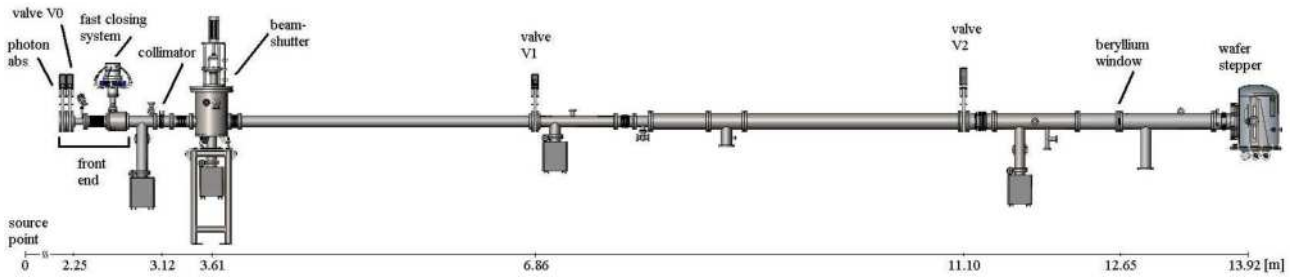

Fig. 2: Schematic layout of the beamline BL1. The front-end section, the collimator behind the front-end, the beamshutter as well as the beryllium window and the wafer stepper within the stepper chamber are shown.

The thickness of the beryllium window is 127 μm with an aperture of 110 x 10 mm^2 (horizontally x vertically) which ensures that the entire beam can pass. The window separates the ultra high vacuum section from the high vacuum region and absorbs the long-wavelength radiation below 0.8 keV. This is important because the long-wavelength radiation causes a heating of the resist and the mask resulting in the distortion of the structure. The thickness of the window is a compromise between transparency for x-ray energies above 2 keV and breaking resistance. The photon energy spectrum at the exposure endstation can be seen in Fig.3. The full spectrum produced by the bending magnet is described by the red line. The consideration of the 127 μm thick beryllium window at the exposure endstation yields the spectrum displayed by the green line. The critical energy at 2.2 keV is indicated by the vertical line.

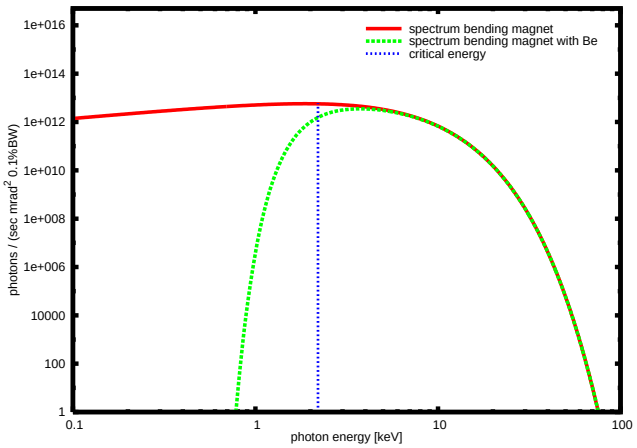

Fig. 3: Photon energy spectrum of a 1.5 T DELTA bending magnet (red solid line). The spectrum is calculated for a beam current of 130 mA. The green dashed line shows the spectrum at the endstation under consideration of a 127μm thick beryllium window. The critical energy is indicated by the vertical line at 2.2 keV.

The wafer stepper at the endstation moves the wafer and the mask vertically through the beam with a constant velocity to guarantee a uniform illumination. The usage of a wafer stepper is the standard method to produce structures for micromechanical components. Thus the set-up at BL1 at DELTA is comparable to the deep x-ray lithography beamlines at e.g. ANKA in Karlsruhe or BESSY in Berlin [5, 6, 7]. The beamlines use shadow projection, moving the wafer with the mask through a broad white beam.
Currently, at beamline BL1 the vacuum sections from the source to the exposure endstation are installed, leak tested and under vacuum. Also the experimental hutch is constructed. At the end of 2009 the beamline will be commissioned and it is planned to start user operation in spring 2010.

Acknowledgement

We would like to thank the DELTA machine group for providing synchrotron radiation and for technical support. We also would like to thank Dr. A. von Bohlen for his help and support during the test experiments carried out at ISASline BL2 at DELTA.

References

[1] V. Saile, U. Wallrabe, O. Tabata, J.G. Korvink, O.Brand, G.K. Fedder, C. Hierold (Eds.), *LIGA and its applications*, Wiley-VCH (2009).

[2] A.v. Bohlen, M. Krämer, R. Hergenröder, U. Berges, *AIP Conference Proceedings* ***879***, 852 (2007).

[3] G. Aigeldinger, C.Y.P. Yang, D.M. Skala, D.H. Morse, A.A. Talin, S.K. Griffiths, J.T. Hachmann, J.T. Ceremuga, *Microsystem Technologies - Micro- and Nanosystems-Information Storage And Processing Systems* ***14***, 277 (2008).

[4] M. Körfer, *Entwurf und Aufbau einer Bestrahlungsanlage für die Röntgentiefenlithographie mit periodischer Bewegung der Synchrotronstrahlung am Speicherring Delta*, PhD Thesis, Dortmund (1997).

[5] J. Göttert, H.O.Moser, F.J. Pantenburg, V. Saile, R. Steininger, *Microsystem Technologies* ***6***, 113 (2000).

[6] ANKA Instrumentation Book (2006), *http* : *//ankaweb.fzk.de/_file/extras/extras_download_3.pdf*.

[7] *http* : *//www.bessy.de/bit/bit_station_list.php* (13.10.2009).

Report - U250 PGM Beamline 5

Angle- and spin-polarized photoemission system with the upgraded *in –situ* sample preparation system

Participants:
Daniel Gottlob, Matthias Gulik, Alexej Herdt, Lukasz Plucinski, Stefan Cramm, Frank Matthes, Bernd Küpper and Claus M. Schneider

Institute of Solid State Research, IFF-9 “Electronic Properties“
Research Centre Jülich, 52425 Jülich, Germany

Contact: daniel.gottlob@uni-dortmund.de

Motivation

Nowadays photoemission experiments feature a variety of different applications, from basic spectroscopy to angle-, spin- or time-resolved measurements. At the Beamline 5 in DELTA we combine into a one spectrometer system a conventional high resolution angle-resolved photoemission with one-dimensional spin-polarized photoemission. During the last year this setup has been enhanced by a new preparation chamber capable of producing complex sample structures *in-situ* and serving multiple users at once.

Experimental Setup

The new preparation chamber is built to supply three users with means of sample preparation. For this purpose the experimental platform has been enlarged by 30% and new equipment has been mounted:

- 8 evaporator cells featuring two Focus EFM3T triple evaporators,
- Ion gun for Ar_+ sample cleaning,
- Commercial LEED, Auger, and MOKE systems,
- Quartz Monitor to measure the evaporation thickness per minute,
- UHV manipulator with 2D rotation, liquid Nitrogen cooling and sample heating up to 550°C,
- Base pressure of about 1E-10, accomplished by a turbomolecular-, an ion-getter-, and a titanium sublimation pumps.

This preparation chamber offers the possibility of preparing complex sample structures while another user is able to collect PES data on an already prepared sample in the main chamber. The two chambers are connected to each other by an UHV transfer system to swap used and a freshly prepared sample.

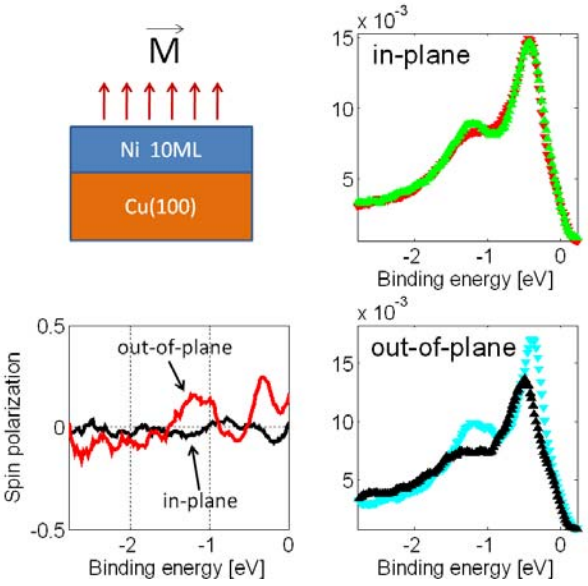

Figure 1: Normal emission spin-polarized spectra of 10ML Ni/Cu(100) at hv=50eV.

A detailed description about the detector setup can be found in the last year’s DELTA User Meeting issue. In short, the unique measurement system of the main chamber features a delay-line-detector and a SPLEED detector which allow to take angle resolved photoemission spectra and spin resolved one-dimensional data simultaneously. Furthermore in-plane- and out-of-plane-magnetization components are measured simultaneously by the SPLEED detector.

Recent projects

In the past year the research at the beamline concentrated on the various properties of magnetic thin films. We have extensively measured magnetic linear dichroism (MLD) on Co/Cu(100) as well as spin-reorientation transitions in Fe/Ag(100) and Ni/Cu(100). A typical example is presented in Fig. 1 where spin-polarized photoemission spectra of 10ML Ni film deposited on Cu(100) surface is shown. Since the experiments are made in remanence it is clear that easy magnetization axis of the film is perpendicular to the film plane, since the magnitude of the in-plane magnetization component is within the noise range.

Ongoing projects

Heusler Alloys

Due to their high Curie temperature, structural relation to conventional semiconductors and theoretically predicted spin polarization of 100% Heusler Alloys receive a lot of interest in the latest condensed matter research. These characteristics make them look promising as material for spin filters, tunnel junctions and GMR devices for spin injection. Our research focuses on the electronic structure, as the spin polarization effects at the Fermi level play a major role in further utilization of Heusler Alloys.

MgO/Fe/GaAs(100)

In recent years, there have been significant advances in the preparation of single crystalline magnetic tunnel junctions (MTJs) based on MgO(100) insulating barriers. Experimentalists confirmed theoretical values for the tunneling magnetoresistance (TMR) of several hundred percent. Details of the electronic structure at the interface between the ferromagnet and insulator can strongly influence the magnitude of the TMR ratio, especially for thinner insulator barriers. Within this study we would like to investigate the minority surface states of Fe(100) [1] and check if they still exist as interface states in MgO/Fe(100).

NiPd/Cu_3Au

On this compound, we want to watch the electronic and magnetic properties with regard to the thickness and the composition of the ultrathin Ni_xPd_{1-x} layer. This composition differences should be reflected in an inverse spin-reorientation transition [2]. We would like to see differences in the spin-orbit coupling caused by the structural differences, obtained by different evaporating parameters.

Summary

A major upgrade of the experimental system is completed. Number of improvements has been made, which sum up to an experiment that now is faster to execute, more accurate and has a more user friendly environment. This made it possible to start three new promising experiments, which are expected to show some first results soon. The new preparation chamber is now capable of serving all of these experiments, and preparation during measurements. There is no need to interrupt the vacuum or to swap any chambers for running all three experiments.

[1] L. Plucinski, Y. Zhao, C. M. Schneider, B. Sinkovic, and E. Vescovo, Phys. Rev. B (2009, accepted).
[2] F. Matthes, M. Seider, and C. M. Schneider, J. Appl. Phys 91, 8144 (2002).

Commissioning of the YB_{66}-monochromator at DELTA beamline BL8

A. Herdt[a], R. Wagner[b], R. Frahm[b] and D. Lützenkirchen-Hecht[b]
a) Zentrum für Synchrotronstrahlung, TU Dortmund, Maria-Goeppert-Mayer-Str. 2, 44227 Dortmund, Germany. Present address: IFF, FZ Jülich, 52425 Jülich..
b) Fachbereich C – Physik, Bergische Universität Wuppertal, Gaußstr. 20, 42097 Wuppertal.

The materials science beamline BL8 employs the synchrotron radiation emitted by the superconducting asymmetric wiggler which provides intense photon beams in the range from about 1 keV (12.4 Å) to ca. 25 keV (0.49 Å). Three different pairs of monochromator crystals – namely Si(311), Si(111) and YB_{66}(400) – are mounted in the complex triple monochromator of BL8. Each of the first crystals is indirectly water cooled, with the cooling being designed for heat loads of up to 500 W. Two mirror systems may be used as low pass filters and for focussing. More details about the construction and the properties of the beamline instrumentation are given in ref. [1]. Here we will address the low energy YB_{66} monochromator optics, which has been proven to deliver monochromatic X-ray beams in the technologically important spectral range between 1 and 2 keV, enabling e.g. X-ray absorption experiments at the Mg, Al and Si K-edges [2, 3]. The YB_{66}-crystals of about 20 mm width, 10 mm length and 1 mm thickness (see Fig.1) are mounted on the goniometer that also accommodates the Si(111) crystal, and both crystal pairs can be remotely exchanged by a linear translation stage perpendicular to the beam. Due to the large interplanar spacing of 5.86 Å, the YB_{66}(400) crystals are favourable for the low energy spectral range from about 1.1 keV to about 2.1 keV (see e.g. [2, 3]). We have optimized the alignment of the two YB_{66}-crystals by choosing a rather high energy in the vicinity of the Ti K-edge at 4.966 keV (wavelength $\lambda \approx 2.496$ Å) corresponding to a Bragg angle of $\Theta_B \approx 12.299°$.

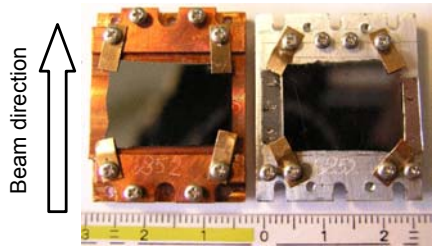

Fig. 1: YB_{66}(400)-monochromator crystals of the DELTA beamline 8. The size of the crystals are about 10 mm in the beam direction, 20 mm width perpendicular to the beam, and 1 mm thickness (Scale at the bottom of the figure). The first crystal (left) is mounted on a water-cooled copper metal crystal holder, the second (right) is mounted on a steel crystal holder.

In Fig. 2, we present a transmission mode near-edge spectrum of a Ti metal foil under ambient conditions using ionization chambers as detectors. As can be seen, the distinct pre-edge feature of metallic Ti directly at the edge cannot be resolved by using the YB_{66}-crystals, while it is easily detectable using Si(111). This is due to the lower energy resolution of the YB_{66}-crystals at this energy, but a convolution of the Si(111) spectrum with a Gaussian of 3 eV full width is able to reproduce the spectrum acquired using the YB_{66} optics. These experiments thus show that an absorption experiment at relatively high energies is well suited for the commissioning and alignment of a YB_{66} double crystal monochromator, even without an evacuated sample stage.

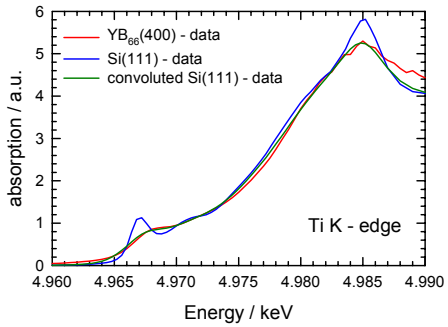

Fig. 2: (a) Transmission mode measurements of a Ti metal foil (7.5 µm thickness) at the Ti K-edge using the YB_{66}(400)- and the Si(111)-monochromators, respectively. If the energy resolution of the YB_{66}-optics (ca. 3 eV) is taken into consideration, the Si(111)-spectrum can be well reproduced.

The experience with the YB_{66} monochromator obtained during commissioning has shown that the Bragg-reflected beam of the YB_{66} monochromator is always contaminated by higher harmonics, especially at lower photon energies < 2 keV. This is not unlikely because the diffraction pattern of those crystals is quite complex (e.g. [3]), and the structure factor of the (12 0 0) and the (16 0 0) reflections are of similar magnitude compared to the fundamental (400) wave. We have therefore employed the double mirror device located downstream the monochromator to reduce the amount of higher harmonics in the beam. Further precautions for experiments at low energies are the use of differentially pumped beam pathways between the different sections of the beamline and the location of the sample, and a specialized vacuum sample stage which is mounted on the diffractometer in the experimental hutch [4]. This way it is guaranteed that the beam path is completely under vacuum, and no parasitic absorption can occur. Our results have shown that a Cr-coated mirror with a grazing angle of 0.8° only transmits the fundamental wave for E < 2 keV, with a cut-off energy of about 4 keV. This can clearly be seen in Fig. 3(a), where fluorescence spectra of a multi-elemental sample are presented for different grazing angles of the Cr-coated double mirror device. More precisely, the intensity of all the lines at higher energies (i.e. those of V, Cr, Fe, Cu) are fully suppressed at Θ=0.8°, while those of Al and Si are still detectable.

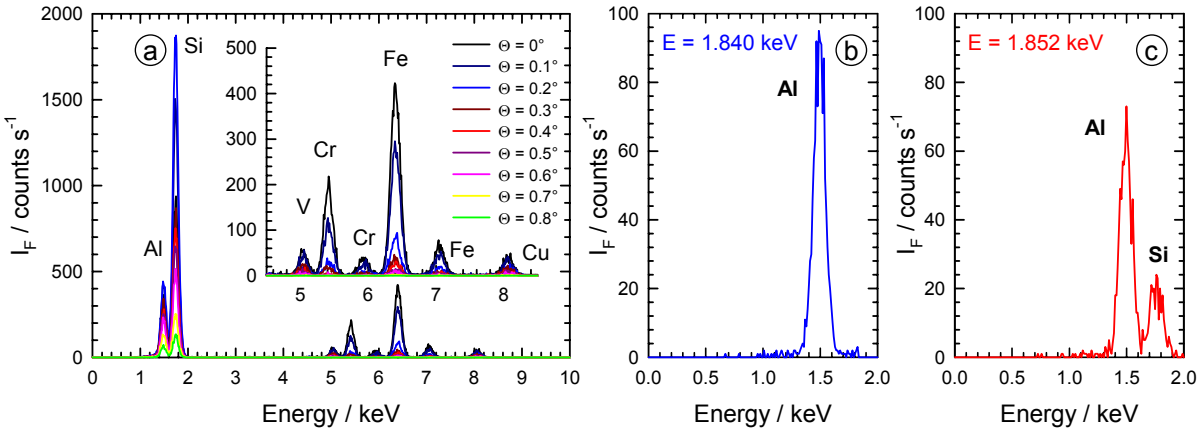

Fig. 3: (a) Fluorescence spectra of a multielemental sample for different incidence angles of the Cr-coated double mirror device. (b) and (c): Fluorescence spectra of an Al/Si-sample obtained in the vicinity of the Si K-edge. Higher harmonics in the beam were suppressed by an incidence angle of the Cr-coated mirror of 0.8°. The excitation energies are 1.840 keV (b) and 1.852 keV (c), respectively.

Fluorescence spectra of a sample containing Al and Si measured using excitation energies in the vicinity of the Si K-edge are presented in Fig. 3(b) and (c). The results show that the higher harmonics of the fundamental wave have successfully been suppressed by the double-mirror device, as no Si fluorescence signals could be detected for an excitation energy of 1.840 keV, while strong Si contributions are found if the excitation energy is increased by only 12 eV, i.e. about 3 eV above the Si K-edge at 1.849 keV (Fig. 3(c)). In conclusion, the presented results have shown that X-ray experiments at low energies in the spectral range between 1 and 2 keV are feasible at DELTA beamline BL 8 making use of the YB_{66} optics, and the setup seems to be promising for X-ray absorption experiments at low energies in the future.

References:

1. D. Lützenkirchen-Hecht, R. Wagner, et al., *J. Synchrotron Rad.* **16,** 264 (2009).
2. T. Kinoshita, Y. Takata, et al., *J. Synchrotron Rad.* **5,** 726 (1998).
3. J. Wong, T. Tanaka, et al., *J. Synchrotron Rad.* **6,** 1086 (1999).
4. A. Herdt, Diploma thesis, Technical University of Dortmund (2009).

Practical courses for physics students using synchrotron radiation at DELTA

D. Lützenkirchen-Hecht, T. Heim, S. Rutkowski, R. Wagner and R. Frahm
Fachbereich C – Physik, Bergische Universität Wuppertal, Gaußstr. 20, 42097 Wuppertal.

As an important part of the physics degree program in Wuppertal University, the physics students have to perform extended practical exercises prior to the beginning of their diploma or masters thesis. In contrast to standard laboratory experiments, these so called "projects" have to be performed in the different working groups and the projects should ideally have a direct link to actual research projects. This way, the students on one hand get a closer insight into contemporary issues and up-to-data research topics, and on the other hand they have for the first time to work continuously on an experiment for a longer period of time. The definition of the project is done by a project leader in close contact with the students, and the students have to prepare their studies which usually last one week.

In the present case, the two students (T.H. and S. R.) should evaluate the possibility of X-ray reflectometry and grazing incidence EXAFS experiments on liquid surfaces using synchrotron radiation at DELTA. Such experiments may yield valuable information about the molecular structure of liquid interfaces, but they are intrinsically restricted to a Θ-Θ-geometry for the incident and reflected beams (see, e.g. [1]), and thus it is necessary to manipulate the beam impinging on the surfaces accordingly. The basic underlying idea was to use the double mirror device which is originally used for the harmonic rejection of low energy beams for this purpose. However, the beam is usually reflected upwards on the first mirror during conventional operation, and the apertures of the Be-window which separates the beamline vacuum against the laboratory air, the vacuum valve and all the other beamline components downstream the mirrors are designed for such an optical path (see [2]). In contrast, the beam needs to be deflected downwards in the present case, and therefore the first task of the students was to evaluate if an X-ray beam can be guided to the diffractometer endstation in the experimental hutch by using the upper mirror of the mirror system in a downwards reflecting geometry, and if so, what is the accessible angular range of the incidence angle Θ?

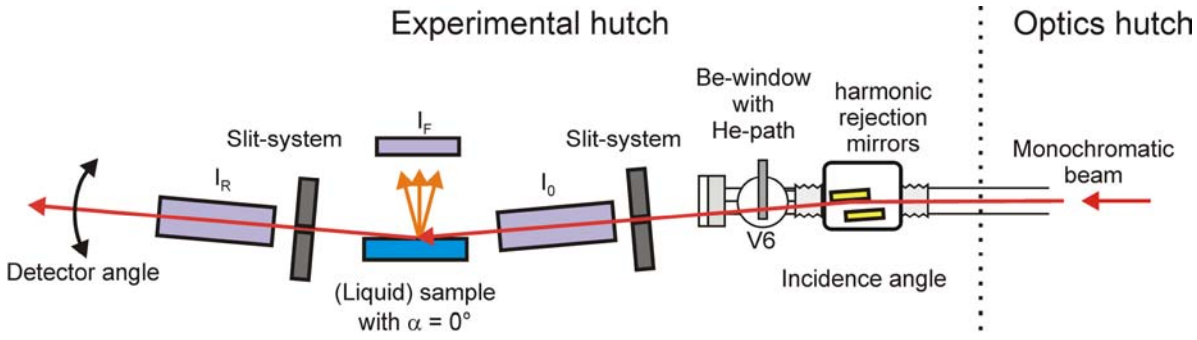

Fig. 1: Setup for the X-ray reflectivity experiments of liquid sample surfaces at BL8 in a Θ-Θ-geometry. The monochromatic beam from the Si(111) double crystal monochromator is reflected downwards by the upper mirror of the double mirror device. The incidence angle on the sample is limited to about 0.3° (5 mrad) by the maximum negative tilt angle of the mirror system and the apertures of the beamline equipment downstream the double mirror device.

As a first result, the students succeeded in receiving well-conditioned X-ray beams for incidence angles of up to $\Theta \approx 0.3°$ - however the change of Θ causes a vertical shift of the beam position, so that the absolute height of the sample and the position of all the slits have to

be optimized after each incidence angle variation. In a second step, model samples consisting of thin sputter-deposited Fe-Cr-oxides of about 5-10 nm thickness have been prepared on glass substrates. Both the new Θ-Θ-geometry suited for the study of liquid surfaces and the conventional Θ-2Θ-geometry were used for X-ray reflectometry and grazing incidence EXAFS measurements, and the obtained results were compared. Furthermore, the feasibility of fluorescence detection was checked. A typical result of a reflectivity measurement in the Θ-Θ-geometry is presented in Fig. 2(a), and both the near edge structure as well as EXAFS oscillations extending to more than ca. 0.4 keV above the edge can be seen. A linear pre-edge background was calculated, and the normalized difference ($R_0(E)$ - R(E)) was calculated as a measure of the absorption. This quantity is compared to near-edge X-ray absorption data of several Fe-O reference compounds in Fig. 2(b). As can be see, the data quality is at least sufficient for a qualitative comparison of the spectra, which leads to the conclusion that the atomic short range order of the thin film is best described by the spectra of β-FeOOH and the Fe_2O_3 references, while all other spectra show significantly different features compared to the thin-film data.

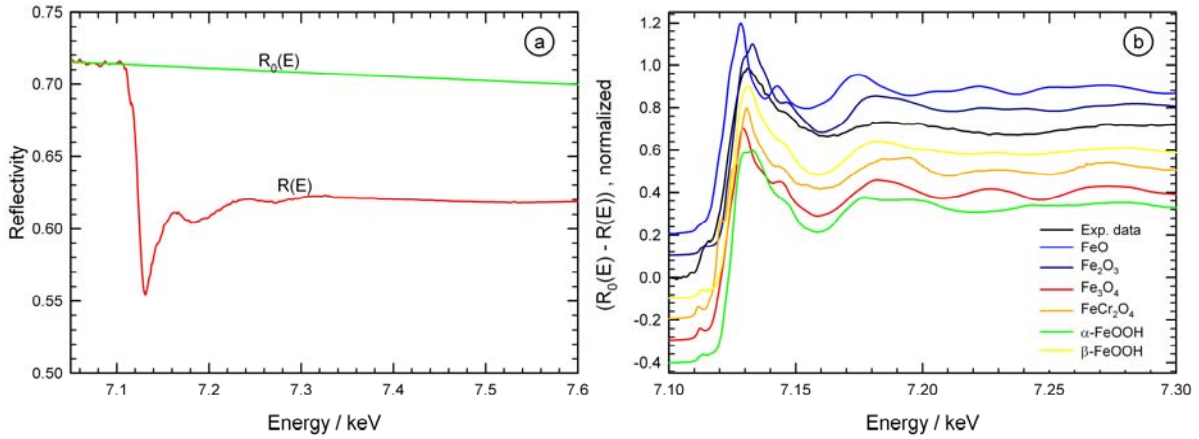

Fig. 2: (a) Reflection mode EXAFS spectrum of a Fe-Cr-oxide thin film (thickness ca. 5 nm) on a glass substrate at the Fe K-edge at an incidence angle of 0.2° using the Θ-Θ-geometry. A linear background $R_0(E)$ is fitted to the pre-edge region of the spectrum, and the difference ($R_0(E)$ - R(E)) was calculated as a measure of the absorption. (b) Comparison of the normalized difference ($R_0(E)$ - R(E)) with Fe K-edge absorption spectra of several different Fe-O reference compounds.

In conclusion, the experiments performed in the present project have proved the feasibility of grazing incidence EXAFS experiments at BL8, both in the reflection mode and using fluorescence detection. The achieved data quality allows a structure determination of thin films of some few nm thickness, so that the setup appears to be in principal suited for the surface analysis of liquid sample systems. As a consequence, in-situ studies of langmuir layers are planned in the near future. Furthermore, keeping in mind that the presented studies have been performed by undergraduate students who did not have any practical experience with accelerator or synchrotron related research before, one can easily judge the unique opportunities of the materials science beamline BL8 at the DELTA storage ring for educational purposes. The students profit from the inspiring atmosphere at DELTA in close contact with many different research teams working in substantially different areas ranging from soft to hard condensed matter, magnetisms, lithography, accelerator physics, chemistry, etc, and the possibility to discuss with other students, researchers and scientists.

References:

1. H. Tanida, H. Nagatani and M. Harada. J. Phys. Conf. Series 83 (2007) 012019
2. D. Lützenkirchen-Hecht, R. Wagner, A. Herdt and R. Frahm. AIP Conf. Proc. (2009), in print.

An EXAFS study of GaN thin films prepared by Pulsed Laser Deposition

J. Brendt, M. Martin
Institute of Physical Chemistry, RWTH Aachen University, 52056 Aachen, Germany
brendt@pc.rwth-aachen.de

Introduction

Amorphous materials exhibit a non-crystalline structure, but most often with well defined short range order, and so they possess unique macroscopic properties. Other materials with interesting properties are non-stoichiometric compounds. The existence of non-stoichiometry causes an increased number of defects in the lattice structure of crystalline substances, such as vacancies or interstitial atoms.

Recently, we have prepared new materials which combine both – an amorphous structure and a highly non-stoichiometric composition. These materials exhibit very interesting and promising properties. We found that in amorphous and non-stoichiometric gallium oxide an insulator-metal transition can be induced by annealing the samples at about 400 °C [1].

Here we report on amorphous and non-stoichiometric gallium nitride thin films prepared by Pulsed Laser Deposition (PLD) [2]. Films were deposited under different gas atmospheres (Ar, N_2, N_2 + N) and at different substrate temperatures (20 – 600 °C).

Elementary analysis of these films by means of Electron Probe Micro Analysis (EPMA) has shown that the gas atmosphere has a big influence on the stoichiometry. Films prepared in Ar ($Ga_1N_{0.66}$) and pure N_2 ($Ga_1N_{0.89}$) have a big nitrogen deficit; in contrast, films prepared in N_2 atmosphere assisted by a nitrogen atom source are stoichiometric ($Ga_1N_{0.97}$).

While the gas atmosphere has a big influence on the stoichiometries of the films, the structural properties are controlled by the substrate temperature. Our aim was to investigate the structural properties (short range order) of the films by *in situ* and *ex situ* Extended X-ray Absorption Fine Structure (EXAFS).

Experiment

The measurements have been done on beamline BL8 at DELTA. *In situ* and *ex situ* XAS experiments were performed in transmission and fluorescence geometry. As fluorescence detector a PIPS (Passivated Implanted Planar Silicon) detector (active area: 3000 mm^2) was used. *Ex situ* experiments were done at RT and *in situ* crystallization experiments were done at temperatures up to 600 °C in argon atmosphere in a specially developed XAS furnace. Fluorescence and transmission signals were recorded simultaneously, but with a much better S/N-ratio of the fluorescence signal.

Results and Discussion

As prepared films

The analysis of the measured spectra has shown that there is a significant difference between the samples prepared in argon, nitrogen and nitrogen assisted by a nitrogen atom source (Fig. 1). The sample prepared in argon shows the smallest amplitude in the first coordination shell, which gives evidence of a smaller averaged coordination number in the 1st shell. This is in agreement with the results from the EPMA analysis, where it is shown that the films prepared at a higher nitrogen partial pressure have higher nitrogen content.

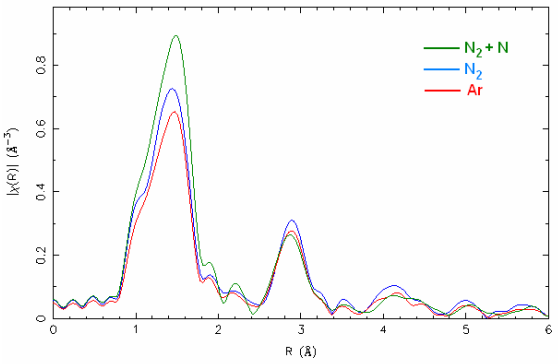

Figure 1: G(R) of GaN samples prepared under different gas atmospheres at 600 °C.

Crystallization

Furthermore the crystallization of amorphous GaN thin films was investigated. *In situ* EXAFS measurements have shown that during the crystallization process there are big changes in the radial EXAFS distribution function (Fig. 2).

While there are only small changes in the first coordination shell, the 2nd and 3rd shell increase drastically. In the as prepared samples there is only short range order. The first peak in the RDF represents the first shell of N atoms around the Ga emitter. This shell does not change much with time, so one can say that there is the same short range order in the crystalline and amorphous GaN phase. The increasing amplitude of the 2nd and 3rd Peak in the RDF can be explained by the ordering process of the atoms and so by an increased long range order.

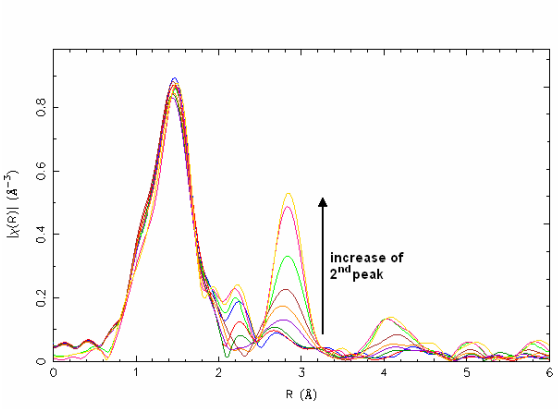

Figure 2: Development of the G(R) of a GaN sample during the crystallization process.

References

[1] L. Nagarajan, R. A. De Souza, D. Samuelis, I. Valov, A. Börger, J. Janek, K.-D. Becker, P. C. Schmidt, M. Martin, Nature Mater. 7 (2008) 391-398.

[2] D. B. Chrisey, G. K. Hubler, "Pulsed Laser Deposition of thin Films", Wiley-Blackwell, 1994.

EXAFS investigations of functionalized ZnO(0001) surfaces

V. Moellmann[a], O. Ozcan[a], C. Kunze[a], P. Keil[b], R. Wagner[c],
D. Luetzenkirchen-Hecht[c], R. Frahm[c], G. Grundmeier[a]
a) Department of Chemistry, University of Paderborn, 33098 Paderborn, Germany
b) Department of Interface Chemistry and Surface Engeneering,
Max-Planck Institut für Eisenforschung GmbH, 40237 Düsseldorf, Germany
c) Fachbereich C - Physik, Bergische Universität Wuppertal, 42097 Wuppertal, Germany

Recently self-assembled monolayers (SAMs) attracted great attention due to their high potential in many industrial applications including electronics and biosensoric [1]. Moreover since SAMs form well organised monolayers over large areas and can be used to tune the characteristics of the surfaces, they are also good candidates as anti-corrosive or adhesion promoting treatments [2]. ZnO in its native form exists abundantly as a passive oxide layer on galvanised steel. Therefore, a detailed understanding of the adhesion mechanisms and stability of organofunctional molecules on ZnO and the properties of the resulting SAMs is necessary for the design of novel and efficient systems.
In this study single crystalline ZnO(0001) and Octadecanethiol (ODT) were chosen as the substrate and the organofunctional molecule respectively. All ZnO substrates were prepared as described in detail elsewhere [3] using 10 minutes of alkaline etching in 3 M NaOH solution. Since the main aim of this study was to investigate the bonding and stability of the ODT-SAM on ZnO surface, three samples were prepared and analysed: The first sample, "etched", which served as the reference sample was measured right after the etching step. The second one, "thiol covered", was exposed to a 1 mM ethanolic solution of ODT for 12 hours with a subsequent rinsing step in pure ethanol. The third sample, "washed", was prepared by placing the monolayer coated substrate in water for 12 hours.
The samples were investigated with grazing incidence EXAFS (beamline 8 at DELTA, Dortmund), Atomic Force Microscopy (AFM) and Diffuse Reflectance Infrared Fourier Transform Spectroscopy (DRIFTS).

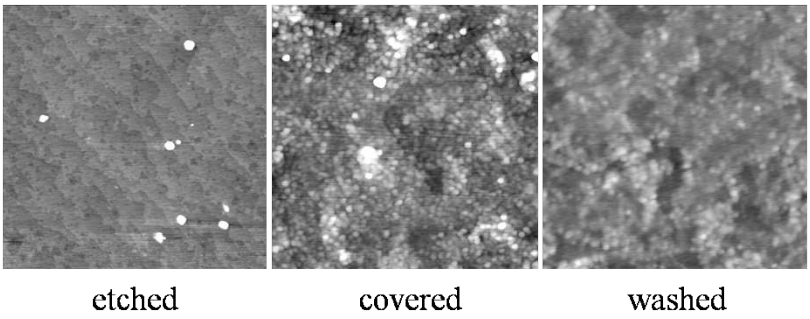

FIG. 1: AFM topography images of the etched (left), thiol covered (middle) and washed (right) surfaces. All images are scaled 1×1 μm.

The AFM-measurements (see figure 1) showed terraces on the bare etched surface. After 12 hours in a solution of 1 mM ODT a strong change in surface topography was observed, the terrace structure disappeared and the surface seemed to be covered by an organic layer. After the washing step the topography of the sample did not show any clear difference.
However although we did not observe an apparent change after the washing step in the topography with AFM, a decrease in the intensity of the symmetric and antisymmetric CH_2 stretching mode could be detected with DRIFTS, which indicates a lower coverage of the surface with Octade-

canethiol.

The EXAFS measurements were done in reflection mode at an angle of incidence of 0.225° for a higher surface sensitivity at the Zn_K edge (9659 eV) at beamline 8. The reflection mode XAS data was then transformed into absorption mode data and a quantitative analysis was made using the IFEFFIT package and the FEFF6 code. A Si 111 double crystal monochromator was used, detuned to 60% at 9.6 keV to reject higher harmonics, the ionization chambers were filled with nitrogen and the apertures were chosen 100 μm before and 600 μm behind the sample.

As seen in the Fourier Transformation of the grazing incidence EXAFS data (figure 2), the intensity of the peak of the first coordination shell, which belongs to the Zn-O distance, decreased after covering the surface with ODT. This can be explained by missing oxygens after bonding of the sulfur of ODT to the zinc of the hydroxylated surface ZnOH releasing one H_2O molecule so that some portion of the surface hydroxlys were replaced with sulphur-zinc bonds.

It was also observed that the Zn-O (first shell) and the Zn-Zn distance (second shell) became longer after covering the surface with ODT and even longer after the washing procedure. So as well the covering as the washing procedure cause some disorder in our system and the relaxation of surface atoms. For a complete understanding of the nature of ODT to ZnO bond and its stability, measurements at the S-edge will be performed in the near future.

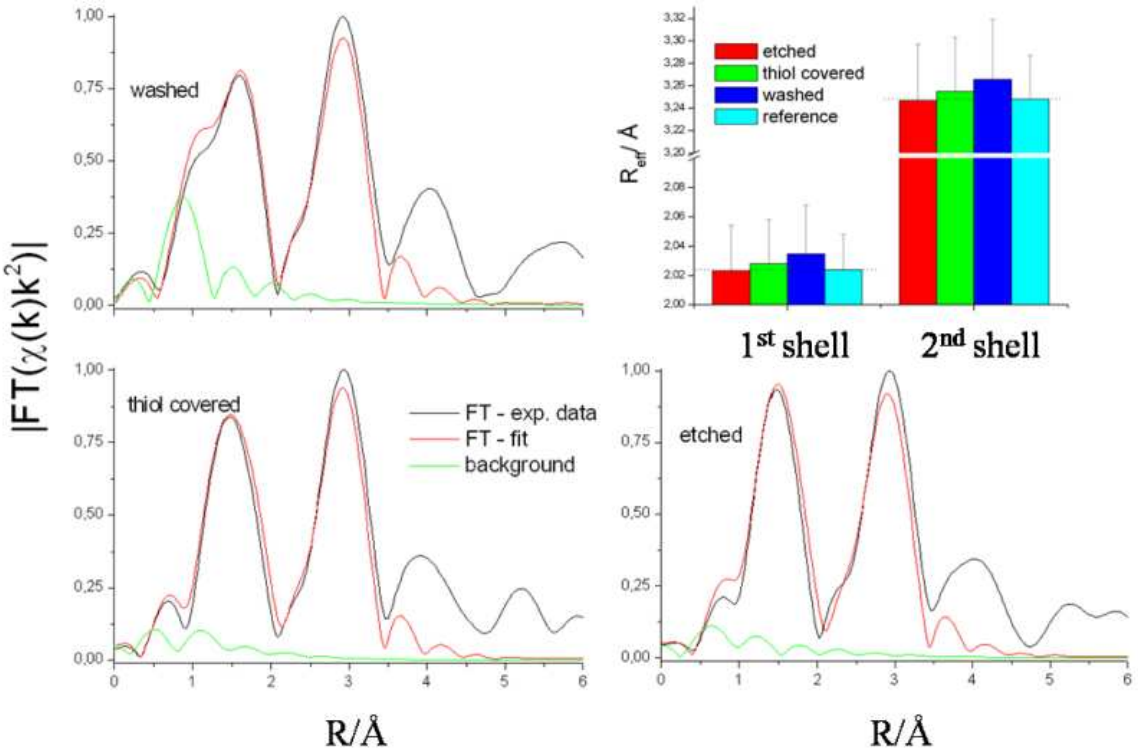

FIG. 2: Fourier Transformation of the grazing incidence EXAFS data of the etched, thiol covered and washed ZnO(0001) surface and the resulting values for R_{eff}. The measurements were done at the Zn_K edge at 0.225° at beamline 8, DELTA.

[1] P. W. Sadik, S. J. Pearton, D. P. Norton, E. Lambers, and F. Ren, Journal of Applied Physics **101**, 104514 (2007).

[2] G. Grundmeier, W. Schmidt, and M. Stratmann, Electrochimica Acta **45**, 2515 (2000).

[3] M. Valtiner, S. Borodin, and G. Grundmeier, Physical Chemistry Chemical Physics **9**, 2406 (2007).

XSW Analyses of dynamical Interface Processes

M. Brücher[1],A. von Bohlen[1,2], B. Holland[1], R. Wagner[2], D. Lützenkirchen-Hecht[2], R. Hergenröder[1]

[1] ISAS Dortmund, Bunsen-Kirchhoff-Str. 11, 44139 Dortmund
[2] DELTA, University of Dortmund, Maria-Goeppert-Mayer-Str. 2, 44221 Dortmund

During the last beamtimes at DELTA, X-ray Standing Waves (XSW) have been used to study the sample composition at different types of interfaces. Experiments were performed to measure the ion distribution at solid/liquid interfaces, from which the interfacial charge could be deduced.[1] Also the pH dependent effect of surface functionalization by aminosilane groups could be observed.
A further sample system were polymer layers used for the development of a new multilyer OLED (organic light emitting diode) fabrication technique. Polymer layers of ca. 130 nm thickness were coated on a Si substrate. A crosslinking reaction initiated by heating transforms the polymer into an insoluble state, so that further layers can be added. The crosslinking process generates a front of sulphur containing ions, which marks the upper limit of the crosslinked sample volume. The position of the S front could be determined using XSW at the expected position, verifying the assumed crosslinking mechanism.

While the former measurements described above were carried out at samples of temporally constant element distribution, recent studies were dedicated to the analysis of dynamical processes at the substrate/solution interface.

Polymer Brushes

Polymer brushes are used for surface functionalisation in microfluidic devices. Their orientation relative to the interface can be controlled by the pH value: for the analysed PAA brushes a pH value of 2 causes them to attach to the interface, making it hydrophobic, while in basic solutions (pH 8) they relax, generating hydrophilic properties. This effect is applied to the development of valves in microchannels.

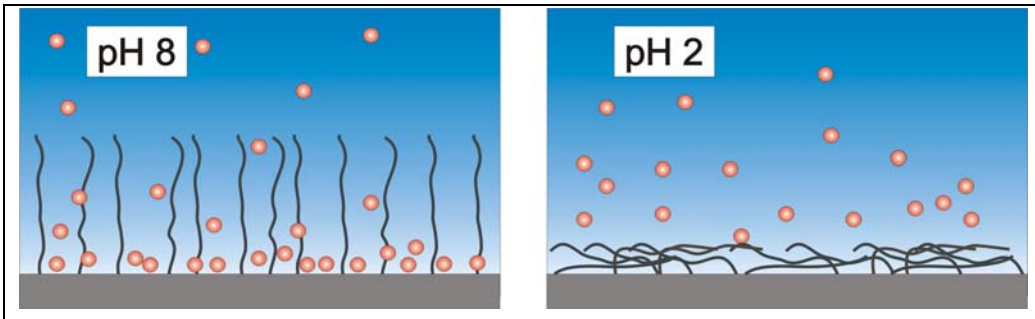

Figure 1. Hydrophilic (left) and hydrophobic (right) interface properties controlled by the pH-dependent orientation of PAA polymer brushes.

XSW measurements have been performed on a PAA sample covered by HCl and KOH solution. It could be seen that for pH 8 (hydrophilic interface) ions could penetrate the brushes and reach the Si surface, whereas in the case of pH 2, the interface-near sample volume was free of ions, demonstration the hydrophobic character of PAA brushes in acid solution.

Initiation of the Polymer crosslinking Process

The start of the crosslinking process described above should be analysed. For this purpose, the sulphur distribution an originally not crosslinked sample was measured repeatedly. Between the measurements, the sample was placed onto a heating plate (T = 130°C) for various time intervals.

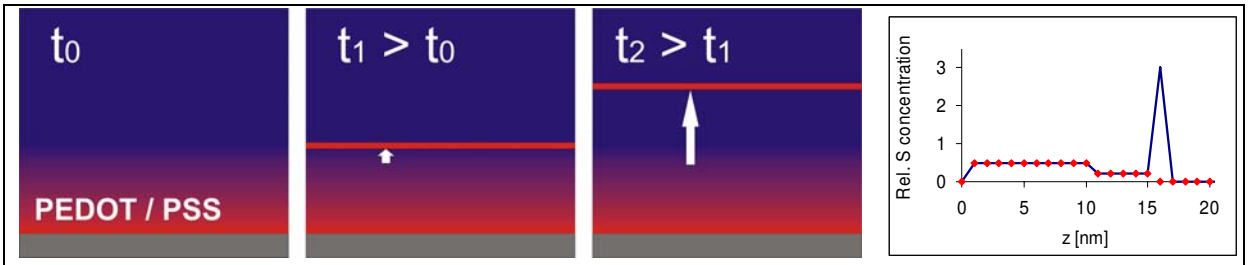

Figure 2. Left: Schematic description of the crosslinking process. The PEDOT/PSS layer contains sulfur atoms/ions initiating the crosslinking process under the influence of sample heating. Further heating causes the progression of the reaction, so the front migrates through the polymer layer. Right: Sulphur distribution profiles deduced from the XSW signal. The red dots mark the S distribution before heating (only PEDOT/PSS), the blue line shows the S distribution (including the front) which can be deduced from the fluorescence curves measured after heating.

Before heating, only the PEDOT/PSS layer could be detected from the angular distribution of sulphur fluorescence. After two heating steps of 30 and 60 seconds, a deformation of the fluorescence curve could be observed, which can be interpreted as a change of sulphur distribution due to the formation of a front of relative high S concentration.

Experiments were performed at beamline 8 at an X-ray energy of 15 keV.

[1] M. Brücher, P. Jacob, A. von Bohlen, J. Franzke, C. Sternemann, M. Paulus, R. Hergenröder, *Langmuir* **2009**, *DOI:10.1021 / la902385d*

Protein Adsorption at Hydrophobic Surfaces

Anne K. Hüsecken*,[a], Florian Evers*,[a], Michael Paulus[a], Christian Sternemann[a], Thorsten Brenner[a], Kaveh Shokuie†,[a], Steffen Bieder[a], Metin Tolan[a] and Claus Czeslik[b]

[a] *Fakultät Physik/DELTA, TU Dortmund, D-44221 Dortmund,*

[b] *Fakultät Chemie, TU Dortmund, D-44221 Dortmund,*

† *now at: Lehrstuhl für Experimentalphysik, Ruhr-Universität Bochum, D-44780 Bochum*

*email: anne.huesecken@tu-dortmund.de, florian.evers@tu-dortmund.de

Introduction

The interaction of proteins with solid surfaces is not only a fundamental phenomenon, but it has also implications in nanotechnology and biomedical engineering [1]. Whenever an aqueous protein solution is exposed to a solid surface, protein molecules will generally tend to adsorb spontaneously at the solid-liquid interface. Many experimental studies indicate that both the adsorption process and the adsorbate structure are influenced by the surface chemistry of the substrate [1, 2]. Depending on surface charge, surface hydrophobicity and solution conditions, the conformation of adsorbed proteins might be changed even leading to denaturation accompanied by a loss of biological activity or leading to surface aggregation. In this regard, self-assembled monolayers, e.g. composed of octadecyltrichlorosilane (OTS) on silica or thiols on Au, exhibit ideal model systems for studying protein adsorption [3] (see report by H. Hähl et al.). Moreover, the hydrophobic OTS-water interface has recently attracted attention as the existence of a water-depletion layer adjacent to the hydrophobic tails, 'the hydrophobic gap', was revealed by high energy X-ray reflectivity [4]. Previous neutron reflectivity studies have shown that a 'two layer model' is suitable to describe the adsorbate structure of β-casein, β-lactoglobulin or lysozyme adsorbed at the hydrophobic OTS surface [5, 6]. This two layer model consists of a compact layer with a high volume fraction adjacent to the surface and a looser, thicker layer protruding into the subphase.

In this study, we examine the adsorption of ribonuclease A (RNase) at the hydrophobic OTS-water interface by X-ray reflectivity. RNase is a model protein with a high conformational stability and has been used in our previous studies [7, 8]. From the analysis of the scattering data, the interfacial adsorbate structure can be obtained and the adsorbed amount of RNase can be calculated. In particular, it will be figured out if the data can be explained by the 'two layer model' and it will be shown how the hydrophobic gap is changed in the presence of the adsorbate. Moreover, we also investigated the effect of non-ionic cosolvents glycerol and urea on the adsorbate structure as a continuation of our previous study (see report by F. Evers et al.).

Experiments and Results

The experimental conditions, the chemicals used and the experimental set-up were the same as in our previous study (report by F. Evers et al.) except that silanized silicon (OTS) wafers were used as substrates which were kindly provided by the group of Prof. Dr. K. Jacobs (Universität des Saarlandes). X-ray reflectivity measurements were performed with a set-up optimized to access solid-liquid interfaces at the beamline BL9 at DELTA [9], which has already been used for protein adsorption studies [10, 11].

Figure 1 displays X-ray reflectivity measurements of RNase adsorption at the hydrophobic OTS-water interface in the absence and presence of 2 M glycerol and 2 M urea. A reference measurement of the pure OTS-water interface is shown for comparison in order to emphasize the effect of the adsorbed protein layer on the reflectivity curve. In the case of pure RNase and RNase in the presence of glycerol, pronounced Kiessig fringes are observed, whereas an additional oscillation occurs in the presence of urea. The complex interfacial structure is described in terms of a layer model as indicated in the electron density profiles shown in Figure 1. The reference system is described by four layers (Si / SiO_2 / OTS head / OTS tail / gap / water). In order to obtain a meaningful refinement of the data, it is necessary to introduce a density depletion layer ('gap') between bulk water phase and OTS tails [4]. The protein adsorbate can be modelled by one (pure RNase, glycerol) or two layers (urea). In the case that one layer was necessary to model the adsorbate structure, a high roughness between adsorbate and protein solution is observed. Hence, the adsorbate structure can be described by a compact part with high volume fraction adjacent to the surface and a thicker loose part protruding into the subphase. Thus, the 'two layer model' is qualitatively corroborated.

Obviously, the hydrophobic gap is present even after the adsorption of RNase. In the presence of glycerol, the depth of the gap is even increased. This observation is in line with a study on the adsorption of BSA and IgG [12], whereas recent studies have suggested that the gap is filled upon the adsorption of BSA and α-amylase on

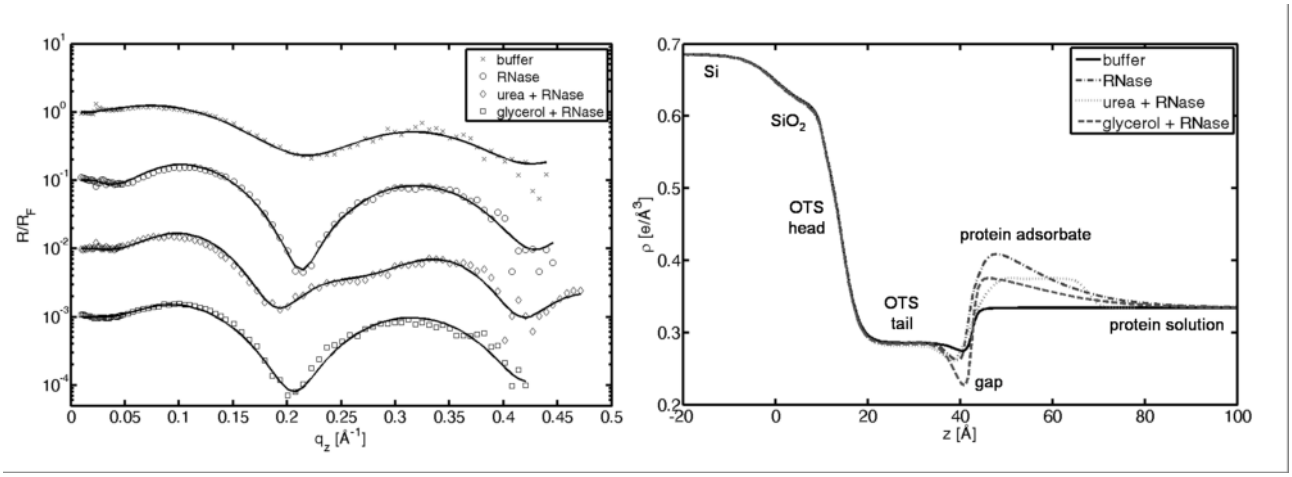

Figure 1: (Left) X-ray reflectivity data (symbols) and refinements (solid lines) of RNase adsorbed at the hydrophobic OTS-water interface with and without cosolvents. (Right) Electron density profiles of RNase adsorbed at the hydrophobic OTS-water interface as obtained by analyzing the reflectivity data.

OTS (report by H. Hähl et al.) and the adsorption of insulin and IAPP on dPS [13]. Further data are needed to clarify the structure of the gap upon protein adsorption.

Γ [mg/m^2]	RNase at OTS	RNase at dPS [14]
w/o. cosolvent	1.6	1.4
glycerol 2 M	1.0	0.8
urea 2 M	0.9	1.0

Table 1: Adsorbed amount as a function of cosolvent content.

The effect of non-ionic cosolvents on protein adsorption is of interest because cosolvents are used to control the conformation of proteins in solution; cosolvents can be used either to denature or to stabilize the protein conformation (see report F. Evers et al.). Recent studies have shown that the addition of cosolvents can lead to a reduction of the interfacial affinity [7, 8, 14]. Here, we find that glycerol and urea significantly decrease the adsorbed amount of RNase, Γ, at the hydrophobic OTS-water interface as listed in Table 1. The same trend has been observed for RNase adsorption at the hydrophobic dPS-water interface by neutron reflectivity measurements [14]. The structure of the protein adsorbate in the presence of urea differs considerably from the two other adsorbate structures shown in Figure 1. In the presence of urea, a more compact adsorbate structure is observed. To uncover the details of the adsorbate structure at hydrophobic OTS surfaces in the presence of cosolvents, further measurements are needed.

Conclusion

In conclusion, X-ray reflectivity has been used to characterize the interfacial structure RNase adsorbed at the hydrophobic OTS-water interface. The adsorbed layer shows two parts: a part adjacent to the surface with a high volume fraction and a loose part protruding into the bulk phase. The hydrophobic gap is still present after adsorption of RNase. Furthermore, first measurements suggest that cosolvents reduce the interfacial affinity of RNase even at hydrophobic OTS surface and it is shown that urea might exert a drastic effect on the adsorbate structure.

Acknowledgments

The DELTA machine group is gratefully acknowledged for providing synchrotron radiation and technical support. It is a pleasure to thank the group of Prof. Dr. K. Jacobs for providing silanized silicon wafers. We would like to thank the Bundesministerium für Bildung und Forschung and the Deutsche Forschungsgemeinschaft for financial support.

References

[1] C. Czeslik, *Z. Phys. Chem.* **218**, 771 (2004).

[2] M. Bellion, L. Santen, H. Mantz, H. Hähl, A. Quinn, A. Nagel, C. Gilow, C. Weitenberg, Y. Schmitt, K. Jacobs *J. Phys.: Condens. Mat.* **20**, 404226 (2008).

[3] K. L. Prime, G. M. Whitesides, *Science* **252**, 1164 (1991).

[4] M. Mezger, H. Reichert, S. Schöder, J. Okasinski, H. Schröder, H. Dosch, D. Palms, J. Ralston, V. Honkimäki , *Proc. Natl. Acad. Sci. USA* **103**, 18401 (2006).

[5] G. Fragneto, R. K. Thomas, A. R. Rennie, J. Penfold, *Science* **267**, 657 (1995).

[6] J. R. Lu, T. J. Su, P. N. Thirtle, R. K. Thomas, A. R. Rennie, R. Cubitt, *J. Coll. Interf. Sci.* **206**, 212 (1998).

[7] J. Koo, T. Gutberlet, C. Czeslik, *J. Phys. Chem. B* **112**, 6292 (2008).

[8] F. Evers, R. Steitz, M. Tolan, C. Czeslik *J. Phys. Chem. B* **113**, 8462 (2009).

[9] M. Paulus, D. Lietz, C. Sternemann, K. Shokuie, F. Evers, M. Tolan, C. Czeslik, R. Winter, *J. Synchrotron Rad.*. **15**, 600 (2008).

[10] F. Evers, K. Shokuie, M. Paulus, C. Sternemann, C. Czeslik, M. Tolan, *Langmuir* **24**, 10216 (2008).

[11] F. Evers, K. Shokuie, M. Paulus, S. Tiemeyer, C. Sternemann, C. Czeslik, M. Tolan, *Eur. Phys. J. Spec. Top.* **167**, 185 (2009).

[12] A. Richter, APS March Meeting 2007, H35.003.

[13] C. Jeworrek, O. Hollmann, R. Steitz, R. Winter, C. Czeslik, *Biophys. J.* **96**, 1115 (2009).

[14] F. Evers, R. Steitz, M. Tolan, C. Czeslik, (unpublished).

Biomineralization at lipid membranes

Steffen Bieder*,[a], D.C. Florian Wieland[a], Martin A. Schroer[a], Michael Paulus[a], Christian Sternemann[a], Patrick Degen[b], and Metin Tolan[a]

[a] *Fakultät Physik/DELTA, TU Dortmund, D-44221 Dortmund,*

[b] *Physikalische Chemie II, TU Dortmund, Otto-Hahn-Str. 6, D-44221 Dortmund*

*email: Steffen.Bieder@uni-dortmund.de

Composite materials which were formed by biomineralization processes can show a well organized and complex structure. Thus, new advanced materials might be produced if the control mechanisms of biomineralization are understood. The biomineralization process in living organisms is controlled by proteins and chemical environment [1, 2, 3]. Studies on different systems show that the formation process is influenced by electrostatic interactions, geometric matching and stereochemical correspondence [4, 5, 6].
In this study the crystallization of iron oxide under an organic monolayer is investigated by grazing incidence diffraction (GID). A Langmuir monolayer of the phospholipid 1,2-dipalmitoyl-glycero-3-phosphocholine (DPPC) mimicing a cell membrane was spread on a liquid solution. The subphase was a 12 millimolar iron(II)-chloride solution. In the case of iron(II)-chloride the biomineralization process is triggered by the change of the pH value. To start the biomineralization process at the membrane ammonium was added to the gas atmosphere (helium) in the sample cell. The diffusion of ammonium to the liquid interface causes a pH change in this region.

The liquid surface sensitive diffraction experiment took place at beamline BL9 at DELTA using the MAR345 detector and a photon energy of E = 13 keV. For the measurement the beam had to be bent down on the liquid surface by using a silicon mirror, resulting in an incident angle of 0.081° [7]. At the sample stage a Langmuir trough was installed into a helium flushed cell (see figure 2). The Langmuir layer was compressed to a surface pressure of $\Pi = 40\ \frac{\mathrm{mN}}{\mathrm{m}}$ at room temperature. After adding ammonium to the helium atmosphere several diffraction patterns were recorded in order to observe the time evolution of the system. Three different diffraction patterns are shown in figure 1 as example.

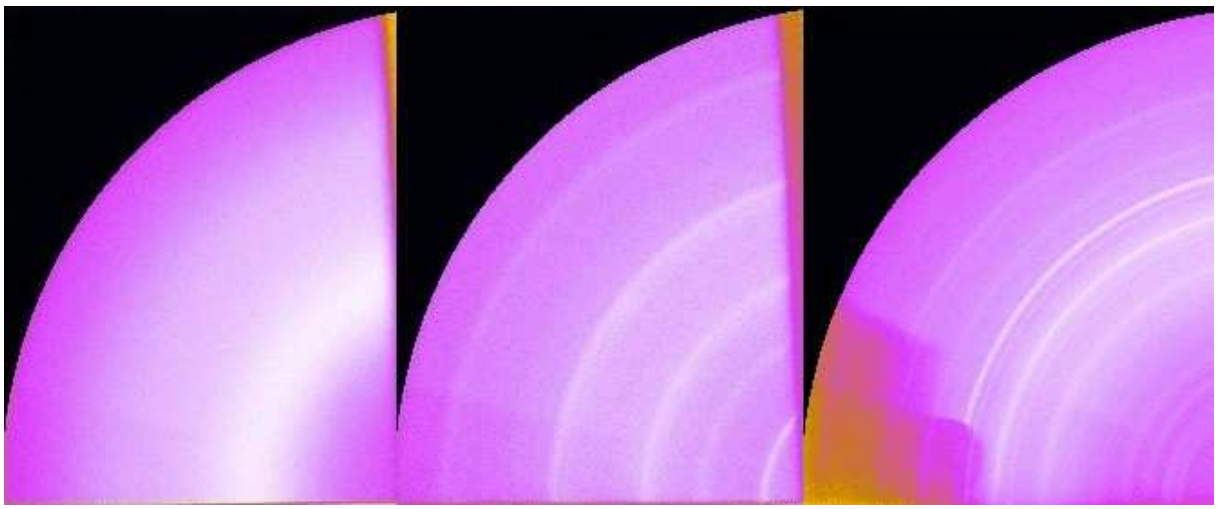

Fig. 1: The left picture shows a diffraction pattern of the sample system before ammonium was added. Only the water structure peak is visible. After adding ammonium the central diffraction pattern was measured. The broad rings indicate the formation of crystalline material at the interface. The result after adding more ammonium is shown the right difraction pattern. The increase of crystallinity becomes clearly visible in the decreasing width of the Debye-Scherrer rings.

The first diffraction patterns showed only the water structure peak. After adding ammonium the appearance of broad rings indicate the formation of material with low crystallinity. When more ammonium was added, the ring positions and widths change drastically (see figure 1, right diffraction pattern). This leads to the conclusion that the recorded patterns show a phase transition from a low- to high-crystalline material. The quantitative data evaluation is still in progress.

Fig. 2: The picture shows the sample cell, which was installed in the six circle diffractometer of BL9 in order to store the samples under a water saturated helium atmosphere.

References

[1] H.A. Lowenstamm, S. Weiner, *On Biomineralization*; Oxford: New York, 1989.

[2] L. Addadi, S. Weiner, *Angew. Chem., Int. Ed. Engl.* **1992**, 31, 153.

[3] L. Addadi, S. Weiner, *Proc. Natl. Acad. Sci. U.S.A* **1985**, 82, 4110.

[4] E.M. Landau, M. Levanon, L. Leiserowitz, M. Lahav, J. Sagiv *Nature* **1985**, 318, 353.

[5] S. Mann, D. Archibald, J.M. Didymus, T.Douglas. B.R. Heywood, F.C. Meldrum, N.J. Reeves *Science* **1993**, 261, 1286.

[6] J.H. Fendler *Chem. Mater.* **1996**, 8, 1616.

[7] C. Krywka, M. Paulus, C. Sternemann, M. Volmer, A. Remhof, G. Nowak, A. Nefedov, B. Pöter, M. Spiegel, M. Tolan *J. Synchrotron Rad.*, **2007**, 13, 8

SAXS studies on proteins under extreme conditions

Martin A. Schroer*,[a], Victor Khangulov[b], Jean-Baptiste Rouget[c], Julien Roche[c], Christoph Jeworrek[d], Michael Paulus[a], Christian Sternemann[a], Heiko Conrad[a], Christoph J. Sahle[a], Andre Steffen[a], D.C. Florian Wieland[a], Catherine A. Royer[c], Bertrand Garcia-Moreno[b], Metin Tolan[a], and Roland Winter[d]

[a] *Fakultät Physik/DELTA, TU Dortmund, Maria-Goeppert-Mayer-Str. 2, D-44227 Dortmund, Germany;*

[b] *Department of Biophysics, Johns Hopkins University, 3400 North Charles Street, Baltimore, MD 21218, USA;*

[c] *3 CNRS, UMR5048, Centre de Biochimie Structurale, F-34090 Montpellier, France;*

[d] *Physikalische Chemie I, TU Dortmund, Otto-Hahn-Str. 6, D-44227 Dortmund, Germany;*

*email: martin.schroer@tu-dortmund.de

In this report we describe recent results of our small angle x-ray scattering (SAXS) studies on the unfolding properties of proteins in aqueous solution performed at the synchrotron radiation facility DELTA, TU Dortmund.

As proteins are ubiquitous in all biological processes, the detailed knowledge of the mechanisms that lead to folding, unfolding and misfolding are of significant scientific interest. In this context the influence of electrostatic interactions in proteins is of major importance. Internal ionizable residues are essential for various energy transduction processes common to living organisms like H^+-transport [1] or light-activated processes [2]. Hence, studies of the effect of ionizable amino acids on the stability of proteins are subject of current research [3, 4].

In our SAXS studies we performed measurements on different mutants of the small monomeric protein Staphyloccocal Nuclease (SNase) whose stability and that of some of its mutants were already analyzed in previous scattering studies [5, 6, 7, 8]. The variants studied here were T62P, a natively unfolded protein, and Δ+PHS-V66K, which contains an ionizable lysine residue within its hydrophobic core.

Measurements were performed at beamline BL9 of DELTA employing the SAXS setup already described in Ref. [9]. A photon energy of 10 keV and a sample-to-detector distance of about 1080 mm allowed to cover a q-range from 0.3 up to 4.0 nm^{-1}. The exposure time was chosen to be 1800 s due to the low concentrations used. Low proteins concentration were used to avoid protein aggregation and to be able to determine the form factor of the proteins without contributions of an intermolecular structure factor. In no case radiation damage was observed.

The scattering signals of the proteins in solution were obtained by measuring the protein solution, the pure buffer solution and subtracting the azimuthal averaged buffer data from the scattering data of the protein solutions.

The SAXS data of the SNase mutant T62P were recorded as a function of the pH value. The pH range from 2.0 to 7.0 was covered in 0.5 steps. Figure 1 exemplarily shows the background-corrected scattering curves for pH 2.0 to 4.5. Obviously, increasing the pH results in significant changes of the SAXS profiles reflecting a pH induced structural modification of the protein.

A detailed analysis of the SAXS data of T62P as a function of pH in comparison to the wildtype protein SNase shows, that this mutant, even though denatured under all pH conditions studied, becomes more compact when the pH value is increased. In addition, at higher pH values the affinity to formation of dimers increases due to a reduction of the Coulomb repulsion and an enhanced hydrophobic interaction, thus leading to a larger radius of gyration, R_g.

Our data further reveal that the unfolded state of wildtype SNase at pH 2.0 is more compact than that of the highly denatured T62P, which can be described by a random coil conformation. (*paper in preparation*)

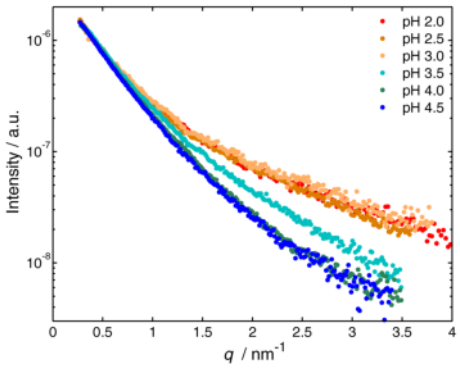

Figure 1: Scattering curves for T62P at different pH values.

To further study the influence of ionizable residues inside the protein on the overall stability, high pressure SAXS measurements were carried out on another SNase mutant, Δ+PHS-V66K. The pK_a value of the residue lysine (K) inside the hydrophobic core is at about 5.5 [10]. Thus, at a pH value of 4.5 this residue is positively charged, whereas at pH 6.0 it is essentially uncharged. These pH changes allow us to study this mutant in two different charged states.

High pressure has been proved a valuable tool to study the plasticity of proteins in solution [11]. To achieve pressures up to 3 kbar a hydrostatic high pressure cell employing to flat diamond windows was used [12]. These measurements were supplemented with experiments carried out at BW4, HASYLAB.

Depending on the pH value adjusted, Δ+PHS-V66K exhibits a different stability against pressure-induced unfolding. Figure 2 depicts the radius of gyration, R_g, as a function of pressure for two different pH values.

In the uncharged state (pH 6.0), we detect only a slight increase of R_g as the pressure is raised, reflecting some small structural changes only, whereas in the charged state (at pH 4.5) unfolding of the protein occurs already at 1 kbar.

A detailed analysis of these SAXS data in combination with the results of other techniques (high pressure NMR) yields a detailed picture of the networks of interactions which underlies the cooperativity of folding and the conformational dynamics of the protein. (*paper in preparation*)

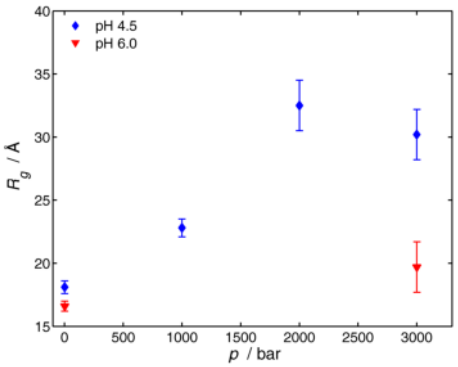

Figure 2: Radius of gyration, R_g, for Δ+PHS-V66K as a function of pressure for different pH values.

In our SAXS studies we could show that there may exist different unfolded state stuctures of a small monomeric protein induced by a single-point mutation and the solvent's pH value. Furthermore, the plasticity and stability are already largely influenced by minor changes in the electrostatic interactions inside the protein. Both the effects of varying pH value and of pressure on the conformation of small globular proteins were studied at beamline BL9 with high accuracy. In addition, supplemental measurements on a non-globular repeat protein, the ankyrin domain of the protein Notch, were also performed at DELTA (data not shown) [13].

The authors like to acknowledge the DELTA machine group for providing synchrotron radiation and technical support.

References

[1] S. Yoshikawa, K. Shinzawa-Itoh, R. Nakashima, R. Yaono, E. Yamashita, N. Inoue, M. Yao, M.J. Fei, C.P. Libeu, T. Mizushima, H. Yamaguchi, T. Tomizaki, T. Tsukihara, *Science* **280**, 1723 (1998).

[2] H. Luecke, J.K. Lanyi, *Adv. Protein Chem.* **63**, 115 (2003).

[3] D.G. Isom, B.R. Cannon, C.A. Castaneda, A. Robinson, B. Garcia-Moreno E., *Proc. Natl. Acad. Sci.* **105**, 17784 (2008).

[4] N.C. Fitzkee, B. Garcia-Moreno, *Protein Sci.* **17**, 216 (2008).

[5] G. Panick, R. Malessa, R. Winter,G. Rapp, K.J. Frye, C.A. Royer, *J. Mol. Biol.* **275**, 389 (1998).

[6] G. Panick, G.J.A. Vidugiris, R. Malessa, G. Rapp, R. Winter, C.A. Royer, *Biochemistry* **38**, 4157 (1999).

[7] M. Schroer, *Röntgenkleinwinkelstreuung an dem Protein Staphylokokken Nuklease und dessen Mutanten*, Diploma thesis, TU Dortmund (2008).

[8] M.A. Schroer *et al.*, *in preparation.*

[9] C. Krywka, C. Sternemann, M. Paulus, N. Javid, R. Winter, A. Al-Sawalmih, S.B. Yi, D. Raabe, M. Tolan, *J. Synchrotron Rad.* **14**, 244 (2007).

[10] C.A. Fitch, D.A. Karp, K.K. Lee, W.E. Stites, E.E. Lattman, B. Garcia-Moreno E. *Biophys. J.* **82**, 3289 (2002).

[11] J.L. Silva, D. Foguel, C.A. Royer, *Trends Biochem. Sci.* **26**, 612 (2001).

[12] C. Krywka, C. Sternemann. M. Paulus, M. Tolan, C. Royer, R. Winter, *ChemPhysChem.* **9**, 2809 (2008).

[13] J.-B. Rouget *et al.*, *submitted to J. Mol. Biol.*

Bulk amorphous SiO studied by SAXS

Martin A. Schroer*,[a], Christoph J. Sahle[a], Omid M. Feroughi[a,b], Christian Sternemann[a], Achim Hohl[c], and Metin Tolan[a]

[a] *Fakultät Physik/DELTA, TU Dortmund, 44221 Dortmund,Germany,*

[b] *Lehrstuhl für Werkstofftechnologie, TU Dortmund, Leonhard-Euler-Str. 2, 44227 Dortmund, Germany,*

[c] *Institute for Materials Science, Darmstadt University of Technology, 64287 Darmstadt, Germany*

*email: martin.schroer@tu-dortmund.de

Changes in the microscopic structure of bulk amorphous SiO_x (a-SiO_x, $x \approx 1$) are studied by small angle X-ray scattering (SAXS). The results foster the interpretation of other data (see e.g. [1, 2]) and are in line with a structural model of a-SiO where nanometer sized regions of Si and SiO_2 are separated by ultra–thin sub–oxide interfaces (schematic drawing in Figure 1). [3]

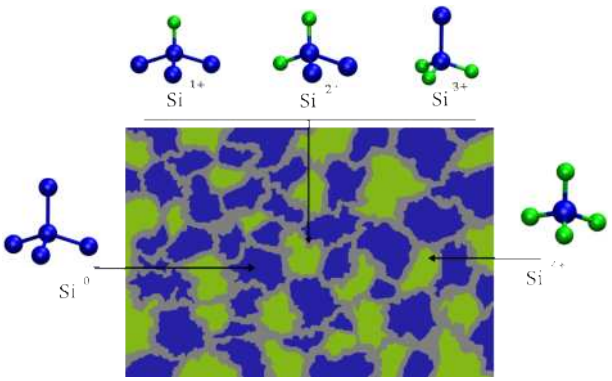

Figure 1: Schematic drawing of the microscopic structure of a-SiO according to the ICM model.

a-SiO, analogous to a-GeO [4, 5, 6], represents a promising starting material for the development of new (opto-) electronic and semiconductor technology. Since SiO shows a temperature induced phase separation that is accompanied by the formation of Si nanocrystals (NC) in an oxide matrix [2, 7] the mentioned technological applications seem feasible, yet, little is understood about the NC formation mechanisms. In this context SAXS can be of great avail as this technique is capable of probing nanometer sized structures both in ordered and disordered systems.

SAXS measurements on a-SiO were performed at beamline BL9 of DELTA. [8] A photon energy of 10 keV and a sample–to–detector distance of about 108 cm allowed to measure q-values of up to 4 nm^{-1}. Exposure times between 600 and 800 seconds were chosen. a-SiO samples were synthesized as described in detail in Ref. [3] and were annealed *ex situ* for one hour in a quartz–glass tube furnace under a steady nitrogen flow at temperatures between $T = 600 - 1200$ °C.

Figure 1 depicts the scattering intensity for samples annealed at different temperatures. Significant changes in the data as a function of annealing temperature are obvious. In order to analyze the SAXS signal the linear part of the scattering curves in a double-logarithmic representation were fitted by the following equation:

$$I(q) = A \cdot q^{-p}.$$

Here, A is a constant, $q = \frac{4\pi}{\lambda} sin(\frac{2\Theta}{2})$ is the wave vector transfer and p is the scattering object's fractal dimension. [9, 10] A value of $1 \leq p \leq 3$ characterizes scattering from mass fractals. A diluted percolation system, diluted gels and colloidal aggregates, branched polymers or a two phase system where ramified domains exist are examples; whereas $3 \leq p \leq 4$ reflects scattering from surface fractals, e.g. Euclidean bodies where the surface fractal dimension quantifies their roughness.

As shown in Figure 2, up to a temperature of about $T = 900$ °C the increase of p is sparse. This implies that in this temperature regime the recorded SAXS signal can mainly be attributed to the sub–oxide interfaces, which mass–fractalic plunges the native sample. At higher temperatures the decay power p increases drastically reflecting scattering from surface fractals. In addition to this rise in p a shift of the linear regime in $I(q)$ towards smaller q values, i.e. larger structures, is evident. Both the increase in p and the shift in the linear regime in q suggest a growth of Si and SiO_2 domains at the expense of the sub–oxide interfaces.

Overall, these data point to an intepretation of the native a-SiO structure as nanometer scaled dendritic regions of Si and SiO_2 that are separated by thin sub–oxide interfaces. Temperature treatment leads to a phase separation within the sub–oxide interfaces which results in an obliteration of these interfaces and a growth of Si and SiO_2 regions, accordingly.

In conclusion, SAXS may be used to monitor the change of a system's morphology on the nanometer scale. The temperature dependence of the fractal dimension p can be correlated to the process of the temperature induced phase separation and nanocrystal formation in a–SiO, analogous to a–GeO [6] as was confirmed using X–ray Raman scattering (XRS) and X–ray diffraction (XRD). [2] Thus, combining complementary scattering techniques such as SAXS, XRS or XRD allows one to study this process on different length scales.

The authors would like to acknowledge the DELTA machine group for providing synchrotron radiation. This

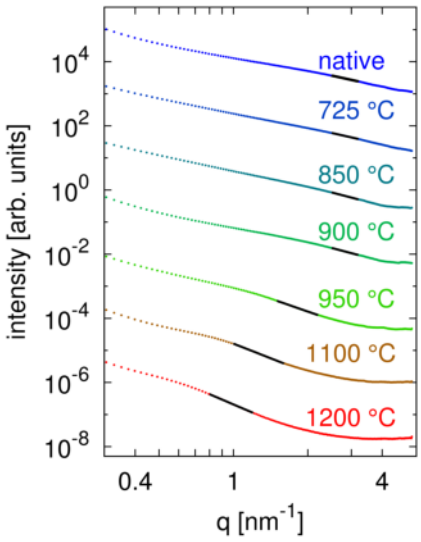

Figure 2: SAXS signal of differently annealed a-SiO samples. Black solid lines represent least square fits which were used to estimate the decay power.

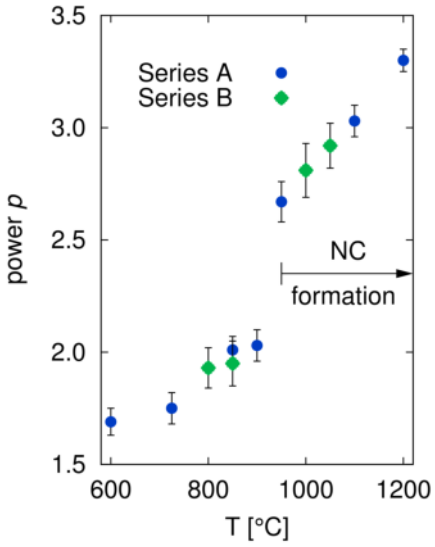

Figure 3: Decay power p as function of annealing temperature T.

work was supported by DAAD (313-PPP-SF/08-IK and 1127504), DFG (TO 169/14-1) and the Academy of Finland (1110571, 1127462).

References

[1] A. Sakko, C. Sternemann, Ch.J. Sahle, J.A. Soininen, H. Sternemann, O.M. Feroughi, H. Conrad, F. Djurabekova, M. Tolan, K. Hämäläinen in preparation

[2] O.M. Feroughi, C. Sternemann, Ch.J. Sahle, M.A. Schroer, H. Sternemann, H. Conrad, A. Hohl, G.T. Seidler, T.T. Fister, J. Bradley, M. Balasubramanian, A. Sakko, K. Pirkkalainen, K. Hämäläinen, and M. Tolan, submitted to *Appl. Phys. Lett.*

[3] A. Hohl, T. Wieder, P.A. van Aken, T.E. Weirich, G. Denninger, M. Vidal, S. Oswald, C. Deneke, J. Mayer, H. Fuess, *J. Non-Cryst. Solids* **320**, 255 (2003).

[4] Ch.J. Sahle, C. Sternemann, A. Hohl, H. Conrad, A. Herdt, O.M. Feroughi, R. Wagner, D. Lützenkirchen-Hecht, A. Sakko, R. Frahm, K. Hämäläinen, and M. Tolan, *Delta User Meeting Report* 2008/2009.

[5] A. Schacht, C. Sternemann, A. Hohl, H. Sternemann, Ch. Sahle, M. Paulus, and M. Tolan, *J. Non-Cryst. Solids* **355**, 1285 (2009).

[6] Ch.J. Sahle, C. Sternemann, H. Conrad, A. Herdt, O.M. Feroughi, M. Tolan, A. Hohl, R. Wagner, D. Lützenkirchen–Hecht, R. Frahm, A. Sakko, and K. Hämäläinen, *Appl. Phys. Lett.* **95**, 021910 (2009).

[7] V. Kapaklis, C. Politisb, P. Poulopoulos, and P. Schweiss, *Appl. Phys. Lett.* **87**, 123114 (2005).

[8] C. Krywka, C. Sternemann, M. Paulus, N. Javid, R. Winter, A. Al-Sawalmih, S. Yi, D. Raabe, and M. Tolan, *J. Synchrotron Rad.* **14**, 244 (2007).

[9] D.W. Schäfer, B.C. Bunker, and J.P. Wilcoxon, *Proc. R. Soc. Lond. A* **423**, 35 (1989).

[10] P.W. Schmidt, *J. Appl. Cryst.* **24**, 414 (1991).

Structure determination of polyethylene materials by means of x-ray diffraction

Saskia Schmacke*,[a], Michael Paulus[a], Christian Sternemann[a], Dirk Grahl[b], Thomas Theisen[b], Metin Tolan[a]

[a] *Fakultät Physik/DELTA, TU Dortmund, D-44221 Dortmund,*
[b] *RWE Vertrieb AG, Freistuhl 7, 44137 Dortmund.*

*email: Saskia.Schmacke@uni-dortmund.de

Polyethylene (PE) is a widely used material in many fields of daily life like automotive industry (wheels, interior), packing industry and building industry. The materials studied in this work are polyethylene gas pipes, which have been in use around 30 years.

Polyethylene is a macromolecule, consisting of a long chain of ethene units. The examined PE gas pipes were made of PE63. The solid body is composed of crystalline and amorphous areas. In the crystalline parts the chains order in an orthorhombic unit cell (space group P*nam*) with cell parameters a = 7.4241 Å, b = 4.9491 Å and c = 2.5534 Å in the case of a bulk material [1]. The polyethylene chains are oriented in the direction of the c axis of the unit cell. In the amorphous regions, the polyethylene molecules are randomly distributed. With increasing amorphous fraction the elasticity increases and the the brittleness decreases [2]. Thus, the composition of crystalline and amorphous areas effects the macroscopic behaviour of the material.

The task is to obtain information about the structure of bulk polyethylene at room temperature and the ageing behaviour by means of thermal and pressure treatment. The goal is the prediction of material failure. X-ray diffraction is a proper tool to analyse the crystalline and amorphous contributions within the samples and to establish a connection between molecular structure and macroscopic properties such as material stability.

The examined samples were prepared from a 30 years old PE63 gas pipe. Two parts of this pipe have been artificially aged in a temperature and pressure bath with different parameters. For sample preparation a 1 cm broad stripe was cut out of the pipe along the longitudinal axis. This stripe was divided in four equal cuboids. Each of the cuboids was cut in four slices from the outer wall over two volumes slices and a fourth slice from the inner wall. The dimensions of each slice were 10x20 mm^2 with a thickness of 2 mm. These samples were annealed in a temperature range of 90 – 140 °C.

The diffraction experiments took place at the wiggler beamline BL9 at DELTA [4]. Diffraction patterns were measured at a wavelength of $\lambda = 0.459$ Å using a MAR345 image plate scanner. The distance between the sample and the detector was 352.52 mm. The samples were tempered in an oven at each temperature for 15 minutes. Afterwards, ex situ diffraction experiments of the differently annealed samples were carried out. The average exposure time was 300 s. After the measurements the 2d data were integrated with the program Fit2D [5], followed by the data analysis.

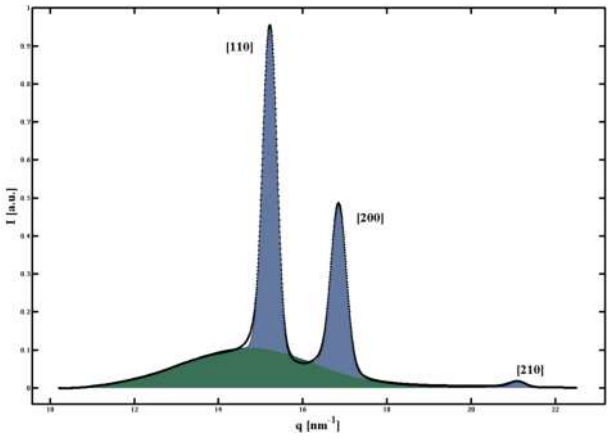

Fig. 1: Decomposition of a typical x-ray diffraction spectrum after background correction in crystalline (blue area) and amorphous (green) contributions.

Since the samples are neither completely amorphous nor completely crystalline, scattering experiments yield both crystal reflections and a broad amorphous scattering halo. The region of the [110] and [200] reflections as well as the strong amorphous scattering halo have been used for the analysis of the samples crystallinity. Exemplarily for a single sample pseudo Voigt profiles (Laurentzian $L(q)$ and Gaussian $G(q)$) are selected as profile functions for the crystalline reflections and a Gaussian in the case of the amorphous contribution. This function is fitted to the background corrected data set. From the positions of the reflections follow the cell parameters. Integration of the amorphous scattering contribution (I_{am}) as well as contribution of the [110] and [200] reflection (I_{cryst}) and calculation of the ratio of both yields the relative crystallinity χ of the sample:

$$\chi = \frac{I_{cryst}}{I_{cryst} + I_{am}}.$$

Figure 1 shows a typical 1D diffraction pattern for an annealed polyethylene sample after background correction. Profile fitting and integration of the crystalline and amorphous contributions lead to the samples crystallinity.

Figure 2 shows the temperature dependence of the crystallinity χ for two native samples, a surface slice (blue markers) and a volume slice (green markers). The crystallinity starts with a relatively constant value of $\chi = 62\%$ between 90 and 110 °C. A further increase of the heating temperature leads to an increase in the crystallinity of approximately 1.5 %. This increased crystallinity can be associated with a change of Young's modulus [2]. An increase of χ by this value results in a difference in the Young's modulus of 14 %. A higher brittleness (and lower elasticity) is connected to an increased probability for material failure because of a relatively high stiffness of the material. The lower the Young's modulus, the more flexible is the material and the more external stress it can stand. At a temperature of around 135 °C the melting of the polyethylene starts.

Further experiments with systematic examination of the temperature behaviour of the material as well as measurements with spatial resolution have been carried out. The data analysis is still in progress and will complete the presented results.

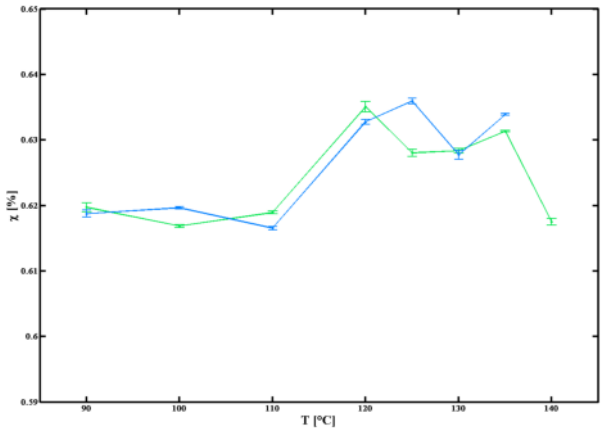

Fig. 2: Relative crystallinity of two native slices depending on the annealing temperature. Clear increase of χ with temperature up to around 120 °C, then relatively constant till 135 °C, when the melting starts.

The author wants to thank *RWE Vertrieb AG* for financial support of the work and the DELTA institute for beamtime.

References

[1] R. Caminiti, L. Pandolfi, P. Ballirano, *J. Macromol. Sci – Phys.*, B39(4), 481492 (2000)

[2] H. Gräfen, „Lexikon der Werkstofftechnik", VDI-Verlag Düsseldorf, 779-785 (1993)

[3] H.M. Rietveld, *J. Appl. Cryst.* 2, 65 (1969)

[4] C. Krywka, C. Sternemann, M. Paulus, N. Javid, R. Winter, A. Al-Sawalmih, S. Yi, D. Raabe, and M. Tolan, *J. Synchrotron Rad.*, **14**, 244 (2007).

[5] http://www.esrf.eu/computing/scientific/FIT2D

Self-assembly of iron oxide nanoparticles characterized by X-ray scattering

D. Mishra, [1] M.J. Benitez, [1, 2] O. Petracic, [1] P. Szary, [1] F. Brüssing, [1] M. Feyen, [2] A. Lu, [2] H. Zabel[1]

[1] Institut für Experimentalphysik / Festkörperphysik, Ruhr-Universität Bochum, 44780 Bochum, Germany.

[2] Max-Planck-Institut für Kohlenforschung, Mülheim an der Ruhr, Germany.

Magnetic nanoparticles are the building blocks for bottom up nanofabrication. Several applications have already been realized in medicine, biology and other fields. There are many potential promising applications to be seen in near future e.g. in high density data storage, logic devices and quantum information technology [1]. Self-assembly or templated self-assembly is one of the ways for realizing these bottom up nanostructures. Since the nanoparticle size (and size distribution) as well as internal structure determine the magnetic and electrical properties it is important to study the structure for better device fabrication.

We present here a detailed study of self assembled iron oxide nanoparticles of 20nm diameter coated with oleic acid and spin coated on Si (100) substrate. The self-assembly of one monolayer (1ML) and multilayer systems were characterized by X-ray reflectivity, in plane scattering at small angles and rocking scans using beamline BL9 in DELTA at an energy setting of 11keV. Furthermore, the internal crystalline structure was studied with out-of-plane Bragg scans to analyze and distinguish different oxide phases present in the sample. The synthesis of nanoparticles is described in more detail in Ref [2].

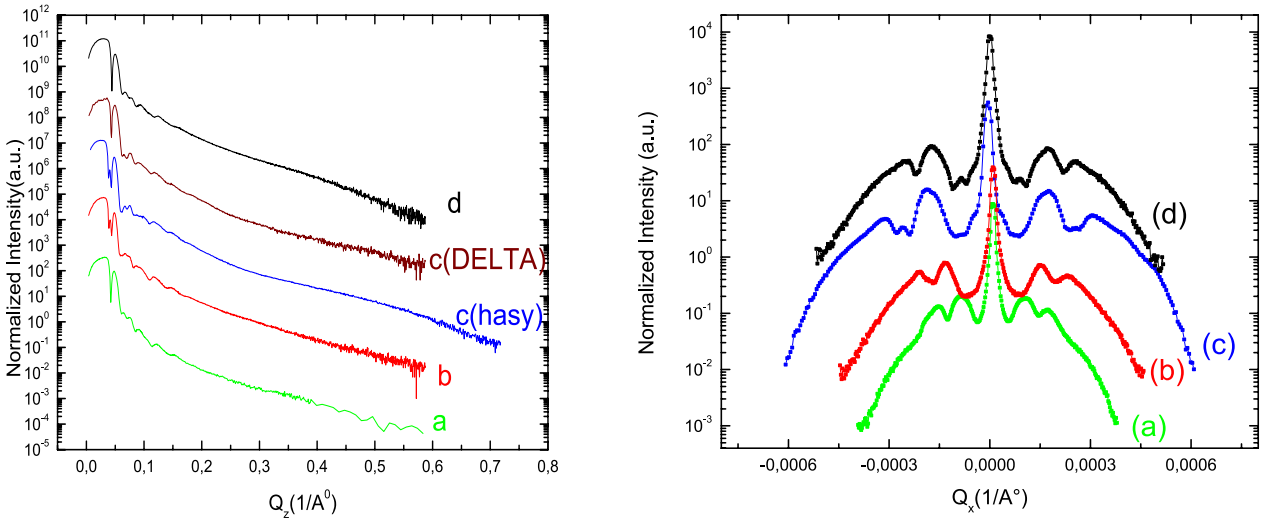

Fig 1: X-ray Reflectivity (left) and rocking scan (right) at 0.069 $Å^{-1}$ of 5ML films annealed at (a) 80°C in air (b) 170°C in air (c) 230°C in vacuum (d) 500°C in vacuum for 20 minutes.

Fig. 1 shows the reflectivity and rocking scans of a 5 ML film annealed at different temperatures and atmospheres. The reflectivity which probes the electron density perpendicular to the sample surface shows a Bragg peak due to multilayer periodicity, which corresponds to a periodicity of 13nm. From this periodicity we infer a close packing of nanoparticles. The absence of higher order Bragg peaks as well as the fast damping of Kiessig-fringes indicate a high roughness of the film, which is intrinsic due to the spherical size of the nanoparticles.

The unchanged multilayer Bragg peak position for different annealing temperatures indicates that the ordering and size of the particles is not affected by heat treatment. The in plane rocking scans on the right panel of Fig. 1 reveals an additional ordering of 1µm and 6µm respectively. Its origin is not clear to us at the present time. In order to observe the in-plane interparticle distance GISAXS experiments are required.

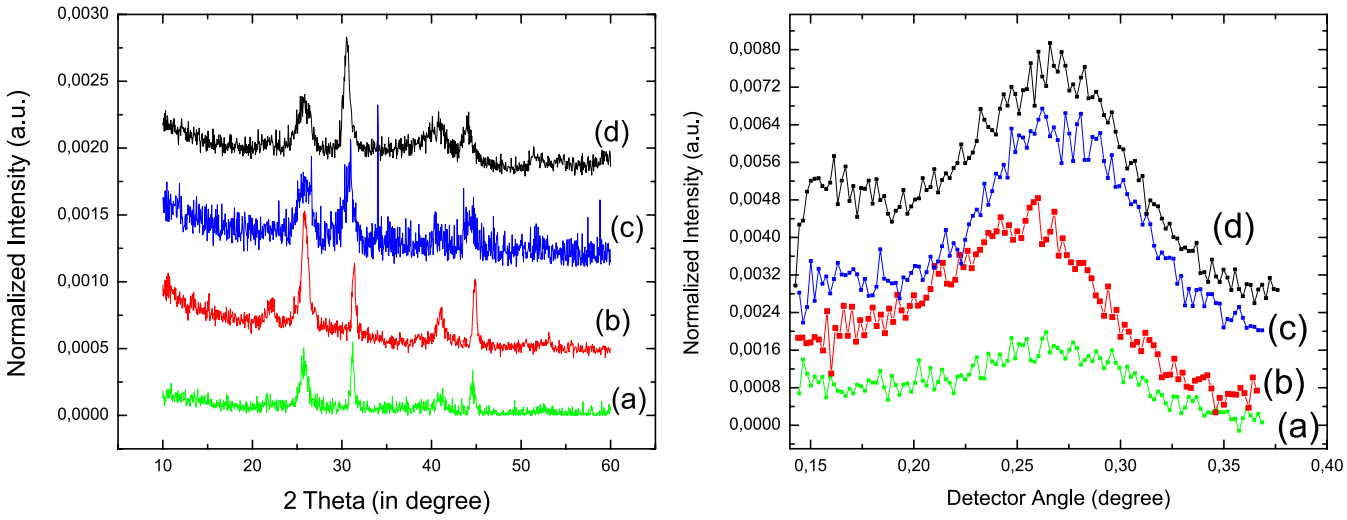

Fig 2: X-ray diffraction (left) and in plane scattering (right) of 5ML films annealed at (a) 80°C in air (b) 170°C in air (c) 230°C in vacuum (d) 500°C in vacuum.

We have also studied the internal crystalline structure with grazing incidence X-ray diffraction as a function of annealing temperature which is shown in the left panel of Fig. 2. The incidence angle was 0.2° and the detector was scanned from 10° to 60° with a step size of 0.05°. The X-ray diffraction pattern shows a mixed iron oxide phase consisting of FeO and γ-Fe_2O_3/Fe_3O_4. Their proportion changes as a function of annealing temperature. It is difficult to distinguish between γ-Fe_2O_3 and Fe_3O_4 from X-ray diffraction. Magnetic measurements also confirm a mixed phase iron oxide with antiferromagnetic FeO residing in the core and γ-Fe_2O_3/Fe_3O_4 forming the ferromagnetic shell [3]. The right panel on Fig. 2 shows the in-plane scattering due to particle size, which corresponds to a particle size of 23nm.

Acknowledgement:

Authors would like to acknowledge the immense help provided by the beamline scientists of BL9 Dr. Michael Paulus and Dr. Christian Sternemann during the measurement at DELTA. D. Mishra would like to acknowledge financial support through fellowship from the research school "Forschung mit Synchrotronstrahlung in den Nano- und Biowissenschaften".

References

1. S. Sun, C. B. Murray, D. Weller, L. Folks, A. Moser Science **287,** 1989 (2000).
2. J. Park, K. An, Y. Hwang, J. park, H. Noh, J. Kim, J. Park, N. Hwang, T. Hyeon Nature Materials **3**, 891 (2004).
3. M.J. Benitez et al (unpublished).

The adsorption of nanoparticles at interfaces

Thorsten Brenner*,[a], Michael Paulus[a], Patrick Degen[b], Sebastian Tiemeyer[a], Heinz Rehage[b] and Metin Tolan[a].

[a] *Fakultät Physik/DELTA, TU Dortmund, D-44221 Dortmund, Germany,*

[b] *Fakultät Chemie, TU Dortmund, D-44221 Dortmund, Germany.*

*email: thorsten.brenner@tu-dortmund.de

In our x-ray reflectivity (XRR) study we have analysed the adsorption of maghemite (γ-Fe_2O_3) nanoparticles with hydrodynamic diameters between 10 nm and 30 nm at the solid/liquid interface between an aqueous solution and a silicon (Si) surface.

Nanoparticle materials are frequently used in industry e. g. in the production of cosmetics, for the design of surface coatings and in medical applications. The adsorption of nanoparticles is determined by particle-particle and particle-interface interactions. Here the van-der-Waals and electrostatic interaction play a major role [1, 2]. Effective interaction potentials can be obtained by Derjaguin-Landau-Verwey-Overbeek (DLVO) theory [3, 4].

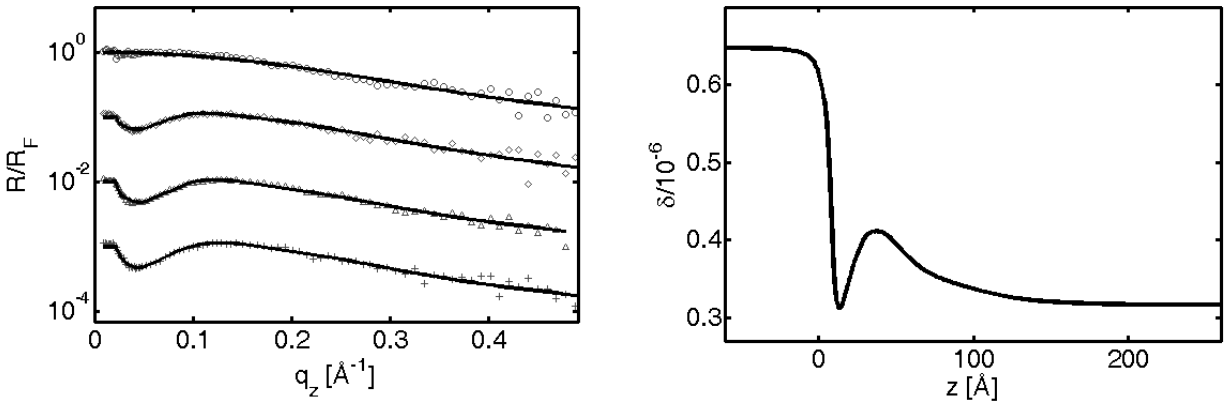

Figure 1: Left: X-ray reflectivities of the silica/aqueous nanoparticle solution interface taken before preparation and 35, 120 and 185 minutes after preparation (top to bottom). The reflectivities are normalized by the Fresnel reflectivity. Refinements are shown as solid lines. Right: Dispersion profile obtained by a refinement of the reflectivity taken 185 minutes after preparation.

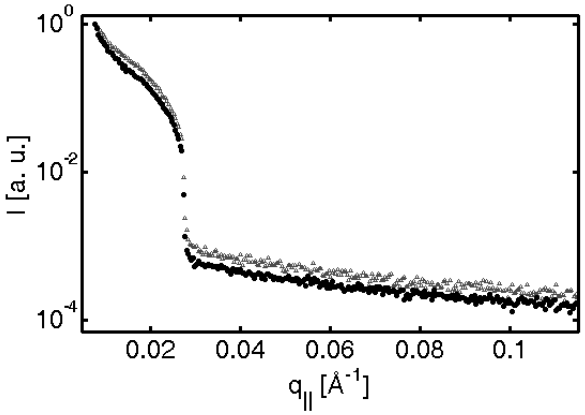

Figure 2: Diffuse scattering signal nominated on the main intensity of a silicon substrate without nanoparticles (filled points) and with dried-up maghemite nanoparticles (unfilled triangles). Raw data is shown. The isotropic bulk scattering has not been subtracted.

The production process for a maghemite nanoparticle solution is described in [5]. The measured zeta potential of the solution was between $\zeta = +40\,\mathrm{mV}$ and $\zeta = +60\,\mathrm{mV}$. The maghemite concentration in the aqueous solution is about 0.7 g/l.

The XRR measurements of the silica/aqueous solution interface were performed in-situ using a photon energy of 27 keV at beamline BL9 at DELTA [6]. A drop of maghemite solution was placed onto water at pH3. The maghemite particles diffuse through the water and adsorb finally onto the silicon substrate. The reflectivity curves reflect the adsorption of the positively charged particles on the negatively charged silicon interface. Figure 1, left-hand shows a series of in-situ XRR measurements of the silicon nanoparticle solution interface normalized by the Fresnel reflectivity. Figure 1, right-hand depicts the dispersion profile of the reflectivity taken after 185 minutes. The dispersion δ and the electron density ρ are related by $\delta = \lambda^2/(2\pi) \cdot r_\mathrm{e}\,\rho$ (λ wave length, r_e classical electron radius). A model of hard spheres was used to interpret the electron density profile. In this model the size distribution of the polydispers particles plays a major role. From dynamic light scattering data of maghemite solution we maintain a log-normal size distribution with a maximum at $(15 \pm 1)\,\mathrm{nm}$. The results of the XRR measurements indicate the adsorption of small particles from the solution with a most common diameter of $d = (3.1 \pm 0.1)\,\mathrm{nm}$.

The lateral structure of dried-up nanoparticles on a silicon substrate had been investigated by measurements of the diffuse scattering. Figure 2 shows the results. Laterally there is no long ranged order detectable. A reason for this could be the size distribution of the particles or a averagely long distance between the particles on the substrate. The slight difference between silicon and silicon with nanoparticles could indicate a wide structure peak or the form factor of the particles.
Another XRR measurements were performed with gold nanoparticles. Their zeta potential was negative. The reflectivities show no adsorption of particles onto a silicon substrate. Consequently the electrostatic forces are dominating the adsorption process. To prove the reversibility of the adsorption process the silicon wafer was sprayed with water. Reflectivity curves of this sprayed silicon wafer show no significant reduction of adsorbed particles on the substrate.
Similar results were found investigating the free interface between an aqueous nanoparticle solution and air. Here x-ray reflectivities were measured with a Bruker D8-Advanced diffractometer in theta-theta geometry with a photon energy of 8 keV. Even without strong electrostatic interactions between the gas phase and the aqueous solution there is a weak adsorption of particles at the interface preferencing particles with smaller diameter.

References

[1] M. Paulus, P. Degen, S. Schmacke, M. Maas, R. Kahner, B. Struth, M. Tolan, and H. Rehage, *Eur. Phys. J. Special Topics* **167** (2009) 133-136.

[2] P. Degen, M. Paulus, M. Maas, R. Kahner, S. Schmacke, B. Struth, M. Tolan, and H. Rehage, *Langmuir* **24**, 12958 - 12962 (2008)

[3] B. V. Derjaguin, L. D. Landau, *Acta Physicochim. URSS* **14** (1941) 633.

[4] E. J. W. Verwey, J. T. G. Overbeek, Theory of the stability of hydrophobic colloids, *Elsevier Science Publisher*, Amsterdam (1948).

[5] Y. S. Kang, D. K. Lee, C. S. Lee, and P. Stroeve, *Journal of Physical Chemistry B* **106** (2002) 9341 - 9346.

[6] M. Paulus, D. Lietz, C. Sternemann, K. Shokuie, F. Evers, M. Tolan, C. Czeslik, and R. Winter, *Journal of Synchrotron Radiation* **15** (2008) 600 - 605.

The X-ray investigation of GaAs nanorods grown onto Si[111] substrate

A. Davydok[a], A. Biermanns[a], U. Pietsch[a] , S. Breuer[b], L.Geelhaar[b]

[a]*Festkörperphysik, Universität Siegen, Walter-Flex-Str. 3,57072, Siegen, Germany*
[b]*Paul-Drude-Institut für Festkörperelektronik, Hausvogteiplatz 5-7,10117 Berlin, Germany*

Nanorods (NR) growth is typically realized using vapor-liquid-solid (VLS) mode in MOVPE [1] or MBE onto [111] planes of a zinc-blende or diamond type semiconductor by solution from a molten eutectic alloy formed by metallic seed. Diameter and position of grown NRs crucially depends on the statistical process of the metallic droplet and alloy formation. The spatial position and the diameter of the molten seed (typically Au) determine position and size of the grown NRs onto the substrate [2]. It was found that nearly any $A^{III}B^{V}$ semiconductor material can be grown as NRs onto another $A^{III}B^{V}$ or group IV [111] substrate independent from lattice mismatch [3].

In recent experiments we were investigating the lattice accommodation between GaAs NRs onto Si[111] substrate grown by MBE via gold precursor. Home measurements at a completed NR sample revealed that the GaAs NRs are grown with lattice parameters known from bulk material. Therefore the huge lattice mismatch has to be accommodated within the first few monolayers or in a wetting layer next to the substrate.

In order to determine the particular influence of stacking faults on strain accommodation we focused our attention measurements of reflection oblique to the [111] growth direction which might be particularly sensitive to stacking faults. For growth along [111]ZB, reflections like (105) wurzite are highly sensitive. In addition the 311 reflection appears only in case of a zinc-blende structure.

During the experiment at DELTA BL9, NRs were inspected in high-resolution setup using an analyser crystal in front of the detector.

Fig. 1 shows a radial scan through the Si(111) reflection. Intense peaks are observed corresponding to GaAs NR's appearing at qz=19.29 and at Si position at qz=20.06. The later peak was used for internal calibration of the angular scale.

Reflection curves measured in asymmetric scattering geometry are shown in Fig.2 Results show that both peaks, i.e. 311 ZB and 105 wurzit,e show certain small deviation from

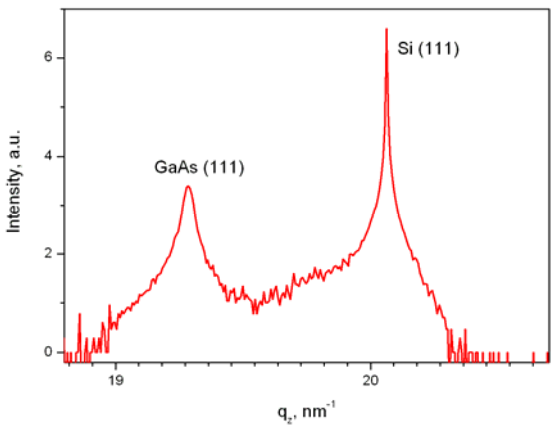

Fig.1 Radial scan through the Si(111) reflection

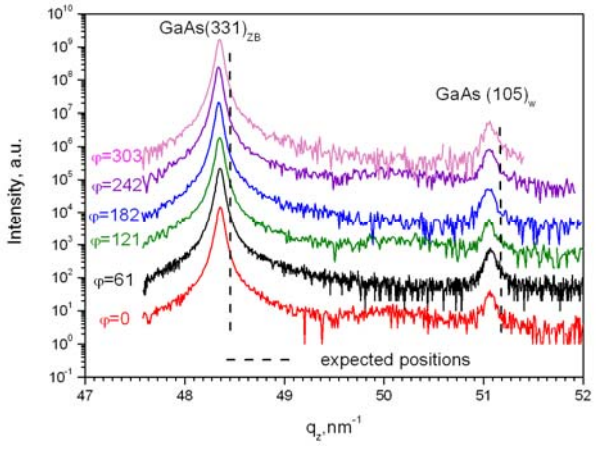

Fig.2 Asymmetric diffraction curve measured in different azimuth positions from 1800s sample

expected qz position. Appearance of both zb and wurzite reflection reveals the existence of stacking faults. The hexagonal symmetry of wurtzite structure was verified by recording the (105) reflection in six azimuth positions appearing with same intensity. In addition we

observed the 331 reflection at six azimuth positions as well. Because zb symmetry would require 120 degree rotational symmetry the existence of six peaks with almost same intensity refers to the existence of so called rotational twins, i.e. zb phases which 60° azimuth twinning against each other.

By comparison of reflection positions receiving from experimental result and theoretical calculations we may estimate strains in sample. For GaAs (331) lattice mismatch equal to 0.11%, for wurtzite GaAs (105) it is 0.75% with respect to bulk GaAs.

References

[1] J. Fan, P.Werner and M. Zacharias Small 2, No 6, (2006) 700-717
[2] J. Noborisaka, J. Motohisa and T. Fukui, Appl. Phys. Lett. 86 (2005)), 2903
[3] J. Bauer, U. Pietsch, A. Davydok, A. Biermanns, J. Grenzer, V. Gottschalch, G. Wagner, Appl. Phys. A 96(2009), 851-859

Phase separation and nanocrystal formation in GeO_x

Christoph J. Sahle*,[a], Christian Sternemann[a], Achim Hohl[b], Heiko Conrad[a,c], Alexej Herdt[a,d], Omid M. Feroughi[a,e], Ralph Wagner[f], Dirk Lützenkirchen-Hecht[f], Arto Sakko[g], Ronald Frahm[f], Keijo Hämäläinen[g], and Metin Tolan[a]

[a] *Fakultät Physik/DELTA, TU Dortmund, Maria-Goeppert-Mayer-Str. 2, 44221 Dortmund, Germany,* [b] *Institute for Materials Science, Darmstadt University of Technology, 64287 Darmstadt, Germany,* [c] *HAYSLAB at DESY, Notkestrasse 85, 22607 Hamburg (Germany),* [d] *Institut für Festkörperforschung Forschungszentrum Jülich, 52425 Jülich, Germany,* [e] *Lehrstuhl für Werkstofftechnologie, TU Dortmund, Leonhard-Euler-Str. 2, 44227 Dortmund, Germany,* [f] *Fachgruppe Physik, Bergische Universität Wuppertal, 42097 Wuppertal, Germany,* [g] *Department of Physics, POB 64, FIN-00014 University of Helsinki, Finland*

*email: christoph.sahle@tu-dortmund.de

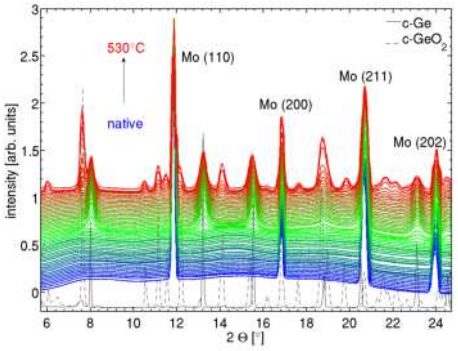

Figure 1: XRD patterns of the *in situ* annealed a-GeO sample E; poly–crystalline Ge (solid line) and GeO_2 (dashed line) reference spectra.

The temperature–induced phase separation, i.e. the disproportionation of GeO into Ge and GeO_2, and the formation of Ge nanocrystals (NC) in bulk amorphous germanium monoxide (a–GeO_x, $x \approx 1$) are studied both *in situ* and *ex situ* by measurements of the x–ray absorption near–edge structure (XANES) at the Ge K–edge and x–ray diffraction (XRD). The studies have been carried out at DELTA beamlines BL8 and BL9. The results provide important information for the production of Ge nanocrystals embedded in amorphous oxide matrices. Oxide matrix embedded Ge or Si nanocrystals belong to a class of materials that has attracted much attention in recent years due to the unique (opto–) electronic properties they inhere. [1, 2, 3] Some of these properties are: visible photoluminescence from oxide matrix embedded Ge NC [4] which is valuable for highly efficient photoluminescent devices and high charge retention properties important for advanced non–volatile flash memories. [5] Bulk amorphous GeO_x ($x \approx 1$) shows a temperature–induced phase separation [6, 7] and can thus be used as a starting material for the production of Ge nanocrystals.

Amorphous GeO was synthesized as described in Ref. [7]. Several series of samples annealed *ex situ* (Series A and series of samples taken from Ref. [7]) and samples annealed *in situ* (samples B, C, D, E) were measured. The samples were treated as described in detail in Ref. [8].

All samples were characterized by XRD in their native and annealed state at the DELTA multipurpose beamline BL9. [9] The results of an *in situ* XRD study of a-GeO (sample E) are shown in Figure 1, exemplarily. The sample in its native state clearly has an amorphous structure, Bragg reflections observed for temperatures below 470 ± 20 °C can be assigned to the metallic molybdenum sample substrate. The formation of Ge NCs sets in for annealing temperatures above 470 ± 20 °C and the peak widths of the Ge reflections yield a mean NC size of $d = 3 \pm 1$ nm. Further annealing also leads to the crystallization of GeO_2. As a reference the XRD patterns of polycrystalline Ge and GeO_2 reference samples are also shown in Figure 1.

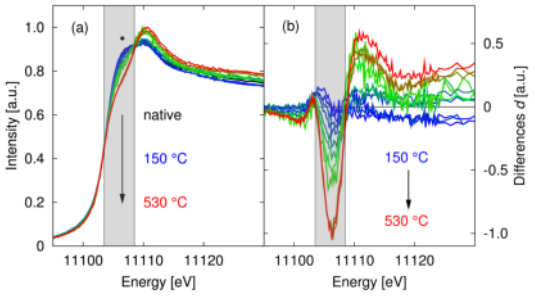

Figure 2: (a) Ge K–edge of the native and differently annealed a-GeO sample B. The spectral features related to the sub–oxide content in the samples are shaded grey. (b) Differences d between the annealed and the native sample.

The disproportionation (GeO → Ge + GeO_2) was studied at the materials science beamline BL8 of DELTA [10] using XANES spectroscopy at the Ge K–edge. The incident energy was scanned between 10988 and 11148 eV and the fluorescence yield was detected by an Amptek XR–100CR Si–pin detector under an angle of 90° suppressing elastic and Compton scattering. XANES spectra of the Ge K–edge of the native and *in situ* annealed a–GeO sample B are shown in Figure 2 (a), exemplarily. The strong shoulder (shaded area in Figgure 2 (a)) in the spectrum of the native sample can be attributed to the sub–oxides and clearly looses spectral weight with increasing annealing temperature and is even more prominent in the differences d of the spectra of the differently annealed and native sample, hence Figure 2 (b). To quantify the phase separation (disproportionation), the energy integral

$$A(T) = \int_{E_1}^{E_2} \mid I_{annealed} - I_{native} \mid dE \tag{1}$$

of the spectral differences d in the energy region between $E_1 = 11103.5$ eV and $E_2 = 11108.5$ eV is calculated and corresponding results are shown in Figure 3. From these results a start and endpoint of the phase separation can be estimated to 260 ± 20 °C and 450 ± 18 °C, respectively.

In order to measure the time dependence of the phase separation, sample D was annealed *in situ* at $T = 530$ °C and XANES scans were performed continually at 7 minutes intervals. The inset of Figure 3 shows this time dependence in terms of the phase separation parameter A vs. the annealing time. Structural changes are evident only within the first 20 minutes of heat exposure.

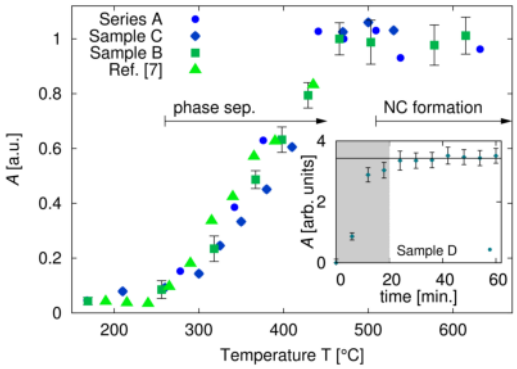

Figure 3: Phase separation parameter $A(T)$ of different sample series.

XRD and XANES data provide a complete picture of the phase separation and nanocrystal formation processes in GeO_x with $x \approx 1$. Temperature treatment of a–GeO leads to a disproportionation and results in the formation of oxide matrix embedded Ge nanocrystals of a few nm in diameter. The different crystallization temperatures of Ge and GeO_2 allow the production of Ge nanocrystals of tunable size embedded in an amorphous oxide matrix. The phase separation is almost completed after 20 minutes of heat exposure. These findings are important for the production of highly efficient (opto–) electronic devices such as light emitting diodes and non–volatile flash memory.

The authors would like to acknowledge the DELTA machine group for providing synchrotron radiation and Prof. H. Fuess (TU Darmstadt) for supporting the sample production. This work was supported by DAAD (313-PPP-SF/08-IK and 1127504), DFG (TO 169/14-1) and the Academy of Finland (1110571, 1127462).

References

[1] S.S. Iyer and Y.-H. Xie, *Science* **260**, 40 (1993).

[2] L. Pavesi, L. Dal Negro, C. Mazzoleni, G. Franzo, and F. Priolo, *Nature* **408**, 440 (2000).

[3] K.D. Hirschmann, L. Tsybeskov, S.P. Duttagupta, P.M. Fauchet, *Nature* **384**, 338 (1996).

[4] Y. Maeda, N. Tsukamoto, Y. Yazawa, Y. Kanemitsu and Y. Masumoto, *Appl. Phys. Lett.* **59**, 3168 (1991).

[5] Y. Batra, D. Kabiraj, D. Kanjilal, *Solid State Comm.* **143**, 213 (2007).

[6] A.V. Kolobov, S.Q. Wei, W.S. Yan, H. Oyanagi, Y. Maeda, and K. Tanaka, *Phys. Rev. B* **67**, 195314 (2003).

[7] A. Schacht, C. Sternemann, A. Hohl, H. Sternemann, Ch. Sahle, M. Paulus, and M. Tolan, *J. Non-Cryst. Solids* **355**, 1285 (2009).

[8] Ch.J. Sahle, C. Sternemann, H. Conrad, A. Herdt, O.M. Feroughi, M. Tolan, A. Hohl, R. Wagner, D. Lützenkirchen–Hecht, R. Frahm, A. Sakko, and K. Hämäläinen, *Appl. Phys. Lett.* **95**, 021910 (2009).

[9] C. Krywka, C. Sternemann, M. Paulus, N. Javid, R. Winter, A. Al-Sawalmih, S. Yi, D. Raabe, and M. Tolan, *J. Synchrotron Rad.* **14**, 244 (2007).

[10] D. Lützenkirchen-Hecht, R. Wagner, U. Haake, A. Watenphul, R. Frahm, *J. Synchrotron Rad.* **16**, 264 (2009).

Structural changes of a metal-organic framework under temperature load

D.C. Florian Wieland*,[a], Osama Shekhah[b], Martin A. Schroer[a], Michael Paulus[a], Christian Sternemann[a], Metin Tolan[a], and Christof Wöll[b]

[a] *Fakultät Physik/DELTA, TU Dortmund, 44221 Dortmund Germany,*

[b] *Physikalische Chemie, Ruhr-Universität Bochum, Universitätsstrasse 150 44780 Bochum Germany*

*email: florian.wieland@tu-dortmund.de

In recent years the class of metal-organic frameworks (MOFs) has attracted much attention due to their high porosity and tunable coordination space which makes them interesting candidates for applications in the field of gas storage, gas sensing or gas separation. These zeolithe type structures are composed of organic ligands held together by inorganic junctions. Thus the directed modification of the network properties on a molecular level by the exchange and variation of single components can be achieved. [1]

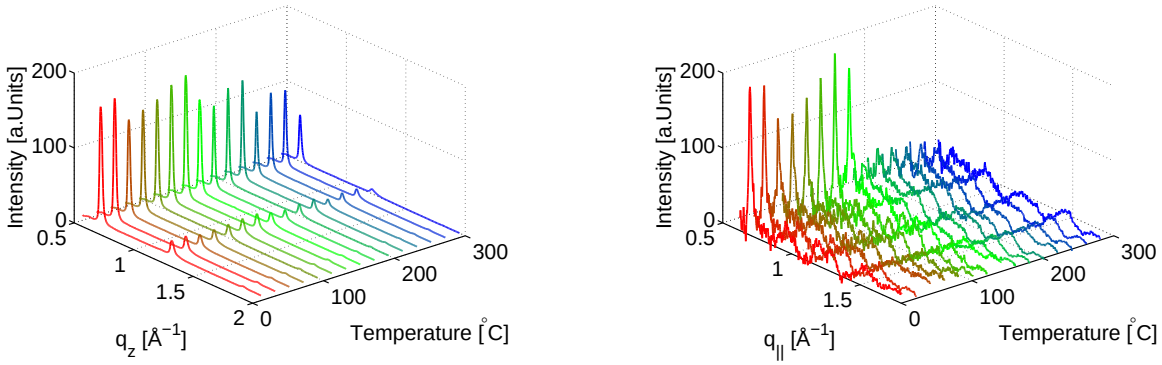

Figure 1: Out-of-plane x-ray diffraction spectra of CuBDC at different temperatures (*left*). In-plane x-ray diffraction spectra of CuBDC at different temperatures (*right*).

These networks can be chemically connected to surfaces like silicon, silicondioxid and aluminium to fabricate so called surface MOFs (SurMOFs). This composite material offers unique opportunities to engineer new gas selective membranes, gas sensors or to grow defined structures on top of surfaces for miscellaneous applications. [2] An important key component for such applications is the ability to grow highly ordered films of controlled thickness and high crystallinity. One potential synthesis route to assemble such films is the production protocol developed by Wöll et. al..[3] This protocol uses a highly ordered self-assembled mono-layer which serves as a two-dimensional nucleation site. In the ongoing synthesis process the MOF is deposited in a step-by-step fashion resulting in a layer like growth. Following this synthesis protocol it was possible to fabricate a complete new SurMOF structure which has no corresponding bulk phase. This SurMOF structure CuBDC consists of benzendicarboxylic acid joined by copper atoms. Up to now the three dimensional structure is not known. The sample was grown on a gold covered silicon wafer covered by a self-assembled mono layer (16-mercaptohexadecanoic acid ($HS(CH_2)_{15}COOH$)). In the following the wafer was alternatingly flushed with a solution of benzendicarboxylic acid and copper acetat solved in ethanol resulting in a crystalline growth.

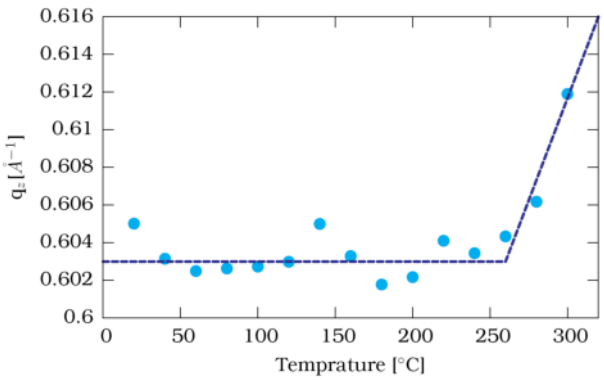

Figure 2: Position of the first out-of-plane reflection as function of the temperature.

In order to characterize structural changes of CuBDC induced by heat load x-ray diffraction measurements at different temperatures were performed. The measurements were carried out at the multi-purpose beamline BL9 using the two-dimensional MAR345 detector. [4]

The experiment was performed under vacuum at a pressure of P=10^{-1}Pa in the temprature range from RT to T=300°C. The scattering patterns were analyzed for different scattering planes using the program package FIT2D. The out-of-plane spectrum, which gives information about the structure perpendicular to the surface and the in-plane spectrum, which is determined by the lateral structure, are shown in Figure 1 as a function of temperature. The out-of-plane spectrum shows two reflections while the in-plane spectrum shows just one. The in-plane reflection vanishes at a temperature of T=160°C. For a more detailed analysis the position of the first out-of-plane reflection is plotted as a function of the temperature in Figure 2. The data shows that at a temperature of T=300°C the diffraction peak shifts with higher temprature to higher q values which indicates a shrinking of the lattice constant perpendicular to the surface.

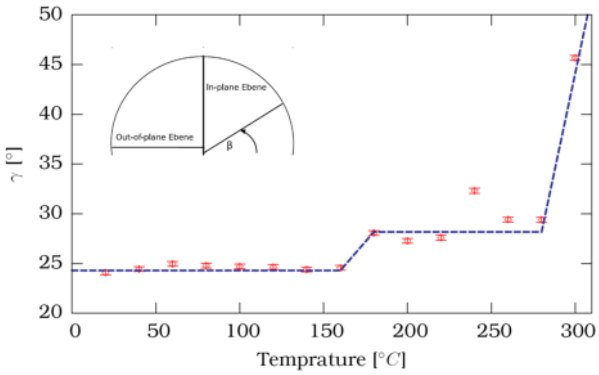

Figure 3: Full width of half maxiumum γ of the first out-of-plane reflection in the direction of β as function of the temperature (lines are guides to the eye).

To obtain information about changes in the ordering of the film the scattering data was analyzed along the azimuthal angle β and Gaussian functions were fitted to the data in order to obtain the full width of half maximum γ of the maxima, see Figure 3.

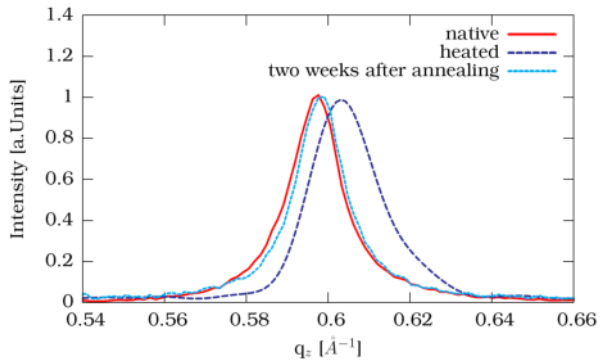

Figure 4: Out-of-plane diffraction pattern of the sample at different states (lines are guides to the eye).

The data shows two jumps, one at a temperature of T=160°C and a second at a temperature of T=300°C. Combining this information with the scattering information of the in-plane spectra it seems that the SurMOF crystallites undergo a distortion process regarding the degree of orientation due to heating. The measurements were stopped at a temperature of T=300°C. Higher tempratures could nit be achieved using the sample cell. At a temperature of T=300°C the sample still shows Bragg reflections indicating a stable crystalline network.

After heating the sample was stored at ambient conditions. After a period of two weeks again a scattering pattern was recorded. The out-of-plane signals of the native sample, the heated sample and the heated sample after two week are shown in Figure 4. The spectra clearly show that the SurMOF network relaxes to its former lattice constants. The observed effect of this reversible change of the lattice constant can be explained by the interaction of guest molecules in the network which has also be observed by other MOF networks. [5] Due to the temperature rise molecules stored by the network desorb which leads to a contraction of the unit cell. By storing the MOF under ambient conditions molecules are resorbed which leads to the relaxation of the network.

References

[1] M. O'Keeffe, M. Eddaoudi, H. Li, T. Reineke, and O.M. Yaghi *J. of Sol. St. Chem.* **152**, 3 (2000).

[2] O. Shekhah, H. Wang, S. Kowarik, F. Schreiber, M. Paulus, M. Tolan, C. Sternemann, F. Evers, D. Zacher, R.A. Fischer, and C. Wöll, *J. Am. Chem. Soc.* **131**, 15118 (2007).

[3] S. Hermes, F. Schröder, R. Chelmowski, C. Wöll, and R.A. Fischer, *J. Am. Chem. Soc.* **127** , 13744 (2005).

[4] C. Krywka, C. Sternemann, M. Paulus,N. Javid, R. Winter, A. Al-Sawalmih, S. Yi, D. Raabe, and M. Tolan, *J. Synchrotron Rad.* **14**, 244 (2007).

[5] P. Llewellyn, G. Maurin, T. Devic, S. Loera-Serna, N. Rosenbach, C. Serre, S. Bourrelly, P. Horcajada, Y. Filinchuk, and G. Ferey, *J. Am. Chem. Soc.* **130**, 12808 (2008).

The Structure of Protein Adsorbates Affected by Short- and Long-Range Forces Studied by X-Ray Reflectivity

Hendrik Hähl[a], Florian Evers[b], Michael Paulus[b], Anne K. Hüsecken[b], Thorsten Brenner[b], Christian Sternemann[b], Samuel Grandthyll[a], Metin Tolan[b] and Karin Jacobs*,[a]
[a] *Experimentalphysik, Universität des Saarlandes, D-66041 Saarbrücken,*
[b] *Fakultät Physik/DELTA, TU Dortmund, D-44221 Dortmund*

*email: k.jacobs@physik.uni-saarland.de

Introduction

Protein adsorption onto solid surfaces plays a central role in numerous processes in medicine, biotechnology and daily life [1]. Recent studies have shown that the substrate strongly influences the enzymatic activity of adsorbed proteins, its orientation on the surface and the kinetics of the adsorption process [2, 3]. The latter studies revealed that already slight changes in the substrate's subsurface composition influence the kinetics of protein adsorption.

Proteins tend to adsorb spontaneously on almost all solid surfaces. Many parameters influence this adsorption process, e.g., pH value, ionic strength, temperature and protein concentration [1, 3, 4, 5]. In the majority of studies, the influence of the substrate on the adsorption is described by the sign and strength of the surface charge, the roughness of the surface and the surface free energy, i.e. the chemical composition of the surface. However, the influence of the bulk substrate should not be neglected, as van der Waals forces range over tens of nanometers, depending on the geometry of the interacting objects. It could already be shown that van der Waals forces govern the stability of thin polymer films [6]. Moreover, it could be demonstrated that the adsorption kinetics of large, deformable proteins is affected by different van der Waals forces [2, 3]. Hence, we hypothesize that the final state of adsorbed protein films might alter (e.g. in protein orientation or conformation) with different subsurface compositions.

In this study, we applied X-ray reflectivity in order to investigate the structure of adsorbed α-amylase and BSA under variation of short- and long-range forces.

Experiments and Results

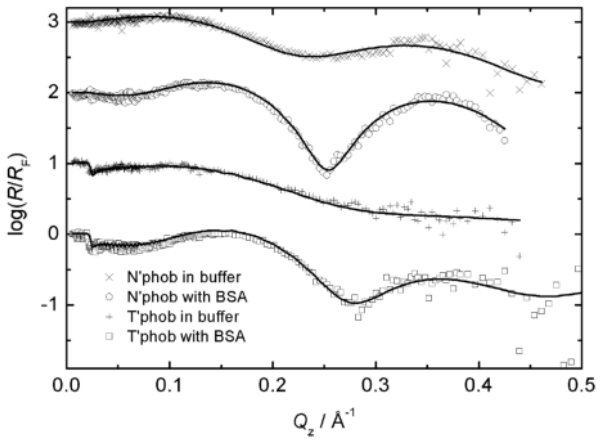

Figure 1: X-ray reflectivity data (symbols) and refinements (solid lines) of the hydrophobic model surfaces with native (N'phob) and thick (T'phob) oxide layers. To emphasize the effect of adsorbed proteins on the reflectivity curves, data of the pure model surface in buffer and in the presence of a protein (BSA) solution are shown.

We used silicon wafers with a natural silicon oxide layer of 1.7(3) nm (Wacker Siltronic AG, Burghausen, Germany) and wafers with a thermally grown amorphous silicon oxide layer, exhibiting a thickness of 151(1) nm (Silchem, Freiberg, Germany) as characterized by ellipsometry. The wafers were cleaned in piranha solution and became hydrophilic with a contact angle of less than 5°. Moreover, wafers could be covered with a self-assembled monolayer of octadecyltrichlorosilane (OTS). After this treatment, the substrates exhibit hydrophobic surfaces with water contact angles of 107° and 112° for receding and advancing contact angles respectively. Thus, a set of four different model substrates was obtained: hydrophilic and hydrophobic wafers (abbreviated as "phil" and "phob", respectively) with either a thin (called "N" for native) or a thick (called "T") amorphous silicon oxide layer. BSA and α-amylase were used as model proteins. They were dissolved in 10 mM phosphate buffer with a pH of 7. Wafers and protein solution were placed in a teflon sample cell with a protein concentration of 0.1 mg/ml. Reflectivity measurements were carried out on the beamline BL9 at the DELTA synchrotron light source with the X-ray reflectivity set-up in a θ-2θ geometry and a photon energy of 27 keV optimized to access solid-liquid interfaces [7]. As previous studies have shown [4, 5], this methodology is well-suited for the study of adsorbed protein films at solid-liquid interfaces.

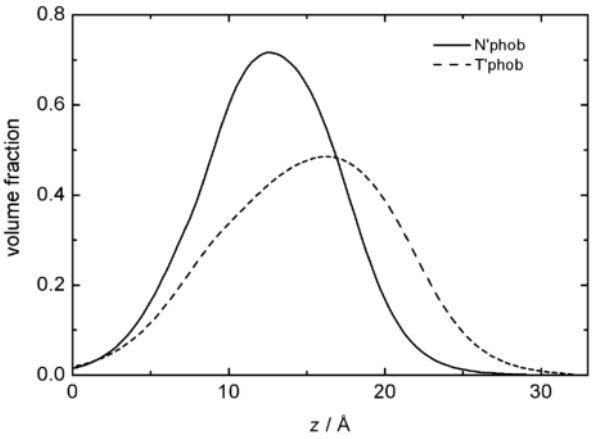

Figure 2: Volume fraction profiles of BSA adsorbed at the N'phob and T'phob substrates as obtained by analyzing the reflectivity data shown in Figure 1.

Figure 1 shows X-ray reflectivity measurements of the adsorption of BSA at the hydrophobic OTS-water interface (N'phob and T'phob) as an example. We present data with and without protein in the buffer solution in order to highlight the alteration of the reflectivity curve in the presence of a protein adsorbate. The reference measurements characterizing the OTS-water interface are well in line with previous studies [8] regarding the structure of the OTS layers. These results indicate that these well-prepared model substrates are ideally suited to study protein interfacial affinity [9]. The presence of the adsorbed biofilm is indicated by an increase in the oscillation amplitude of the Kiessig fringes. The data could be modelled using a layer model (Si/SiO_2/OTS-head/OTS-tail/hydrophobic gap/adsorbate/solution). A dense, thin adsorbed layer at hydrophobic interfaces is observed in the volume fraction profiles displayed in Figure 2. By integrating the volume fraction profiles [5], adsorbed amounts of $1.1(2)\,\mathrm{mg/m^2}$ (for N'phob) and $1.0(2)\,\mathrm{mg/m^2}$ (for T'phob) are obtained. Furthermore, the protein adsorbate is thinner and exhibits a higher peak volume fraction at the N'phob surface as compared to the T'phob surface. The volume fraction profiles reveal a clear effect of subsurface composition on protein interfacial structure due to an alteration of protein-surface interactions. Similar trends were observed for α-amylase and at the silica-water interface. The bare silica, however, yields only low contrast towards the proteins used in this study. Further measurements with proteins of different electron densities might solve this problem.

Conclusion

By using X-ray reflectivity, the structure of protein films has been analyzed on a set of substrates allowing for separate change of short- and long-range forces acting between substrate and proteins. Thus, the effect of subsurfaces changes of the substrates composition on the structure of protein films could be detected. Protein films interacting with the silicon through a thin silicon oxide layer are thinner and denser than the films on thick silicon oxide. The observation of the effect of subsurface changes corroborates the results from *in situ* adsorption kinetics studies [2, 3] and confirms the conjectures about different film structures made therein. To further clarify the origin of this subsurface influence, additional measurements at DELTA, complementary to already existing *in situ*-experiments, are needed.

Acknowledgments

The DELTA machine group is gratefully acknowledged for providing synchrotron radiation and technical support. We would like to thank the Bundesministerium für Bildung und Forschung and the Deutsche Forschungsgemeinschaft for financial support under grant number GRK 1276 and GRK 532.

References

[1] C. Czeslik, *Z. Phys. Chem.* **218**, 771 (2004).

[2] A. Quinn et al., *Europhysics Letters* **81**, 56003 (2008).

[3] M. Bellion et al., *J. Phys.: Condens. Mat.* **20**, 404226 (2008).

[4] F. Evers et al., *Langmuir* **24**, 10216 (2008).

[5] F. Evers et al., *Eur. Phys. J. Spec. Top.* **167**, 185 (2009).

[6] R. Seemann et al., *Phys. Rev. Lett.* **86**, 5534 (2001).

[7] M. Paulus et al., *J. Synchrotron Rad.*. **15**, 600 (2008).

[8] M. Mezger et al., *Proc. Natl. Acad. Sci.* **103**, 18401 (2006).

[9] G. Fragneto-Cusani, *J. Phys.: Condens. Mat.* **13**, 4973 (2001).

Effect of Non-Ionic Cosolvents on Protein Adsorption Studied by X-Ray Reflectivity

Florian Evers*,[a], Anne K. Hüsecken[a], Thorsten Brenner[a], Christian Sternemann[a], Christoph Jeworrek[b], Metin Tolan[a] and Claus Czeslik[b]
[a] *Fakultät Physik/DELTA, TU Dortmund, D-44221 Dortmund,*
[b] *Fakultät Chemie, TU Dortmund, D-44221 Dortmund*

*email: florian.evers@tu-dortmund.de

Introduction

In a biological cell, crowding and confinement as well as cosolvents and interfaces may alter the stability, structure and function of proteins [1, 2]. It is common to classify cosolvents in two groups regarding their effect on protein structure: protein-stabilizing cosolvents, such as SO_4^{2-} and glycerol, are called kosmotropes, protein-destabilizing cosolvents, such as guanidinium, SCN^- and urea, are called chaotropes or denaturants. Many studies deal with the structural and thermodynamic effects of cosolvents on proteins in solution [1, 3]; however, their effect on protein adsorption remains largely unexplored.

In previous studies, we have performed first experiments on the effects of ionic and non-ionic cosolvents on the adsorption of ribonuclease A (RNase) at a hydrophilic silica-water and a hydrophobic poly(styrene)-water interface using optical and neutron reflectometry [4, 5]. In the presence of both the kosmotropic glycerol and the chaotropic urea, less RNase is adsorbing at both interfaces. Furthermore, no change in the adsorbate layer thickness could be detected. One may argue that proteins become preferentially hydrated in the presence of kosmotropic cosolvents [1], thereby disfavoring conformational changes at the interface, whereas chaotropic cosolvents are accumulated at the protein surface and weaken hydrophobic protein-substrate interactions [2].

In this study, we applied X-ray reflectivity (XRR) in order to investigate the details of the adsorbate structure of RNase at the silica-water interface in the presence of non-ionic cosolvents.

Experiments and Results

RNase (Sigma, R5500), glycerol (Sigma, G6279), and urea (Merck, 1.08488) were used as received. Protein solutions were prepared by dissolving RNase in a 10 mM phosphate buffer ($H_2PO_4^-$/ HPO_4^{2-}) adjusted to pH 7.0. The protein concentration was 0.1 mg mL^{-1} in the absence and the presence of cosolvents. Cosolvent concentrations of 2 M and 5 M were used. Silicon wafers were kindly provided by Wacker Siltronic. They were cut into pieces of 18×18.8 mm^2 and cleaned with piranha solution. Hydrophilic wafers were put into the sample cell [6], which was mounted on the diffractometer. All reflectivity measurements were performed at room temperature (22°C) and after an equilibration time of at least 1 h. Reflectivity measurements were

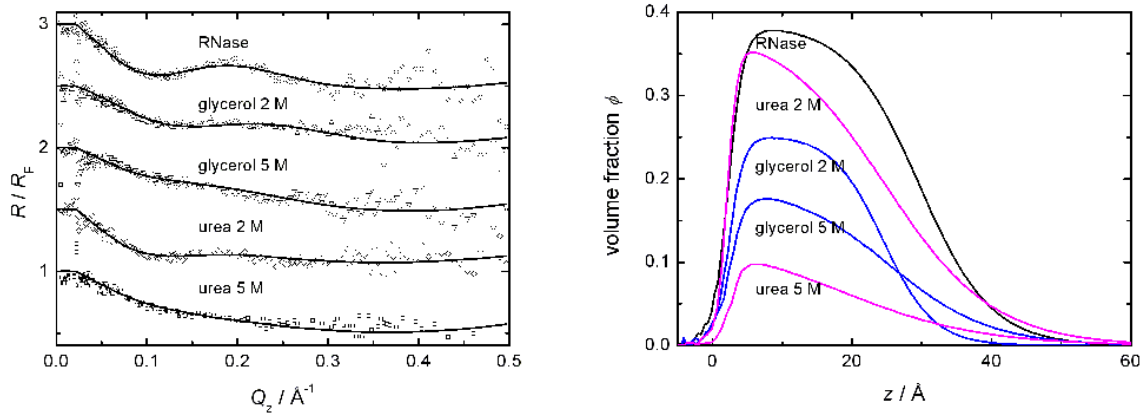

Figure 1: (Left) XRR data (symbols) and refinements (solid lines) of RNase adsorbed at the silica-water interface in the presence of glycerol and urea. (Right) Volume fraction profiles of RNase adsorbed at the hydrophilic silica-water interface as obtained by analyzing the reflectivity data.

carried out on the beamline BL9 at the synchrotron light source DELTA with the XRR set-up in a θ-2θ geometry and a photon energy of 27 keV optimized to access solid-liquid interfaces [6]. We have recently shown

[7, 8] that this methodology is well-suited for the study of adsorbed protein films at solid-liquid interfaces. XRR measurements on the adsorption of RNase at the silica-water interface in the presence of glycerol and urea are presented in Figure 1. The presence of a protein adsorbate is indicated by Kiessig oscillations. Upon addition of glycerol or urea, the amplitude of the Kiessig oscillation decreases hinting at a lower electron density contrast and thus at a reduced volume fraction of the adsorbed layer. The reflectivity curves are simulated using a layer model (Si / SiO_2 / adsorbate / solution). Thus, electron density profiles and volume fraction profiles, $\phi(z)$, of the adsorbed layer can be obtained [7, 8] (Figure 1). The adsorbed amount, Γ, can be calculated from the integral of $\phi(z)$; the values for Γ are listed in Table 1.

	Γ [mg/m^2]
w/o. cosolvent	1.5
glycerol 2M	0.8
glycerol 5M	0.6
urea 2M	1.3
urea 5M	0.3

Table 1: Adsorbed amount as a function of cosolvent content. The error of Γ is estimated to be ± 0.2 mg/m^2.

From the thickness of the adsorbed layers, it can be concluded that RNase forms a monolayer under all conditions studied. Therefore, one can assume that RNase maintains most of its tertiary structure during the adsorption at the silica-water interface – even in the presence of denaturing urea. Both the volume fraction profiles and the values of the adsorbed amount reveal reduced adsorption in the presence of non-ionic cosolvents. Thus, the reduced interfacial affinity of RNase in the presence of these cosolvents as observed by optical and neutron reflectivity [4] is confirmed, although the values of Γ deduced from the X-ray data are lower. Due to the low electron density contrast of the adsorbate, data analysis must be performed with high care and the values of Γ might be underestimated. However, the large range of momentum transfer accessible in XRR leads to detailed volume fraction profiles in which the roughness to the adjacent layers is account for as well. In this regard, XRR measurements bear advantages over similar neutron scattering studies.

The shape of the volume fraction profiles in Figure 1 suggests a compact protein conformation of the adsorbed layer in the absence of any cosolvent and in the presence of 2 M glycerol, whereas the adsorbed layer has a long, rough tail protruding into the subphase in the presence of 2 M urea. Hence, further evidence for the different mechanisms of protein-cosolvent interaction discussed above and their influence on protein adsorption behaviour is given. In the presence of high cosolvent concentrations, the volume fraction and the adsorbed amount are further reduced hinting at a loosely packed adsorbate. Further data on cosolvent-mediated protein adsorption are presented in the report by A. K. Hüsecken et al.

Conclusion

In summary, we present XRR measurements characterizing the interfacial structure of RNase adsorbed at the silica-water interface in the presence of the non-ionic cosolvents glycerol and urea. The data analysis provides further evidence for a reduced adsorbed amount in the presence of non-ionic cosolvents and the volume fraction profiles hint at different mechanisms underlying the similar effects of glycerol and urea. The effect of reduced adsorption in the presence of cosolvents is well in line with previous neutron scattering studies.

Acknowledgments

The DELTA machine group is gratefully acknowledged for providing synchrotron radiation and technical support. We would like to thank the Bundesministerium für Bildung und Forschung and the Deutsche Forschungsgemeinschaft for financial support.

References

[1] S. N. Timasheff, *Annu. Rev. Biophys. Biomol. Struct.* **22**, 67 (1993).

[2] X. Chen, L. B. Sagle, P. S. Cremer, *J. Am. Chem. Soc.* **129**, 15104 (2007).

[3] H. Herberhold, C. A. Royer, R. Winter, *Biochemistry* **43**, 3336 (2004).

[4] J. Koo, T. Gutberlet, C. Czeslik, *J. Phys. Chem. B* **112**, 6292 (2008).

[5] F. Evers, R. Steitz, M. Tolan, C. Czeslik *J. Phys. Chem. B* **113**, 8462 (2009).

[6] M. Paulus, D. Lietz, C. Sternemann, K. Shokuie, F. Evers, M. Tolan, C. Czeslik, R. Winter, *J. Synchrotron Rad.*. **15**, 600 (2008).

[7] F. Evers, K. Shokuie, M. Paulus, C. Sternemann, C. Czeslik, M. Tolan, *Langmuir* **24**, 10216 (2008).

[8] F. Evers, K. Shokuie, M. Paulus, S. Tiemeyer, C. Sternemann, C. Czeslik, M. Tolan, *Eur. Phys. J. Spec. Top.* **167**, 185 (2009).

Ultrathin Co films on glass studied by MOKE, XRR and XRD using the 2D-MAR-detector

Timo Kuschel[1], Tobias Becker[1], Daniel Bruns[1], Martin Suendorf[1], Florian Bertram[2], Christian Sternemann[3], Michael Paulus[3], Lars Böwer[3] and Joachim Wollschläger[1]

[1] *Fachbereich Physik, Universität Osnabrück, Barbarastr. 7, D-49069 Osnabrück*
[2] *HASYLAB at DESY, Notkestrasse 85, D-22607 Hamburg*
[3] *DELTA, Technische Universität Dortmund, Maria-Goeppert-Mayer-Str. 2, D-44227 Dortmund*

In order to study the behavior of ultrathin ferromagnetic films, amorphous and polycrystalline Co films on glass are analyzed. Thinner films (thickness < 30 nm) are assembled by Molecular Beam Epitaxy (MBE) under UHV conditions at the Universität Osnabrück and capped by amorphous silicon to avoid oxidation after leaving the UHV chamber. The thicker ones are provided by the group of Prof. Dr. Paul Fumagalli from the Freie Universität Berlin and are uncapped. The magnetic properties are investigated by Magneto Optical Kerr-Effekt (MOKE) at the Universität Osnabrück, whereas the structural characterization included X-Ray Reflectivity (XRR) and X-Ray Diffraction (XRD) measurements at BL9 at DELTA using a NaI-detector and a 2D-MAR-detector respectively. The photon energy was 15.5 keV.

The magnetization curves of the MOKE measurements show magnetic easy and hard in-plane axes (figure 1a). After plotting the magnetic remanence M_{R} against the azimuthal sample angle Φ, an in-plane two-fold magnetic anisotropy is examined in all Co films (figure 1b) as already reported before [1]. The direction of the magnetic easy axis differ for each sample and can not be correlated to film thicknesses, substrate constitution or preparing conditions [2]. Therefore, we studied the Co films by means of synchrotron radiation to investigate correlations between structure and magnetic properties.

Figure 2 shows the XRR measurement of the thickest investigated Co film. The detected intensity of the reflected light is plotted against the magnitude of the scattering vector q. The analyze tool *i*XRR programmed by Florian Bertram is used for simulating the data [3]. This programm is based on the Parratt algorithm [4]. The data can be fitted using a Co film thickness of 83 nm and a 6 nm oxide film on top due to the missing capping layer. Furthermore 15 and 50 nm Co films were also analyzed.

It has been reported that the crystallite size varies depending on the thickness of the Co films [5]. Different measurements of the diffraction pattern with the 2D-MAR-detector were made to varify this behavior. The incident angle was 0.5°, which is above the critical angle 0.22°. The thinnest film is amorphous, which is pointed out by the missing diffraction rings in figure 3a. In contrast to this the 50 and 83 nm films show rings in the diffraction patterns (figure 3b). This indicates a polycrystalline structure. The integrated intensity of the upper 30° section (limited by the white lines in figure 3a and 3b) is plotted in figure 3c. The scattering angles of the rings fit to the $\{10\bar{1}0\}$, $\{0002\}$ and $\{10\bar{1}1\}$ reflexes of hexagonal Co crystallites. The broad peak is due to the amorphous glass substrate.

In order to test for texture effects as the origin of the magnetic anisotropy, some more measurements with the 2D-MAR-detector were done for different azimuthal sample angles Φ. The analysis of the measurements is still in progress.

Acknowledgements

The author would like to thank Prof. Dr. Paul Fumagalli and his group for providing the uncapped 50 nm and 83 nm Co films.

References

[1] J.B. Wedding et al., J. Magn. Magn. Mater. 204, 79 (1999).
[2] T. Becker, Diplomarbeit, Universität Osnabrück (2008).
[3] F. Bertram, Bachelorarbeit, Universität Osnabrück (2007).
[4] L.G. Parratt, Phys. Rev. 95, 359 (1954).
[5] B. Presa et al., IEEE Trans. Magn. 44, 2788 (2008).

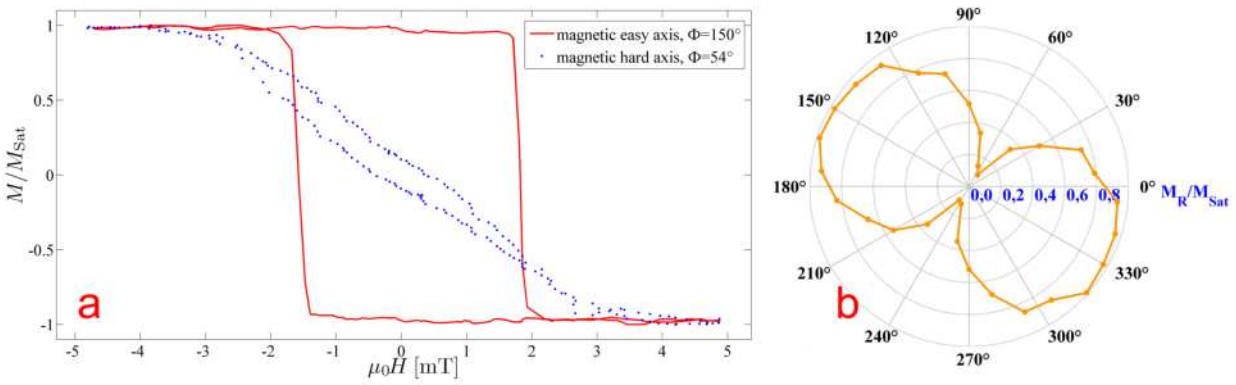

Figure 1: MOKE measurement of 50 nm Co on glass. a: magnetization curve of magnetic easy and hard in-plane axes. b: magnetic remanence plotted against the azimuthal sample angle Φ.

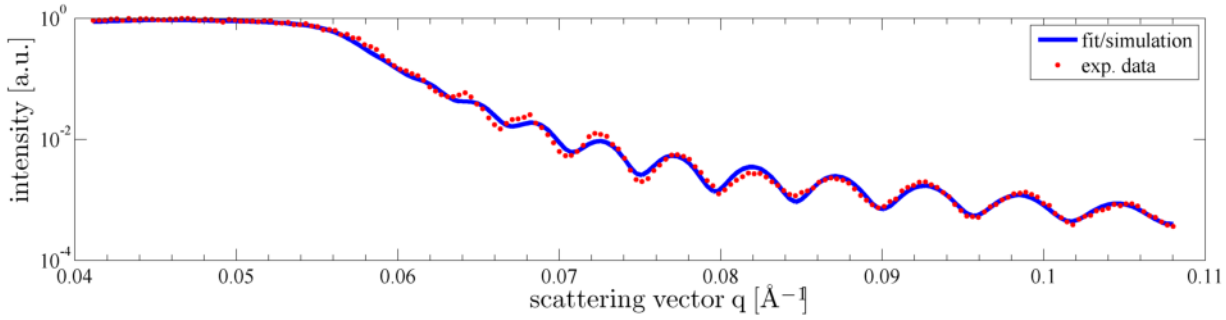

Figure 2: XRR measurement of Co on glass. The simulation curve is due to a model of a 83 nm Co film.

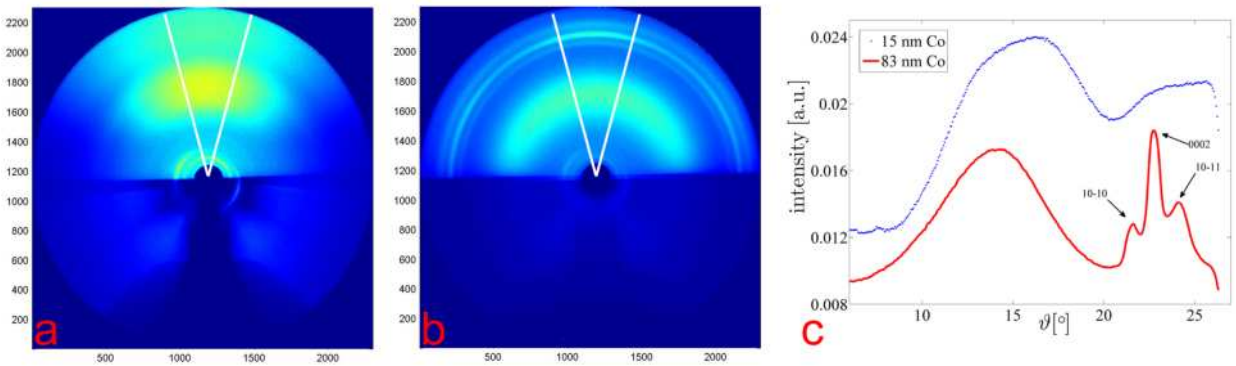

Figure 3: XRD measurement of Co on glass using a 2D-MAR-detector. a: 15 nm Co film. b: 83 nm Co film. c: integrated intensity of the upper 30° section limited by white lines in figure a and b.

Ultrathin Fe films on MgO(001) studied by MOKE, XRR and XRD

Timo Kuschel[1], Hauke Bardenhagen[1], Daniel Bruns[1], Martin Suendorf[1], Bernd Zimmermann[1], Florian Bertram[2], Christian Sternemann[3] and Joachim Wollschläger[1]

[1] *Fachbereich Physik, Universität Osnabrück, Barbarastr. 7, D-49069 Osnabrück*
[2] *HASYLAB at DESY, Notkestrasse 85, D-22607 Hamburg*
[3] *DELTA, Technische Universität Dortmund, Maria-Goeppert-Mayer-Str. 2, D-44227 Dortmund*

In order to study the behavior of ultrathin ferromagnetic films, Fe layers on MgO(001) are assembled by Molecular Beam Epitaxy (MBE) under UHV conditions. Low Energy Electron Diffraction (LEED) and X-Ray Photoelectron Spectroscopy (XPS) was used to check the structure and cleaness. The films are capped by amorphous silicon to avoid oxidation after leaving the UHV chamber. The magnetic properties are investigated by Magneto Optical Kerr-Effekt (MOKE) at the Universität Osnabrück, whereas the structural characterization included X-Ray Reflectivity (XRR) and X-Ray Diffraction (XRD) measurements at BL9 at DELTA. The photon energy was 15.5 keV.

The measured magnetization curves by MOKE show an untypical characteristic as presented in figure 1a. This can be explained by an overlap of linear and quadratic magneto optical Kerr-effects [1]. After plotting the magnetic remanence M_{R} of the linear part against the azimuthal sample angle Φ, an in-plane four-fold magnetic anisotropy is examined in all Fe films (figure 1b). Fe grows in the bcc structure and is 45° rotated in-plane to the rock salt structure of the MgO(001) substrate, so Fe(100) ∥ MgO(110) and Fe(001) ∥ MgO(001) [2]. The four-fold magnetic anisotropy results from the cubic Fe system [3].

Figure 2 shows the XRR measurement of one Fe film. The detected intensity of the reflected light is plotted against the magnitude of the scattering vector q. The analyze tool *i*XRR programmed by Florian Bertram is used for simulating the data [4]. This programm is based on the Parratt algorithm [5]. The data can be fitted using a 5.0 nm Fe film with a roughness of 2 Å. Furthermore Fe films of thicknesses between 1.5 and 12 nm were also analyzed.

XRD measurements were made using ϑ-2ϑ-scans. Thus the 1. and 2. Bragg reflex of MgO as well as the 1. Bragg reflex of Fe can be analyzed for the 00-rod of the reciprocal space. The layer distance of Fe can be calculated by fitting the XRD data as done for the 5.0 nm Fe film for example (figure 3). Here the layer distance is reduced to 2.80 Å compared to the bulk value of 2.87 Å. The FWHM of the Fe peak amounts 0.44° due to a film thickness of 5.3 nm, which is in good agreement to the thickness calculated for the XRR data. Because of the absence of fringes beside the Fe Bragg reflex, the film seems to be very rough. This is contrary to the calculated roughness of the XRR results and has to be analyzed.

Correlations between the quadratic MOKE and the structure of Fe will be examined in the future.

References

[1] K. Postava et al., J. Magn. Magn. Mater. 172, 199 (1997).
[2] J.F. Lawler et al., J. Magn. Magn. Mater. 165, 224 (1997).
[3] J.L. Costa-Krämer et al., J. Magn. Magn. Mater. 210, 341 (2000).
[4] F. Bertram, Bachelorarbeit, Universität Osnabrück (2007).
[5] L.G. Parratt, Phys. Rev. 95, 359 (1954).
[6] H. Bardenhagen, Diplomarbeit, Universität Osnabrück (2009).

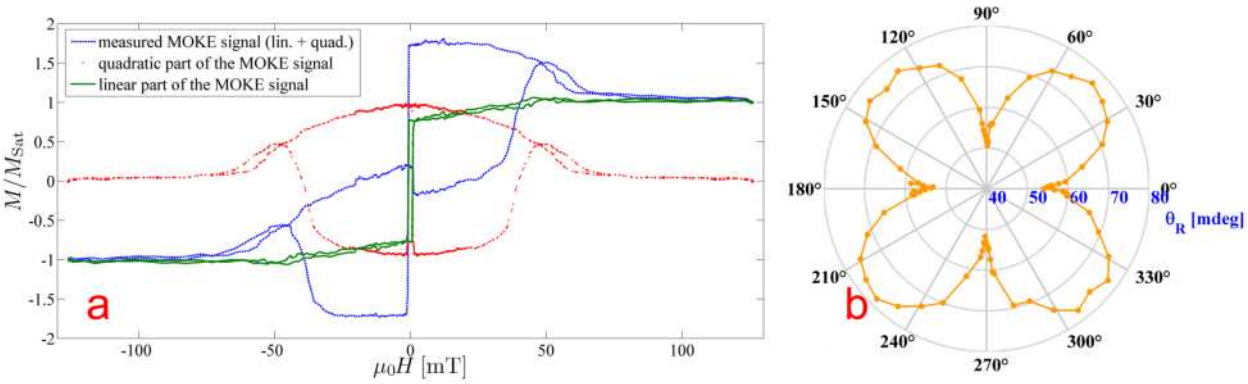

Figure 1: MOKE measurement of 7 nm Fe on MgO(001). a: measured magnetization curve, linear and quadratic part of a magnetic hard in-plane axis. b: magnetic remanence plotted against the azimuthal sample angle Φ[6].

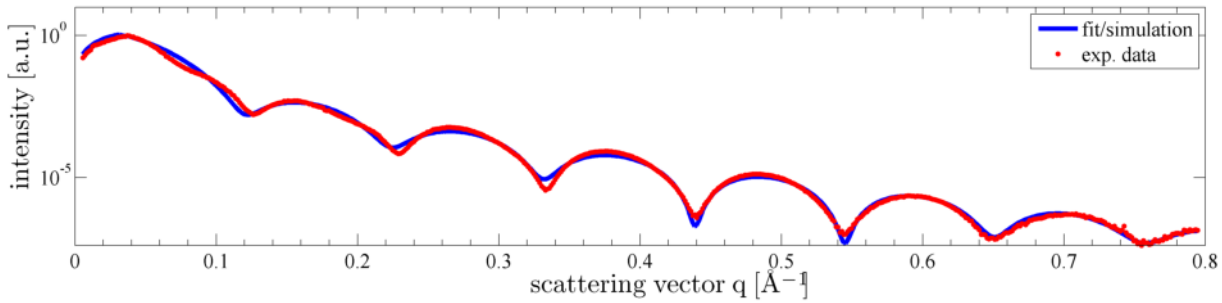

Figure 2: XRR measurement of Fe on MgO(001). The simulation curve is due to a model of a 5.0 nm Fe film.

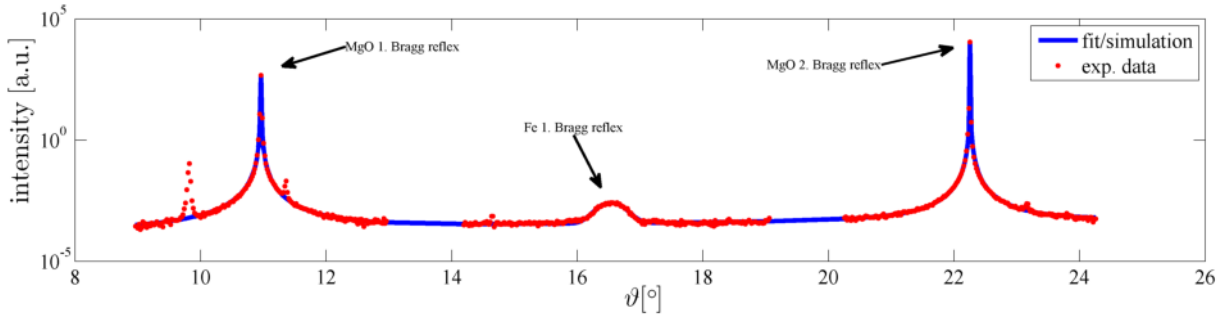

Figure 3: XRD measurement of 5.0 nm Fe on MgO(001). The 1. Bragg reflex of iron is at 16.54°. Therefore the layer distance of iron is 2.80 Å.

Laser-induced strain in InAs/GaAs quantum dots

Sebastian Tiemeyer*,[a], Michael Bombeck[b], Michael Paulus[a], Christian Sternemann[a], D.C. Florian Wieland[a], Manfred Bayer[b], and Metin Tolan[a]
[a] *Fakultät Physik/DELTA, TU Dortmund, D-44221 Dortmund, Germany,* [b] *Experimentelle Physik II, TU Dortmund, D-44221 Dortmund, Germany*

*email: sebastian.tiemeyer@tu-dortmund.de

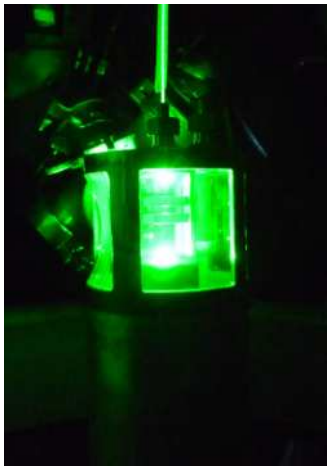

Figure 1: Picture of the in situ cryogenic sample cell. A lense system focused the Nd:YAG laser light on the sample.

Quantum dot heterostructures are a research topic offering both the discovery of principal knowledge in terms of quantum information processing [1] and the development of optoelectronic devices [2]. The confinement of charge carriers to length scales comparable to the de Broglie wavelength in semiconductor heterostructures such as quantum wells and quantum dots leads to a considerable modification of the density of states (DOS). In particular quantum dots represent zero-dimensional structures possessing a DOS similar to that of atoms. Typically, quantum heterostructures feature a size in the nanometer regime demanding investigation methods with an appropriate spatial resolution.
X-rays can easily satisfy these requirements as they exhibit wavelengths between 0.1 Å - 10 Å and thus are perfectly suited to characterize quantum dot heterostructures [3]. Furthermore, X-rays are capable of investigating buried structures [4] allowing in situ measurements of semiconductor devices in operation.
Indium Arsenide (InAs) and Gallium Arsenide (GaAs) exhibit a lattice mismatch of 7% giving rise to strain fields in quantum dot heterostructures. The strain affects significantly the electronic properties of quantum dots e.g. the band structure and gap [5] making so called strain engineered quantum dot devices feasible [6, 7]. Previous X-ray studies have determined the strain distribution in quantum dots and the surrounding crystalline structure (see figure 1) [4, 8]. However, subject to these studies have been passive quantum structures. In the case of excited quantum dots, the injected charge carriers may modify the strain fields and therefore the electronic properties. The lattice distortion by optically excited carriers up to now has been monitored only indirectly by high resolution continuous wave or non-linear time-resolved optical spectroscopy [9–13].
At the beamline BL9 at DELTA [14] we have investigated in situ the laser-induced strain of InAs quantum dots grown on and capped with GaAs by means of high resolution X-ray diffraction (XRD). The measurements were conducted utilizing the 6-circle diffractometer in combination with a 200 mW Nd:YAG @ 532 nm laser system which permits us to excite the quantum dots by laser irradiation. In order to avoid thermal relaxation of the excited quantum dots the sample was cooled down to 15 K by employing an Oxford Instruments closed cycle cryostat. Figure 1 depicts the cryogenic sample cell including a fiber optic and a focusing lense system which ensured the sufficient and homogeneous illumination of the sample. The state of excitation of the quantum dots was detected by photoluminescence spectra.
For the purpose of investigating the structural changes in the quantum dots due to the laser-induced strain, we have collected $\theta - 2\theta$ scans of both the (004) Bragg reflections of InAs and GaAs. Figure 2 shows a comparison between a scan at room temperature with the passive sample (blue line) and a $\theta - 2\theta$ scan under cryogenic conditions including excitation of the quantum dots (red line). As a result of the alloying of InAs and GaAs during the fabrication process of the sample, the $\theta - 2\theta$ scans featured only the (004) GaAs Bragg reflection which exhibits a broad shoulder at smaller angles caused by InGaAs following Vegard's Law [15]. The $\theta - 2\theta$ scan corresponding to the passive measurement at room temperature is characterized by high resolution oscillations due to a phase shift caused by the spatial distance and strain between cap layer and substrate [4]. Unfortunately, in the case of the scan of the laser-excited sample these oscillations were considerably damped by vibrations from the circulation pump of the closed cycle cryostat.
Hence, further measurements have to be conducted employing a vibration free set up which will allow us to exploit the high resolution oscillations in order to analyze the effect of the laser excitation on the structural properties of the quantum dots. In addition, the new set up will feature a direct difference measurement collecting alternately data points with and without excitation of the quantum dots which will reduce systematical errors significant. The refinement of the so far collected data is in progress employing a recursion routine for the Takagi-Taupin equation [16].

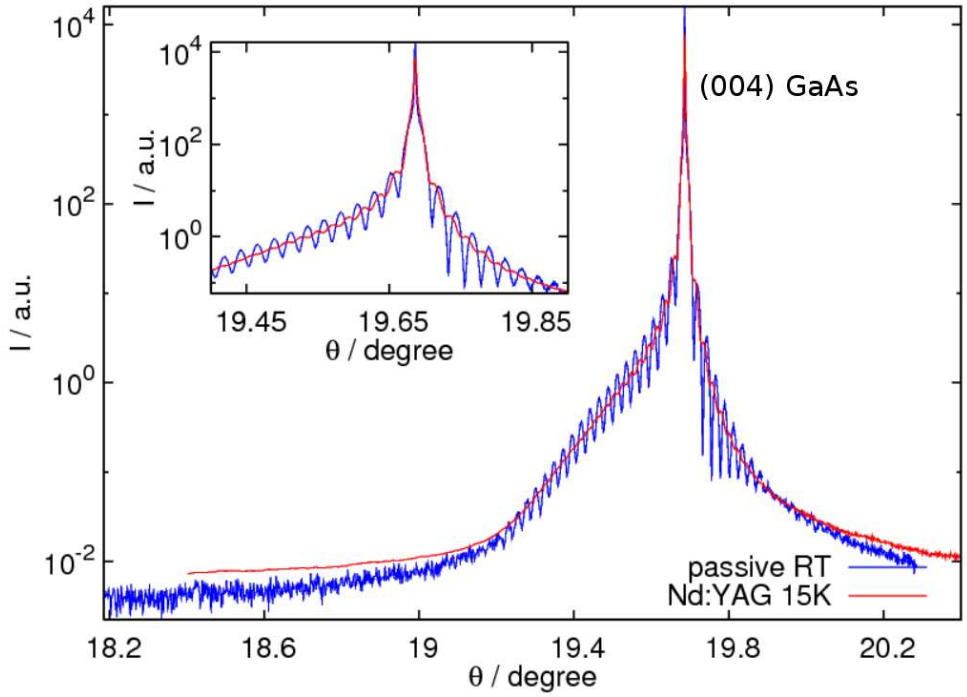

Figure 2: $\theta - 2\theta$ scan of the (004) GaAs Bragg reflection with passive quantum dots at room temperature (blue line) and with excited quantum dots at 15 K (red line).

References

[1] F. Henneberger, O. Benson, Semiconductor Quantum Bits (World Scientific, Singapore, 2008).

[2] D. Bimberg, M. Grundmann and N. N. Ledentsov, Quantum Dot Heterostructures (John Wiley and Sons, Chichester, 1999).

[3] U. Pietsch, T. Baumbach, and V. Holy, High-Resolution X-Ray Scattering from Thin Films and Lateral Nanostructures (Springer, New York, 2004).

[4] A. Krost, F. Heinrichsdorff, D. Bimberg, A. Darhuber, and G. Bauer, *Appl. Phys. Lett.* **68**, 785 (1996)

[5] O. Stier, M. Grundmann, and D. Bimberg, *Phys. Rev. B* **59**, 5688 (1999).

[6] F. Guffarth, R. Heitz, A. Schliwa, O. Stier, N.N. Ledentsov, A.R. Kovsh, V.M. Ustinov, and D. Bimberg, *Phys. Rev. B* **64**, 085305 (2001).

[7] L. Seravalli, M. Minelli, P. Frigeri, S. Franchi, G. Guizzetti, M. Patrini, T. Ciabattoni, and M. Geddo, *J. Appl. Phys.* **101**, 024313 (2007).

[8] I. Kegel, T.H. Metzger , A. Lorke, J. Peisl, J. Stangl, G. Bauer, J.M. Garca, and P.M. Petroff, *Phys. Rev. Lett.* **85**, 1694 (2000).

[9] P. Borri, W. Langbein, S. Schneider, U. Woggon, R.L. Sellin, D. Ouyang, and D. Bimberg, *Phys. Rev. Lett.* **87**, 157401 (2001).

[10] P. Borri, W. Langbein, U. Woggon, M. Schwab, M. Bayer, S. Fafard, Z. Wasilewski, and P. Hawrylak, *Phys. Rev. Lett.* **91**, 267401 (2003).

[11] A. Vagov, V.M. Axt, T. Kuhn, W. Langbein, P. Borri, and U. Woggon, *Phys. Rev. B* **70**, 201305 (2004).

[12] B. Krummheuer, V.M. Axt, T. Kuhn, I. D'Amico, and F. Rossi, *Phys. Rev. B* **71**, 235329 (2005).

[13] A. Krügel, A. Vagov, V.M. Axt, and T. Kuhn, *Phys. Rev. B* **76**, 195302 (2007).

[14] C. Krywka and M. Paulus and C. Sternemann and M. Volmer and A. Remhof and G. Nowak and A. Nefedov and B. Pter and M. Spiegel and M. Tolan, *J. Synchrotron Rad.* **13**, 8 (2006)

[15] S. Adachi, Physical Properties of III-V Semiconductor Compounds, InP, InAs, GaAs, GaP, InGaAs and InGaAsP (Wiley, New York, 1992), p. 4.

[16] W.J. Bartels and J. Hornstra and D.J.W. Lobeek, *Acta Cryst.* **A42**, 539 (1986).

Investigation of Langmuir Films by Grazing Incidence Diffraction

D.C. Florian Wieland*,[a], Steffen Bieder[a], Martin A. Schroer[a], Michael Paulus[a], Christian Sternemann[a], Patrick Degen [b], and Metin Tolan[a]

[a] *Fakultät Physik/DELTA, TU Dortmund, 44221 Dortmund Germany ,*

[b] *Physikalische Chemie II, TU Dortmund, Otto-Hahn-Str. 6, 44227 Dortmund Germany*

*email: florian.wieland@tu-dortmund.de

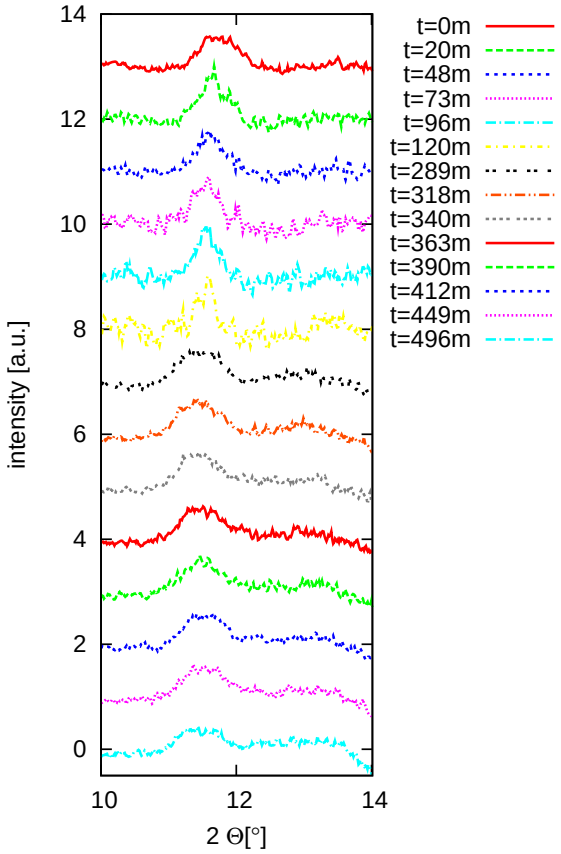

Figure 1: Integrated in-plane spectra from a DPPC monolayer.

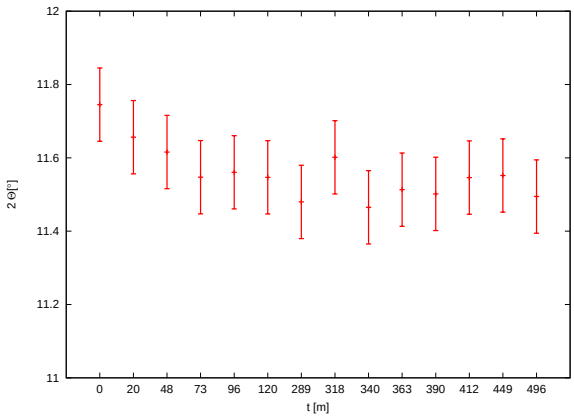

Figure 2: Position of the in-plane reflection from the Langmuir monolayer.

Biomineralization processes provide composite materials which show a hierarchical organization, complex and controlled shapes. By understanding the mechanisms which control the mineralization process new advanced materials could be fabricated. In living organisms the biomineralization process is controlled by proteins and the environment were the process takes place, e.g., the inner cell, sealed compartments or the surface of membranes. [1, 2, 3] Investigations on different systems show that the formation process is influenced by electrostatic interactions, geometric matching and stereochemical correspondence. [4, 5, 6] In this study the effect of the biomineralization of iron(III)-ions on membranes is investigated by grazing incidence diffraction (GID). As a model system for a membrane of a cell a Langmuir monolayer of the phospholipid 1,2-dipalmitoyl-sn-glycero-3-phosphocholine (DPPC) deposited on a liquid solution was chosen. As substrate a 12mmol iron(III)-chloride solution was used. In the case of iron(III)-chloride the biomineralization process is triggered by a change of the pH value. In order to start the mineralization process ammonium was added to the gas atmosphere above the Langmuir monolayer, which diffuses from the gas phase to the liquid interface resulting in a change of the pH value in this region.

The measurements were carried out at the beamline BL9 using the two-dimensional MAR345 detector with a photon energy of E=13keV. The beam was bend down using a Si mirror on the liquid surface resulting in an incidence angle of 0.083°. [7] A Langmuir trough was installed onto the sample stage in order to compress the Langmuir layer to a surface pressure of Π=40$\frac{mN}{m}$ at room temperature. After adding ammonia a series of diffraction patterns was recorded in order to observe the time evolution of the sample system. The amount of ammonia added to the atmosphere is summarized in table 1.

In-plane reflections of the Langmuir monolayer could be observed in GID experiments at BL9. Figure 1 shows the integrated and background corrected spectra of the in-plane scattering reflection as a function of time. For a more quantitative analysis a Gaussian function was fitted to the reflections in order to determine the position of the scattering reflections. Figure 2 shows the position of the Bragg reflection as a function of the time. The data indicates an enlargement of the lattice constant of the Langmuir monolayer with time. The explanation for this observation could be an accumulation of the iron-ions near the interface which might influence the electrostatic

time t	ammonia
0m	50 μl 3% NH_3
50m	50 μl 3% NH_3
160m	100 μl 25% NH_3
289m	100 μl 3% NH_3
363m	50 μl 25% NH_3
749m	100 μl 25% NH_3

Table 1: ammonia added

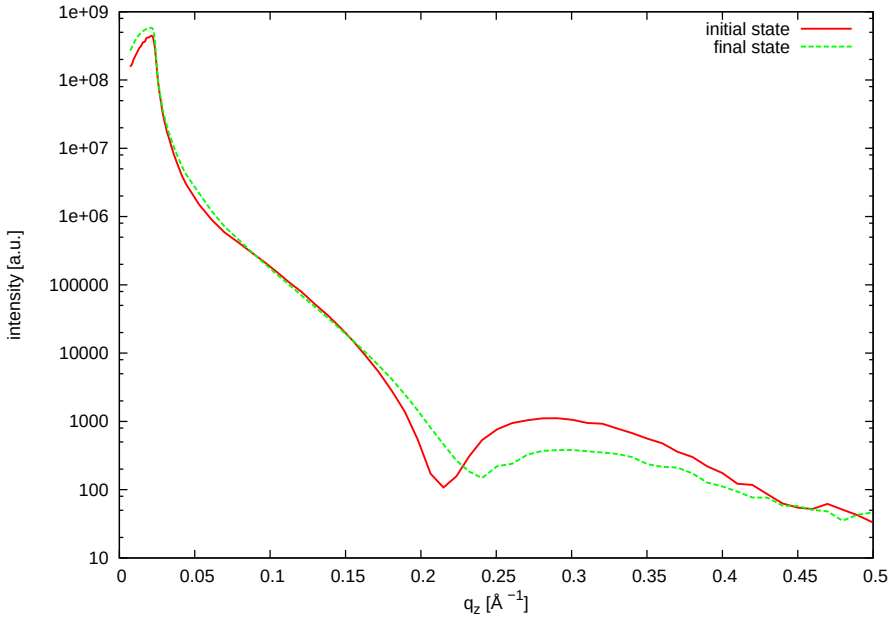

Figure 3: X-ray reflectivity measurements of the initial state and the final state of the Langmuir mono-layer on an Fe(III)-Chlorid subphase.

conditions in the interface region. The scattering patterns show no scattering signal originating from crystalline or amorphus ironoxide.
In order to investigate the vertical film structure x-ray reflectivity measurements (XRR) were performed at a laboratory diffractometer. Figure 3 shows XRR spectra of the initial and final state. The data indicates no change in the vertical structure of the Langmuir film. The quantitative data evaluation is still in progress.

References

[1] H. A. Lowenstam, S. Weiner, On Biomineralization *Oxford: New York*, 1989.

[2] L. Addadi, S. Weiner *Angew. Chem., Int. Ed.* **31**, 153 (1992).

[3] L. Addadi, S. Weiner *Proc. Natl. Acad. Sci.* **82**, 4110 (1985).

[4] E.M. Landau, M. Levanon, L. Leiserowitz, M. Lahav, J. Sagiv *Nature*, **318**, 353 (1985).

[5] S. Mann, D. Archibald, J.M. Didymus, T. Douglas. B.R. Heywood, F.C. Meldrum, N.J. Reeves *Science*, **261**, 1286 (1993).

[6] J.H. Fendler *Chem. Mater.*, **8**, 1616 (1996).

[7] C. Krywka, M. Paulus, C. Sternemann, M. Volmer, A. Remhof, G. Nowak, A. Nefedov, B. Pöter, M. Spiegel, M. Tolan *J. Synch. Rad.* **13**, 8 (2006).

X-ray diffraction studies on cobalt diamond composites

Christian Kronholz*,[a], Andre Steffen**,[b], Manuel Ferreira[a], Michael Paulus[b], Christoph J. Sahle[b], Metin Tolan[b] and Wolfgang Tillmann[a]

[a] *Institute of Materials Engineering, TU Dortmund, Leonhard-Euler-Str. 2, 44227 Dortmund, Germany,*
[b] *Fakultät Physik/DELTA, TU Dortmund, Maria-Goeppert-Mayer-Str. 2, 44227 Dortmund, Germany*

*email: christian.kronholz@udo.edu
**email: andre.steffen@tu-dortmund.de

Diamond grinding tools have widely established its usage in machining and cutting of natural stone and concrete. These diamond-metal composites are mainly fabricated powder-metallurgically in a vacuum sintering or in a hot pressing process [1, 2, 3]. While the vacuum sintering procedure consists of two operational sequences (pressing and sintering), seperated from each other, in the hot pressing technique the diamond-metal powder is compacted and sintered simultaneously in one step. The sintered metal especially serves as a boundary matrix for the embedded diamond (see figure 1), which are primarily responsible for the grinding process [4]. Therefore the bonding type of the diamonds in the metal-matrix is of essential relevance and has to bear up the developing forces at each diamond particle. Simultaneously a constant cutting ability and the so called self sharpening process of the diamond tool is also affected by the interaction between matrix and diamonds. The existence of a chemical bonding in these tools is preferred in contrast to the always given mechanical bonding based on the production techniques. The chemical bonding type results in higher durability and better grinding performance. So it is of important interest if this interface area between diamond and metal matrix consists of metal-carbides, solid solutions of carbon in metal or even graphite. For the extensive analysis of formed reaction products or diffusion zones in the interface area between the embedded diamond and the metal matrix, commercial diamond segments based on a cobalt matrix were produced. For this a cobalt powder with grain size of d≤40 µm and synthetic diamonds (40/50 US-Mesh) was mixed, coldpressed into shape and passed through a freestanding sintering under vacuum. Then the manufactured samples were dissolved in nitric acid and the residual diamonds are analysed regarding metal-carbides or solid solutions. The influence of the phase transition of the metal matrix to the interface area is not clarified yet [5]. It is well known from the literature, that the hexagonal (hcp) phase which is stable at room temperature changes at T≥421°C to cubic (fcc) phase. For powders with small grain size or thin layers a mixture of both phases is also observable at room temperature [6].

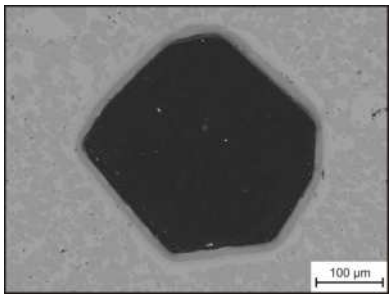

Figure 1: Embedded diamond in a steel-copper matrix.

To investigate the interface area between diamond and cobalt in detail two samples, which were prepared as described above, were each analyzed by x-ray diffraction measurements. All measurements were performed at beamline BL9 of DELTA using the MAR345 detector and transmission geometry [7]. In figure 2 a 2D diffraction pattern is shown exemplarily. All samples show Debye-Scherrer rings as well as high intensive single Bragg reflexions (dark spots in figure 2). This indicates that all samples were composed of both single crystalline and polycrystalline materials. All Bragg reflections which cause single spots in the MAR image can be attributed to the diamond phase. The remaining Debye Scherrer rings can be assigned to polycrystalline cobalt (cubic and hexagonal phases), small amounts of cobalt oxide (CoO and Co_3O_4) and a significant quantity of polycrystalline graphite. The data show no indication of crystalline cobalt carbide structures. Reference measurements with non sintered sample material do not show a graphite contamination. Thus, the graphitization of diamond takes place during the sintering process and is supported by cobalt which acts as a catalyst. Due to its strong scattering signal graphite seems to be the major constituent of the interface area between cobalt and diamond in diamond cobalt composites.

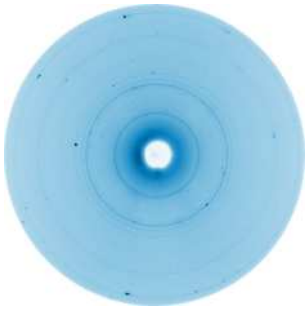

Figure 2: 2D diffraction pattern of diamonds extracted from diamond grinding tools.

To investigate the thermal induced cobalt phase transformation at T=421°C in-situ an x-ray diffraction experiment in transmission geometry consisting of 69 single measurements was performed at beamline BL9 of DELTA using the MAR345 detector with a sample-to-detector distance of about a =350 mm and a photon energy of E_{Ph} =27 keV. The exposure time was t_{ex}=60 s, the detector readout time t_{ro}=117 s. After the first measurement (m=1) at room temperature the sample (ultra fine cobalt powder with grain sizes below 40 μm)

was heated to T=620°C (2≤m≤16) and finally cooled down to T=10°C (m≥17). Diffraction patterns containing Bragg reflections of the Co hcp and Co fcc phases are displayed in figure 3 (left). During the heating process the volume fraction of fcc phase (hcp phase) rises from 44 % to 100 % (falls from 56 % to 0 %) as clearly seen in figure 3 (right side). After cooling the volume fraction is about 92 % (fcc) and 6 % (hcp). 2 % is expected to be cobalt oxide. Additional ex situ measurements of ultra fine cobalt powder which was cooled down in a time period of 24 hours exhibit smaller amount of the cubic phase. Thus, the cooling gradient can be used to adjust a dedicated phase composition in cobalt diamond compounts. More detailes are given in [8].

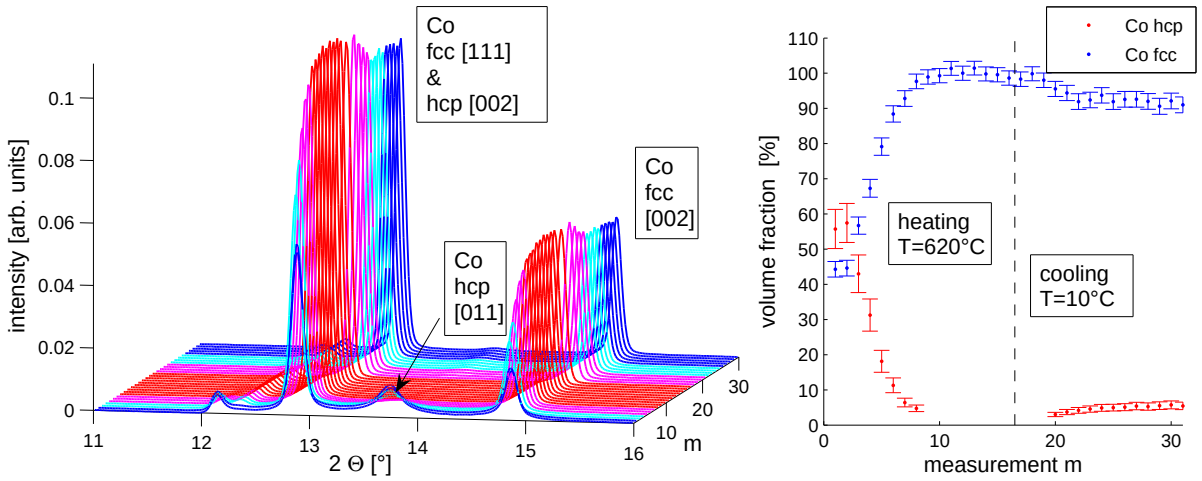

Figure 3: In-situ phase transformation of ultra fine cobalt powder during heating (T=620°C) and cooling (T=10°C). (left): 2Θ diffraction patterns. (right): Refined volume fractions of the hcp and fcc phases.

In our XRD studies on diamond cobalt composites we could not prove the existence of crystalline cobalt carbides in the interfacial volume between diamond and cobalt. A significant amount of polycrystalline graphite in the interface area was detected. By in-situ and ex-situ studies on ultra fine cobalt powder the temperature induced phase transformation between hcp and fcc phase could be monitored. During heating a complete phase transformation hcp→fcc takes place while the the fcc to hcp phase ratio depends strongly on the temperature gradient during cooling.

The authors like to acknowledge the DELTA machine group for providing synchrotron radiation and technical support. A. Steffen thanks the NRW Forschungsschule 'Forschung mit Synchrotronstrahlung in den Nano- und Biowissenschaften' for financial support.

References

[1] Denkena, B.; Tönshoff, H. K.; Friemuth, T.; Gierse, A.; Glatzel, T.; Hillmann-Apmann, H.: *Innovative Trennschleifprozesse in der Natursteinbearbeitung*. Werkstattstechnik online, 6:290-296, 2006.

[2] Konstanty, J.; Bunsch, A.: *Hot Pressing of cobalt powders*. Powder Metallurgy, 34(3):195-198, 1991.

[3] Tillmann, W.; Gathen, M.; Kronholz, C.: *Ein neues Werkstoffkonzept zur trockenen Bearbeitung mineralischer Materialien*. Materialwissenschaften und Werkstofftechnik, 38(2):112-115, 2007

[4] Kieback, B.; Sauer, Ch.; Tillmann, T.: *Optimisation of Metallic Binders used in Diamond Tool production*. Proceedings of the International Workshop on Diamond Tool Production, Turin, 1995, EPMA, S. 57-64

[5] Molinari, A.; Marchetti, F.; Gialanella, S.; Scardi, P.; Tiziani, A.: *Study of the Diamond-Matrix Interface in Hot-pressed Cobalt-based Tools*. Materials Science and Engineering, 130:257-262, 1990.

[6] Schastlivtsev, V. M.; Khlebnikova, Yu. V.; Tabatchikova, T. I.; Rodionov, D. P.; Sazonova, V. A.: *Formation of a Structure in Cobalt Single Crystals at the $\beta \rightarrow \alpha$ Transformation*. Doklady Physics, 54:21-24, 2009.

[7] Krywka, C, Sternemann, C, Paulus, M, Javid, N, Winter, R, Al-Sawalmih, A, Yi, S, Raabe, D, Tolan, M, *The small-angle and wide-angle x-ray scattering setup at beamline BL9 of DELTA*, Journal of Synchrotron Radiation 14, 244 (2007)

[8] Steffen, A.: *Strukturuntersuchungen an Kobalt und Kobalt-Diamant Werkstoffen*. Diploma thesis, TU Dortmund, Fakultät Physik, 2009.

Residual stress measurements on PVD-TiAlN layers of a multilayer coating under low incident beam angle

U. Selvadurai-Lassl, Crostack, H.-A.

Lehrstuhl für Qualitätswesen; Universität Dortmund, Joseph-von-Fraunhofer Str. 20, 44227 Dortmund, Germany

Introduction

Hard PVD- multilayer coatings which consist of ceramic and metallic layers are under development to improve the life time of applications like cuttings tools. Due to the thermal coating process and mismatch of Young's modulus and thermal expansion coefficient between substrate, metallic and ceramic layers residual stresses which can shorten the life-time are induced into the coatings.

Experiments

The residual stress was studied on two multilayer systems which were carefully manufactured by LWT, TU Dortmund without delaminations [l]. The first multilayer system (No. 4028) consists of five metallic Ti-layers (60 nm thick) and five ceramic TiAlN-layers (500 nm thick) which are deposited alternating onto the steel substrate. The complete coating thickness is ≈ 3 µm. In contrast, the Ti-layer thickness of the second multilayer system (No. 7) was increased to 200 nm. Their total coating thickness rise up to 3.5 µm.

The residual stress in the ceramic layers of multilayer was analysed by means of X-ray diffraction and the $d/\sin^2\psi$-method [2] using synchrotron radiation at beamline B9 of DELTA at TU Dortmund, Germany. The high brilliance and intensity of synchrotron radiation allow to analyse reflections under low incident angle with a high accuracy. The energy of 7000 eV which corresponds to a wavelength λ of 0.1771 nm was chosen. By means of this radiation the (200) reflection was analysed at $2\theta \approx 50°$. According to the $d/\sin^2\psi$ method this reflections was analysed at different ψ–angles. This is the angle between the normal of the sample surface and the normal of the lattice plane. It can be chosen by changing the angles χ offset. In a linear case a plot of the measured d-values or the lattice distortions against $\sin^2\psi$ results in a line. The slope of a regression function of this line correlates with the residual stress. The correlation factors are the X-ray elastic constants. Because the X-ray elastic constants of TiAlN are unknown the approximated values were calculated by the Young´s modulus of 428 GPa [3] and Poisson constant of 0.2 [3] according to the Voigt method [4]. The error of the stress values is calculated by the standard deviation from the slope of the straight line.

Due to the low thickness of ceramic layers their reflection intensity is weak in contrast to the ferrite reflections from the substrate. For that reason, both multilayer systems were analysed at a small incident angle θ to increase the penetration path of beam inside the coating. The aim of this experiment was to test different θ angles and to investigate their influence on the residual stress of the ceramic TiAlN-layers.

Results

Different θ angles were chosen to optimise the conditions for measuring the residual stress and its dependency on the depth inside the multilayer coating. At a very small incident angle θ the upper part of the multilayer is analysed, only. With increasing θ angle the deeper parts of the multilayer contribute more and more to the attenuation and the portion of the upper layer is reduced.

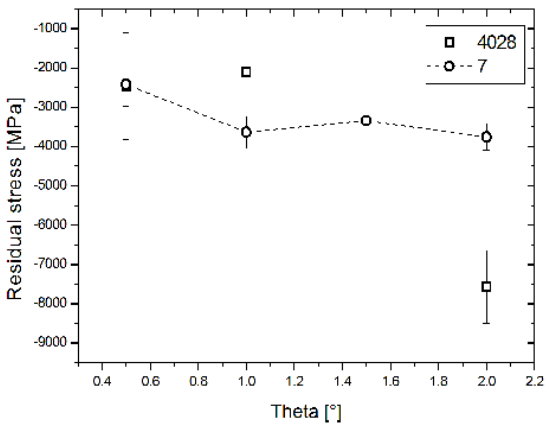

Fig. 1: Influence of incidence angle θ on residual stress of two multilayer systems

In Fig. 1, the measured residual stress values for three and four θ angles are given for the multilayer systems 4028 (thin metal layers) and 7 (thick metal layers), respectively. For both systems the tendency is found, that the compressive residual stress rise up with increasing incident angle θ.

This corresponds to results of FE simulations which show that the residual compression stress in the ceramic layer should increase with increasing depth i.e. with increasing incident angle θ. In sample 7 (thicker metallic layers) the slope of stress-θ curve is relatively small.

This can be reduced to the fact that a high portion of radiation is diffracted by the first ceramic layer for geometric reasons.With increasing θ angle the portion of the second layer increase and the compressive stress values rise up slightly also.

The rapid drop in compressive residual stress of specimen 4028 from θ = 1° and θ = 2° can be ascribed to higher penetration depth due to the lower thickness of metallic layers. Therefore, the contribution of deeper ceramic layers to the average residual stress is higher.

These first measurements prove that residual stress evaluation by means of grazing incidence diffraction on ceramic layer is suitable. Up to θ = 2° no Ferrite reflections were found. Therefore, the penetration path is inside the multilayer. This results show also, that the depth dependency of residual stress in such thin ceramic layers can be analysed by different incident angles. But for this analysis further investigations are needed.

Acknowledgement

The authors would like to acknowledge LWT – TU Dortmund for sample supply.

References

[1] W. Tillmann, E. Vogli: Adv. Eng. Mat., 10, No. 1-2, (2008) 79-84
[2] V. Hauk and E. Macherauch (Hrsg.): Eigenspannungen und Lastspannungen (HTM Beiheft), Carl Hanser Verlag München, Wien (1982)
[3] W. Kress, P . Roedhammer, H. Bilz, W. Teuchert, A.N. Christensen: Phonon anaomalies in transition-metal nitrides: TiN. Phys.Rev. B17 (1978)111
[4] W. Voigt: Lehrbuch der Kristallphysik, Leipzig, B.G. Teuber Verlag (1928)

Structural studies on $Eu_xSr_{1-x}C_2$ by synchrotron powder diffraction

P. Link*, U. Ruschewitz

Institut für Anorganische Chemie, Universität zu Köln, 50939 Köln, Germany.

*email: pspitzer@smail.uni-koeln.de

The structures of ten solid solutions in the system $Eu_xSr_{1-x}C_2$ are investigated by synchrotron powder diffraction at beamline BL9. The results confirm our assumptions of a strainless, Eu^{2+} containing system showing no deviation from Vegard´s law.

Europium is known to exist in two different valence states as Eu^{3+} and Eu^{2+} ion. EuC_2 [1] contains divalent Europium, a fact that leads to a semiconducting behaviour of the compound and shows its similarity to the alkaline earth metal carbides. As the ionic radii of Eu^{2+} (125 pm) and Sr^{2+} (126 pm) are almost the same solid solutions $Eu_xSr_{1-x}C_2$ should be a perfect example of a strain free system following Vegard´s law. We therefore synthesized 10 solid solutions with $0.1 < x < 0.9$ by direct reaction of the elements in an inert atmosphere. The compounds are black powders, no single crystals could be obtained. Due to strong X-ray absorption of Eu conventional Cu$-K_\alpha$ X-ray sources are not feasible for structure determination, moreover Mo$-K_\alpha$ radiation provides powder diagrams with too poor angular resolution. Therefore synchrotron radiation seems to be the appropriate tool to obtain powder patterns with good resolution and minimized absorption.

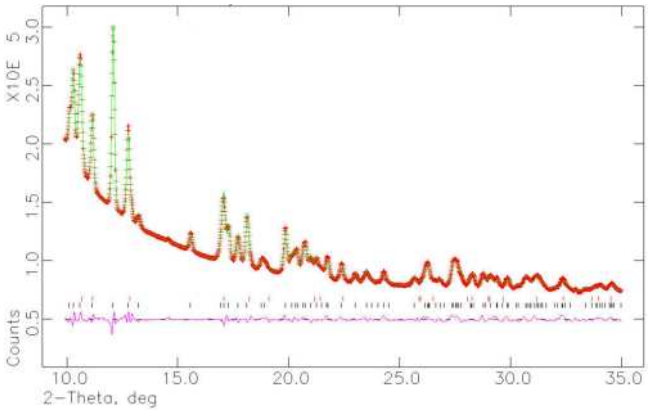

Figure 1: Rietveld plot of $Eu_{0.5}Sr_{0.5}C_2$. Red marks show CaC_2 type structure, black ones show ThC_2 type structure.

10 samples of $Eu_xSr_{1-x}C_2$ with $0.1 < x < 0.9$ were investigated at beamline BL9 of DELTA, 5 of them in the temperature range 300–950 K. A photon energy of 19 keV was used to minimize sample absorption, for fast data collection a MAR345 area detector was chosen. The samples were sealed in quartz capillaries of 0.3 mm diameter as they are very sensitive to air and moisture. All of them were investigated at room temperature, 5 selected ones were additionally attached to a high temperature furnace that was heated to 950 K in steps of 70 K. Due to the good crystallinity of the samples and the high flux of the radiation it was possible to obtain a complete pattern in about ten minutes. Figure 1 shows an exemplary powder diagram obtained at room temperature.

The patterns were first indexed and subsequently refined by the Rietveld method to get exact cell constants. As can be seen in figure 2 the structure of the compounds depends on composition. For $x \leq 0.5$ the tetragonal CaC_2 type structure (I4/mmm, $Z = 2$) coexists with the monoclinic ThC_2 type structure (C2/c, $Z = 4$). For $x > 0.5$ only the ThC_2 type structure is found. All refined volumes per formula unit are in good agreement with Vegard´s law, no strong deviations occur. These findings reinforce our assumptions that Eu is divalent over the whole composition range, as a change in Eu valence would lead to a significant lowering in volume. With two metal ions of nearly the same size these compounds can therefore be regarded as strain free solid solutions.

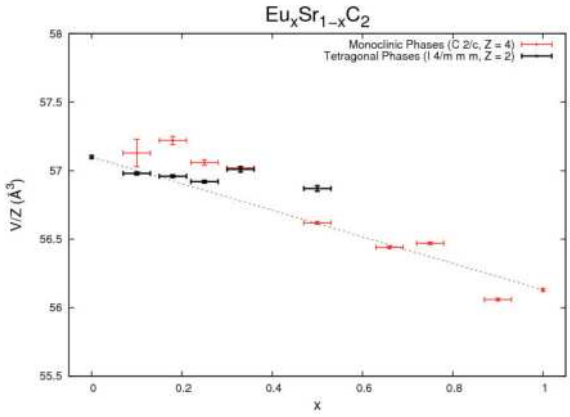

Figure 2: Volume per formula unit of $Eu_xSr_{1-x}C_2$ as a function of x. All values are obtained from Rietveld refinements.

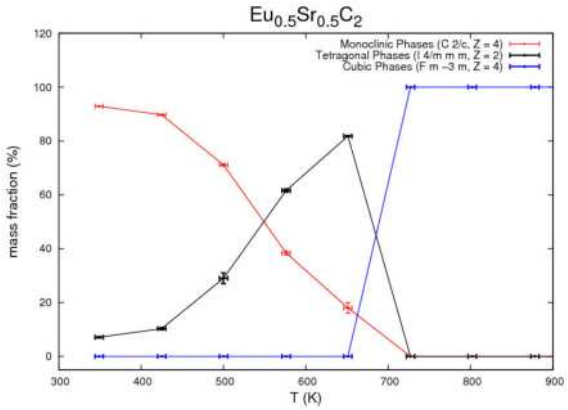

Figure 3: Mass fraction of different modifications in $Eu_{0.5}Sr_{0.5}C_2$ as a function of temperature. All values are obtained from Rietveld refinements.

All temperature dependent measurements show that the CaC_2 type structure is the stable modification at high temperatures, whereas the ThC_2 type structure appears at lower temperatures. This behaviour is also known for pure SrC_2 [2]. The transformation is not sharp but continuous, and it is unknown, whether this is a kinetic or thermodynamic effect. All measured compounds show a sharp transition to the cubic high temperature modification ($Fm\bar{3}m$, $Z = 4$) between 650 K and 720 K. As an example the occurrence of the different modifications in $Eu_{0.5}Sr_{0.5}C_2$ is shown in figure 3. To further validate our findings some complementary analytic measurements are planned. The Eu valency shall be determined by Mössbauer spectroscopy, additionally DTA measurements shall provide the exact values of the transition temperatures to the cubic high temperature modification which contain further information about the strain of the system [3].

We would like to thank the DELTA machine group for providing the synchrotron radiation. This work was supported by the DFG (priority programme SPP 1166).

References

[1] D. Wandner, P. Link, O. Heyer, J. Mydosh, M. A. Ahmida, M. M. Abd-Elmeguid, M. Speldrich, H. Lueken, U. Ruschewitz, *Inorganic Chemistry*, submitted.

[2] V. Vohn, M. Knapp, U. Ruschewitz, *Journal of Solid State Chemistry*, **151**, 111, **2000**.

[3] I. J. McColm, T. A. Quigley, *Journal of Inorganic and Nuclear Chemistry*, **35**, 1931, **1973**.

Structural and morphological changes in P3HT thin film transistors applying an electrical field

D.K. Tiwari[1], S. Grigorian[1], U. Pietsch[1], H.-G. Flesch[2] and R. Resel[2]

[1]Solid state physics, University Siegen
[2]Graz University of Technology

In recent years conjugated polymers have highly increasing interest as active materials in organics electronics. Structural and morphological parameters play an important role in organic transistors performances. It has been already shown that the thermal treatment helps to improve the efficiency of devices [1,2]. The aim of our studies is a correlation between the electrical performance and the structural properties of P3HT films. Especially, to understand how applied electric field can change structural/morphological properties and induce Joule heating caused by high resistance of P3HT films.

Structural and morphological features of poly (3-hexylthiophene) (P3HT) thin films under external electric field were investigated by X-ray scattering technique and Atomic force microscopy (AFM). All x-ray scattering experiments were performed at beam line BL 9 , DELTA, University of Dortmund as well as at laboratory source, at University of Siegen using wavelength of 0.83 Å and 1.54 Å, respectively. All data has been taken using point detector. In order to understand the morphological changes this occurred in polymer thin films with the voltage AFM investigations have been taken at Physical chemistry department (University of Siegen) by using Atomic force microscope (AFM). Samples were prepared on heavily doped n-type Silicon substrate by spin coating and drop casting methods. Gold has been deposited as source/drain electrode above the polymer film with small channel of width of 2 mm. We have done the series of x-ray reflectivity, X-ray grazing incidence out-of-plane and azimuthal scans for various values of applied electric voltage. For X-ray reflectivity, the major change has been found close to critical angle of total external reflection which indicate that thin film becomes less dense and expanded, and, in many cases, an increase of surface roughness with the voltage. This result is correlated with AFM images too. We also investigate structural behaviour with applied electric field in different steps by grazing incidence diffraction. Out-of-plane profiles of the (100) peak revealed that the peak intensity has been decreased with applied electric field. Such kind of structural changes might be caused by Joule heating and current induced defects of the thin P3HT film.

References

[1] Kim et.al.2005 Appl.phys. Letts. 86 063502
[2] Organic Electronics Materials Manufacturing and Applications, 2006 WILEY-VCH Verlag GmbH & Co. KGaA edited by Hagen Klauk.

Structural and Mobility Analysis of Edge on Oriented Poly(3-hexylthiphene) OFET Devices Prepared by Low Temperature Drop Casting Technique

Thankaraj Salammal Shabi, Patrick Pingel, Ullrich Pietsch, Nils Koenen and Ullrich Scherf

Polymer based flexible devices have been started to replace the inorganic based devices due to its good electrical and optical performances, cheap and large area productions. They are cheap because of the nonnecessity of complicated devices like vacuum, evaporating sources etc and they are solution processable. Poly(3-alkylthiophene)s have been placed an important role in the fabrication of organic field-effect transistors (OFET)s [1]. From the thiophene family poly(3-hexylthiophene) has been placed a vital role due to its good electrical performance. It has been realized by the researchers that the mobility of the devices is mostly depending on the regio-regularity (RR), ordering (crystallinity) and molecular weight etc [2, 3 & 4].

Here we have taken effort to solve the crystalline as well as orientation problem evolved in the polymer based devices. We have carried out low temperature growth technique to obtain highly ordered film by controlling the solvent evaporation by the way to control the supersaturation ratio of the solution. The beauty of this technique is that one can grow less thickness film with somehow good surface uniformity as compare to the RT drop casted films. Films were prepared under different temperature with the help of commercial freezer. P3HT films have been grown above Si/SiO_2 substrate, 292 nm thick SiO_2 has been used as an insulator layer and heavily doped n-type Si.

GIXRD analyses were performed at synchrotron source DELTA Dortmund, Germany. 2D images were taken by an image plate with 3450x3450 pixels of 100 µm size, it's fixed at 50 cm far from the sample and samples were probed with a beam size of 0.5x1.5 mm². X-ray of wavelengths 0.83 and 0.93Å has been used for the structural analysis. The incidence angle α_i = 0.13 and 0.14 ° (for the wavelengths 0.83 and 0.93Å respectively) was fixed above the critical angle of the film to enhance the total scattered signal. All the measurements were performed under vacuum in order to avoid the photo oxidation.

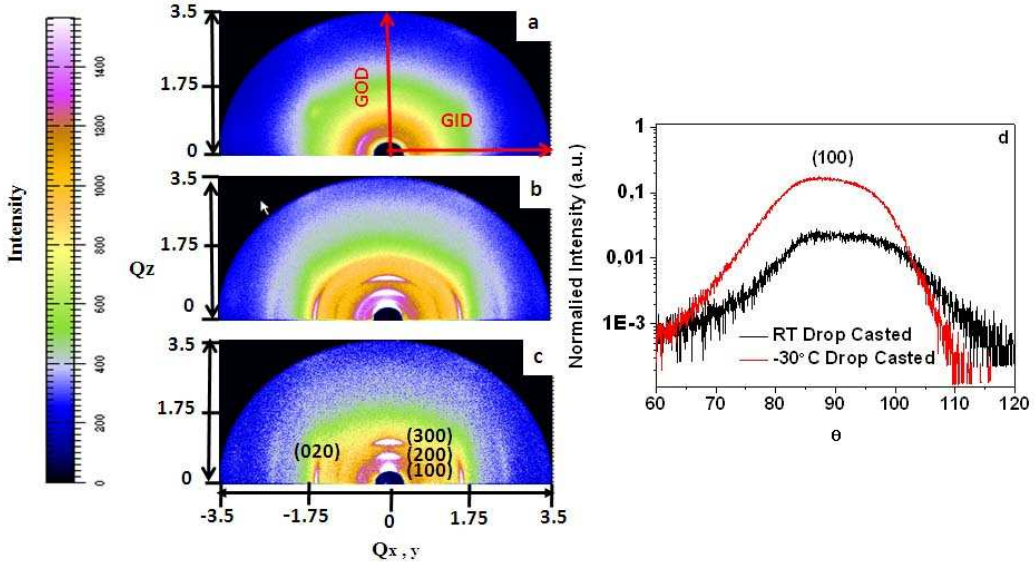

Fig. 1 2D X-ray scattering pattern of spin coated at RT (a), drop casted at RT (b) and -12°C (c) films and Chi scan (d) see right).

X-ray measurements visualize that room temperature (RT) grown film has flat and edge on orientation but in the case of -30°C grown one flat on orientation was completely absent (Fig.1). Chi scans have been performed; it visualizes the tilting of crystallites along in-plane direction. The FWHM of the peak has been reduced from 17.04° to 13.9° while comparing RT with -30°C grown film. The diffraction intensity of -30˚C film is four times higher than the RT grown film. In contrast to X-ray analysis TEM analysis has been performed both are visualizing the same results.

Top contacted mode OFET devices have been prepared to analyze the mobility [1]. Si substrate has been used as a gate electrode; source and drain electrode have been deposited above the polymer film, Au has been used as a metal contact. Mobility measurement reveals that -30°C grown film ($1.5x10^{-3}$ $cm^2V^{-1}s^{-1}$) has one order of mobility higher than the RT ($2x10^{-4}$ $cm^2V^{-1}s^{-1}$) grown one.

References

[1] Organic ElectronicsMaterials Manufacturing and Applications, 2006 WILEY-VCH Verlag GmbH & Co. KGaA edited by Hagen Klauk.
[2] H.Sirringhaus *et al*, Nature. 401 (1999) 685.
[3] Chiatzun Goh *et al*, Appl. Phys. Lett. 86 (2005) 122110.
[4] Li-Min Chen *et al*, Advanced Materials. 21 (2009) 1434.
[5] R. Joseph Kline *et al*, Nature Materials. 5 (2006) 222.

Soft x-ray standing-wave excited photoelectron spectroscopy studies on the system MgO/Fe

S. Döring[1,2,*], F. Schönbohm[1,2], D. Weier[1,2], U. Berges[1,2], R. Schreiber[3], D. E. Bürgler[3], C. S. Fadley[4,5], C. M. Schneider[3], C. Westphal[1,2]

[1] Experimentelle Physik I - Technische Universität Dortmund, Otto-Hahn-Str.4, D 44221 Dortmund
[2] DELTA - Technische Universität Dortmund, Maria-Goeppert-Mayer-Str. 2, D 44227 Dortmund
[3] Institut für Festkörperforschung, IFF-9 „Elektronische Eigenschaften“, Forschungszentrum Jülich GmbH, D 52425 Jülich
[4] Materials Sciences Division, Lawrence Berkeley Laboratory, University of California, Berkeley, CA 94720, USA
[5] Department of Physics, University of California at Davis, Davis, CA 95016, USA
[*] corresponding author: sven.doering@tu-dortmund.de

(October 2009)

In our experiments we investigated the interface between thin MgO and Fe layers. This system represents an important part of a magnetic tunnel junction showing the tunnel magneto-resistance (TMR) effect, which has been used in industrial products like hard-drive read-write heads for some years. Today, it is evident that the properties of the Fe-MgO interface play a crucial role in determining the effect size. Nevertheless, the interface is not easily accessible for analysis.

By combining the element-sensitive x-ray photoelectron spectroscopy (XPS) with the standing-wave technique we are able to address buried interfaces in layered samples. XPS is very sensitive to the elements involved, and additionally their actual chemical states can be identified. This is very useful in order to address and quantify reactions and intermixing at interfaces. The standing-wave field can be scanned through the sample layer by layer. Thus, we are able to determine the thickness of the layers and also the thickness of possible intermixing zones at buried interfaces inside the sample.

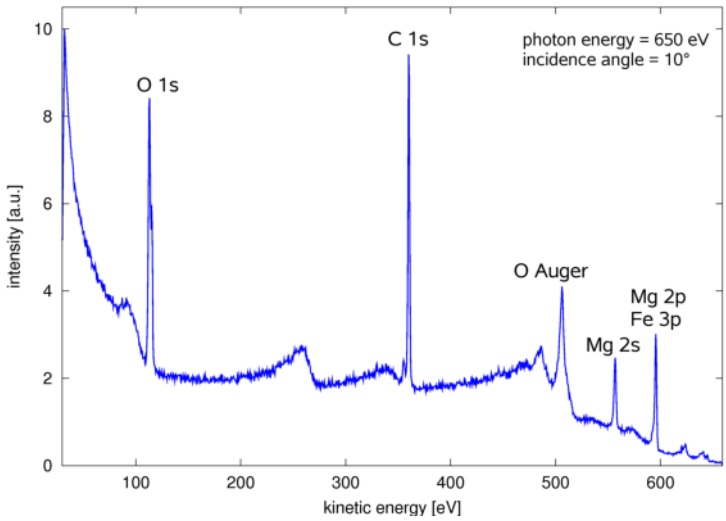

Figure 1: Survey spectrum at $h\nu = 650\,\mathrm{eV}$. The incidence angle was below the first order Bragg-angle. The O1s, C1s, and Mg2p signals were used for further measurements. Close to the Mg2p signal the weak Fe3p signal could be identified when the energy resolution was increased.

A $Si/MoSi_2$ multilayer mirror provides a relative high reflectivity of around 10% even for soft x-rays with an energy of 650 eV and, thus, serves as a substrate. Due to the fact that the standing-wave field is formed by the interference of the incoming and the reflected beam a high reflectivity is required. The Fe and MgO layers were evaporated on top of the mirror. The latter also serves as a protective capping. The sample was prepared at the IFF-9 in Jülich and exposed to ambient air during transportation to BL 11 at DELTA. Thus, we found C and O contamination at the sample surface (Figure 1).

The O1s, C1s, and Mg2p peaks were recorded as a function of the incidence angle. For these measurements the angle was varied in steps of 0.05° over a 3° range around the first order Bragg-angle at $\approx 14.2°$. The intensities of the signals were determined from the spectra and plotted versus the angle to obtain the so-called rocking-curves shown in Figure 2. We analyze these rocking-curves within our analytical model [1] in order to determine the film thicknesses and the thickness of a possible intermixing zone.

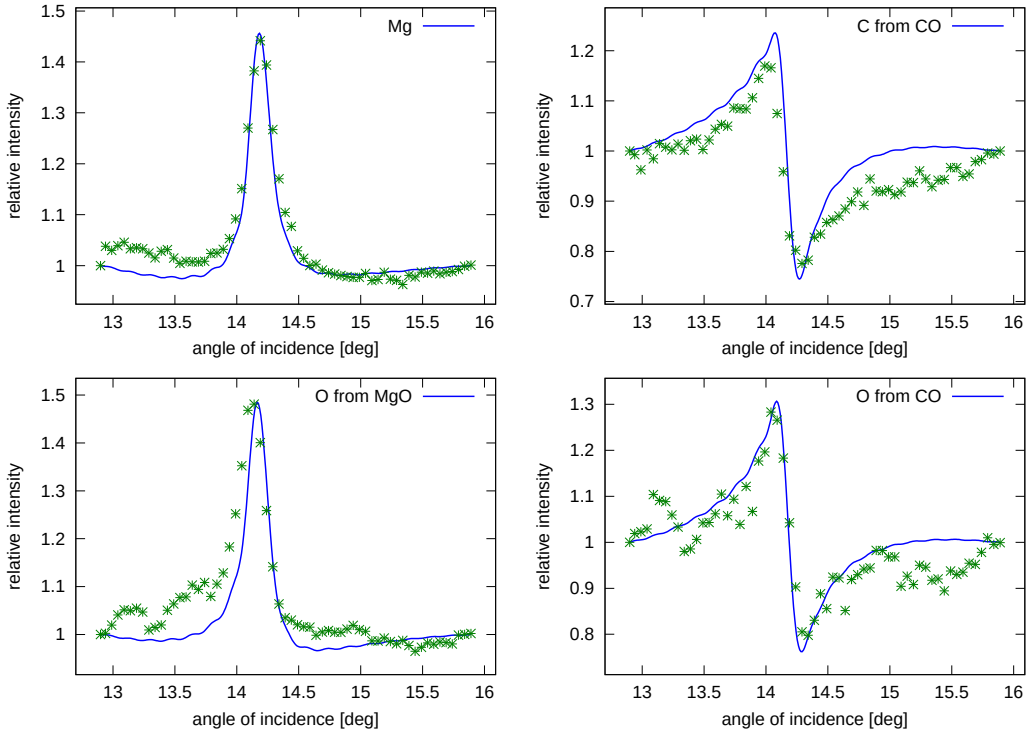

Figure 2: Rocking-curves of Mg2p, C1s, O1s from MgO, and O1s from CO signals measured at $h\nu = 650$ eV. The dots represent the measured data and the lines show simulated curves.

We simulated a full set of rocking-curves, which excellently agree with the experimental data as shown by the blue lines in Figure 2. The Fe, MgO, and surface contamination layers were determined to be 112 Å, 15 Å, and 8 Å thick, respectively. The values for Fe and MgO are in good agreement with the nominal thicknesses. Most importantly, we did not observe intermixing at the MgO/Fe interface.

[1] S. Döring, F. Schönbohm, D. Weier, et al., *„Standing-wave excited photoemission experiments on $Si/MoSi_2$ multilayer mirrors in the soft x-ray regime: an analytical modeling approach“*, submitted to Journal of Applied Physics, Aug. 2009

Photoelectron spectroscopy (XPS) studies on zirconium oxid on nitrided Si(100)

A. Wadewitz[1*], F. Schönbohm[1,2], D. Weier[1,2], T. Lühr[1], C. Westphal[1,2]

[1] Experimentelle Physik 1 - Universität Dortmund, Otto-Hahn-Str. 4, D 44221 Dortmund, Germany
[2] DELTA - Universität Dortmund, Maria-Goeppert-Mayer-Str. 2, D 44227 Dortmund, Germany
[*] corresponding author: anja.wadewitz@uni-dortmund.de

(October 2009)

The ongoing miniaturization of MOSFET semiconductor devices leads to a decreasing thickness of the dielectric gate material. For SiO_2 gate dielectrics, problems occure when the thickness is reduced below 2 nm. The tunneling currents and power consumption of the device increase drastically. This results in a loss of efficiency. Thus, the classically used silicon oxide must be replaced by materials with a higher dielectric constant than SiO_2. One of many promising candidates for high-k dielectrics is zirconium dioxide on which this work focuses on. Within the MOSFET fabrication process, the silicon wafer is being annealed for activation at temperatures above 1000°C. Recent research activities show, that ZrO_2 is thermaly unstable and lacks insulating capabilities above annealing temperatures of 600°C. However a diffusion barrier between ZrO_2 an Si might be a solution for this challenge. In this work the influence of nitrogen as diffusion barrier is studied. Therfore the thermal stability of ZrO_2 on SiN was investigated.

The measurements were performed at beamline 11 of DELTA. The undulator beamline provides a high photon flux and a high energy-resolution at the required soft x-ray energy range. The sample cleaning and preparation was performed in-situ. The base pressure of the chamber was $5{\cdot}10^{-11}$mbar. Sample preparation was started by cleaning the Si(100) surface with annealing at 1050°C. After annealing the sample temperature was slowly decreased within 15 minutes to room temperature, and (2×1)-reconstruction was observed. The surface was checked for impurities by LEED and XPS. In the next step a thin SiN layer is generated at the surface by electron cyclotron resonance plasma evaporation. In order to reduce the thickness of the layer the sample was annealed at 800°C. Subsequently ZrO_2 was evaporated onto the sample at room temperature by means of an electron beam evaporator. After the preparation process the sample was stepwise annealed at increasing temperatures ranging from 500°C to 875°C in order to study the surface variations in dependence on the annealing temperatures. This layer stack was examined by means of XPS and XPD.

The high resolution spectra of Zr 3d and Si 2p signals are presented in Fig.1. For temperatures above 800°C the O1s intensity decreases rapidly. At 825°C the Zr 3d signal decreases as well, while the silicon intensity increases, especially on the bulk-side of the spectra. The Zr 3d spectra show a small shift to lower binding energies at elevated temperatures. This shift is caused by an increased number of zirconium atoms being bond to nitrogen atoms within the diffusion barrier. At temperatures of 825°C the oxygen is removed from the surface. At 825°C a new peak can be observed in the Zr 3d spectra due the formation of zirconium nitride at the surface.

Fig. 2 shows Zr 3d XPD pattern recorded at different temperatures. The first diagram shows a pattern without stuctured order of the amorphous interface, recorded after annealing at 600 °C. For temperatures above 777°C a structured pattern was obtained indicating a crystalline interface between ZrN and SiN.

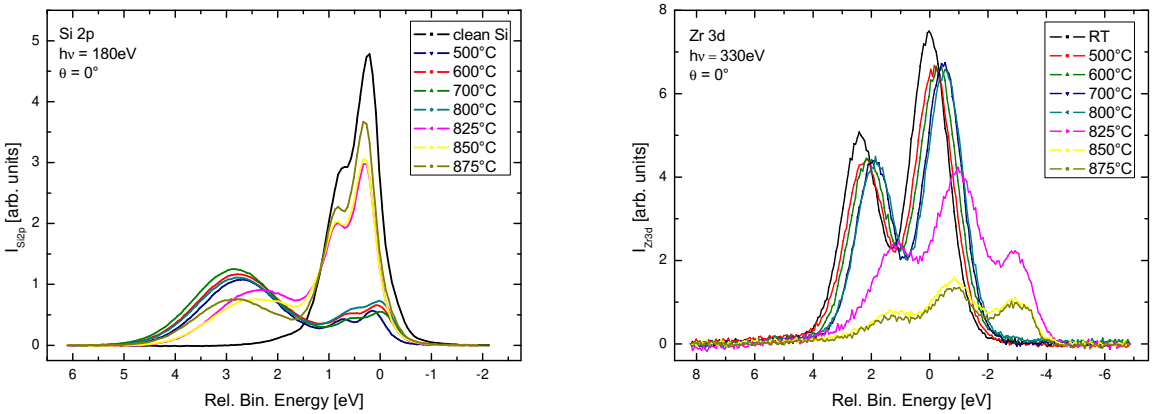

(a) Si 2p signal

(b) Zr 3d signal

Figure 1: XPS signals of Si 2p and Zr 3d for different temperatures

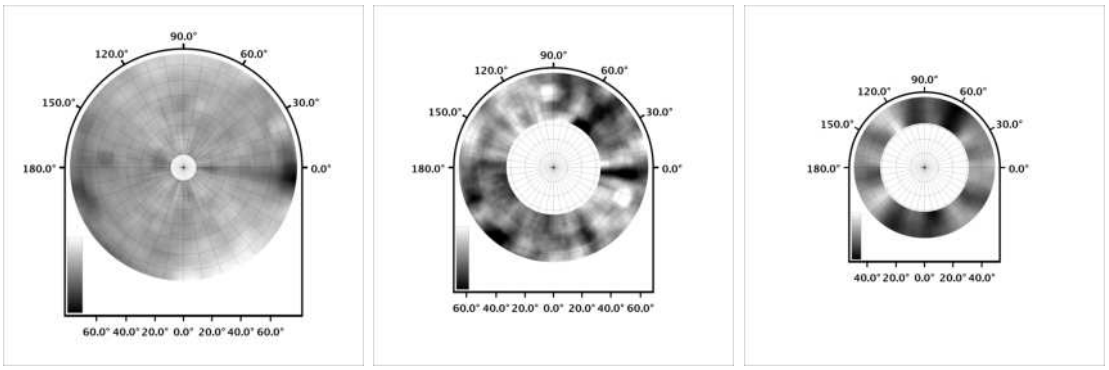

(a) Zr 3d at 600°C

(b) Zr3d at 777 °C

(c) Zr3d at 825 °C

Figure 2: XPD pattern of Zr 3d signal for after annealing at different temperatures

Acknowledgements: The authors would like to thank DELTA staff for continuous support during the beamtimes.

X-PEEM OF ANTIFERROMAGNETIC DOMAINS IN SINGLE CRYSTALLINE NICKEL OXIDE

F. Nickel[1], C. Wiemann[2], U. Berges[1], C. Westphal[1] and C.M. Schneider[2]

[1] Experimentelle Physik I - TU Dortmund
[2] Institute of Solid State Research, IFF-9, Research Center Jülich,
contact: florian.nickel@uni-dortmund.de

Antiferromagnetic (AFM) domains at the (100)-surface of single-crystalline NiO were investigated by X-Ray Photoemission Electron Microscopy (X-PEEM). To access the AFM structure we used X-Ray Magnetic Linear Dichroism (XMLD). Our results represent the first magnetic imaging at DELTA.

Experimental Setup

In order to perform magnetic imaging experiments the PEEM technique was set up in Spring 2009 at Beamline 11. The Beamline provides soft x-rays with energies ranging from $h\nu$ =55 eV up to 1500 eV. Fig. 1.1 shows a schematic sketch of the PEEM used. Since Summer 2009 the system comprises:

- Experimental setup based on STAIB PEEM 350 (details discussed below).
- UHV Manipulator which allows movement for 5 degrees of freedom (x,y,z, rotation, and tilt).
- Sample preparation system for evaporation, sputtering, and annealing up to 1500 K under UHV conditions.
- Load-lock system which enables sample changes without breaking the vacuum in the experimental chamber.

For the future an evaporator system is planed for in-situ preparation of single-crystal films.

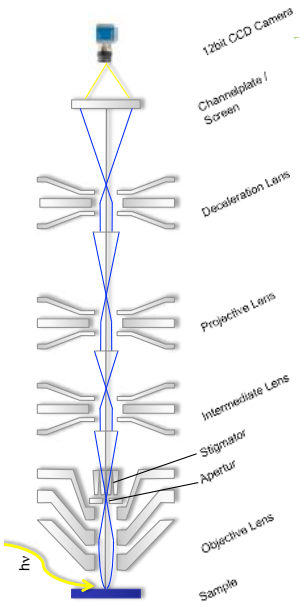

Figure 1.1 – Schematic set-up of the used photoemission electron microscope.

The STAIB PEEM works with fully electrostatic lenses. The sample is located 2 - 3 mm in front of the objective immersion lens and illuminated by a linear polarized soft x-ray-beam. In order to achieve a large acceptance angle, the photoelectrons are strongly accelerated by an electrostatic field ($\approx$5 kV mm^{-1}). This leads to reduced aberration and improved lateral resolution. The instrument operates with a fixed contrast aperture. The electron-optical image is magnified and transfered via the electron-optics onto a channelplate with fluorescent screen. Additionally there is a stigmator stage creating a octupole-field correcting for astigmatic errors of the objective lens. The screen converts the electron-optical into a light-optical image which is in turn read-out by a slowscan 12 bit CCD-Camera.

During the first commissioning in Fall 2009 a lateral resolution of 220 nm was achieved. The signal-to-noise ratio of the light-optical unit is lower than 1% for exposure times less than 4 s. The measured magnification of the system goes up by a factor of 1000.

First Experiments and Results

Sample Preparation

For the experiments high quality NiO(100)-surfaces were obtained by *ex-situ* cleaving followed by *in-situ* sputtering and annealing cycles.
Due to the polar nature of the ionic NiO crystal, (100) surfaces can be easily obtained by cutting the crystal with a knife parallel to a (100) plane. After mounting the cleaved crystal on the sample holder, the sample is introduced into the UHV preparation chamber with a base pressure of $5 \cdot 10^{-8}$ mbar. For cleaning the sample, it was sputtered with Ar^+ ions with a kinetic energy of 4 keV while the Ar^+ partial pressure was kept at $1 \cdot 10^{-6}$ mbar. After 15 min sputtering the sample was annealed by electron-beam heating at 950 K for 2 h in an oxygen atmosphere. The O_2 partial pressure was kept at $1 \cdot 10^{-5}$ mbar.

Microspectroscopy

For the microspectroscopic approach a 3-dimensional (3D) stack $I(x, y, E)$ of images was recorded. This was carried out by tuning the photon-energy stepwise over the 2p resonances of NiO and measuring a single image for each interval. In Fig. 1.2 the resulting spectra are presented. Due to integration of

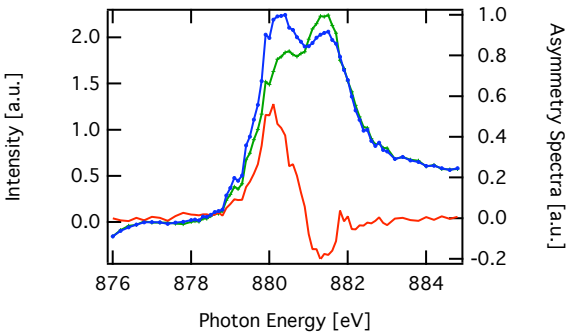

(a) XMLD intensity (blue, green) and asymmetry spectra (red).

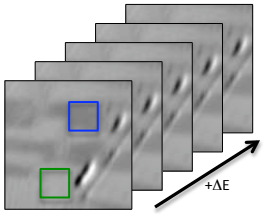

(b) 3D Stack of Images.

Figure 1.2 – Example of the microspectroscopic approach of PEEM.

areas with different contrast (blue and green squares) as shown in Fig. 1.2(b) spectra of different domain states are accessible (Fig. 1.2(a)). The spectra clearly show the change of magnetic contrast on both L2 multiplet peaks. The difference is calculated as the XMLD asymmetry (red). The latter shows the typical s-shaped trace. It has to be noted that the XMLD in antiferromagnets is significantly smaller than the XMCD in ferromagnets and its measurement therefore represents a challenge. Fig. 1.2 demonstrates that this experiment is feasible at DELTA. An improvement of the monochromator-undulator control to continuously scan the photon energy will help to further improve the signal-to-noise ratio.

Magnetic Imaging

Images were recorded with the photon energy tuned to the Ni L_{2a} edge at 880.1 eV and L_{2b} at 881.3 eV. A single X-PEEM image $I(x, y)$ contains both magnetic and non-magnetic contrast. Due to the reversal of the magnetic contrast at the L_{2a} and L_{2b} multiplet peaks a quantity is defined to enhance magnetic contrast by calculating the asymmetry function:

$$A = \frac{I_{L_{2a}}(x, y) - I_{L_{2b}}(x, y)}{I_{L_{2a}}(x, y) + L_{2b}(x, y)} \tag{1.1}$$

A result of this procedure is shown in Fig. 1.3. Due to the rather weak difference of the domain contrast in the directly recorded pictures it is difficult to identify AFM domains, as displayed in Fig. 1.3(a) and 1.3(b). By calculating the asymmetry the image reveals a clear internal structure given by the AFM domains, which is presented in Fig. 1.3(c). Dark and bright areas in the Image correspond to AFM domains with different spin orientation.

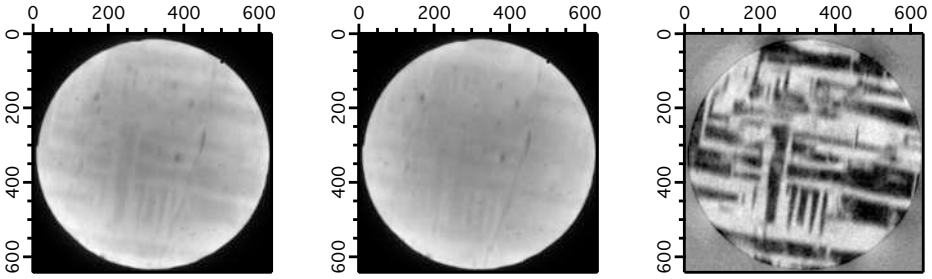

(a) L2a Image (b) L2b Image (c) Asymmetry Image

Figure 1.3 – Enhancement of magnetic contrast by means of calculating the asymmetry. Dark and bright areas in the picture correspond to regions with different magnetization and different AFM-domains, respectively. Field of view is 60 μm.

Conclusion and Outlook

Our results demonstrate for the first time that both microspectroscopy and magnetic domain imaging in antiferromagnets - an important material class for spintronics - are feasible at DELTA.

Acknowledgements

The authors would like to thank Bernd Küpper and Konrad Bickmann for their help during construction works. F.N. would like to thank A. Kaiser, I. Krug and A. Wadewitz. Thanks go to the DELTA staff for continuous support during beamtime.